Universidad del País Vasco Euskal Herriko Unibertsitatea

NAZIOARTEKO BIKAINTASUN CAMPUSA
CAMPUS DE EXCELENCIA INTERNACIONAL

Pharmacokinetics evaluation of new drugs with potential application in Duchenne muscular dystrophy using Positron Emission Tomography and complementary techniques

Rossana Passannante

Doctoral Thesis

Donostia-San Sebastián, 2021

Supervisors:

Dr. Jordi Llop Roig

(CIC BiomaGUNE)

Prof. Jesús Mª Aizpurua Iparraguirre

(UPV/EHU Department of Organic Chemistry I)

List of Abbreviations and Acronyms

ACN	Acetonitrile
ADME	Absorption, Distribution, Metabolism and Elimination
AUC	Area Under the Curve
$C_6H_{16}N_2$	Tetramethylethylenediamine
$C_6H_5NH_2$	Aniline
CH_3I	Iodomethane
CH_3OH	Methanol
Cl	Clearance
CT	Computed Tomography
CYP	Cytochrome
EMA	European Medicines Agency
ERS	Early Stage Researcher
Et_3N	Triethylamine
F	Bioavailability
FDA	Food and Drug Administration
FDG	2-deoxy-2-[^{18}F]fluoro-D-glucose
FOV	Field of View
GLP	Good Laboratory Practice
HCT	Hematocrit
HPLC	High Performance Liquid Chromatography
HPLC-MS	High Performance Liquid Chromatography - Mass Spectrometry
IDIF	Image Derived Input Function
IF	Input Function
IV	Intravenous
LOR	Line of Response
MA	Molar Activity
MDCK-MDR1	Madin Darby Canine Kidney cells with the MDR1 gene
MeOH	Methanol
MRT	Mean Residence Time
MSCA-ITN	Marie Skłodowska Curie Actions – Innovative Training Network

NaOH	Sodium Hydroxide
OR	Oral
PBIF	Population Based Input Function
Pd/Ca_2CO_3	Palladium on calcium carbonate
PET	Positron Emission Tomography
POE	Proof of Efficacy
POM	Proof of Mechanism
POT	Proof of Target
RBC	Red blood cell
RC	Recovery coefficient
RCY	Radiochemical Yield
SA	Specific Activity
SC	Spillover coefficient
$t_{1/2}$	Elimination half-life
TAC	Time Activity Curve
TFA	Trifluoroacetic Acid
TOF	Time of Flight
UGT	UDP-glucuronosyltransferase
V_d	Volume of Distribution
VOI	Volume of Interest
WP	Work Package

Table of Contents

SUMMARY

Drug development is a complex process aimed to evaluate the safety, toxicity, and efficacy of new drugs. Despite the effort in improving the entire process, this is still high time and money consuming. With the aim to reduce drug failure and facilitate a smarter drug development, the incorporation of imaging as technique has gained significant popularity in recent years. Among the different imaging modalities available, Positron Emission Tomography (PET) has played an important role in providing valuable data for the early identification of molecules with the optimum characteristics. It represents the most sensitive nuclear imaging technique based on the administration of compounds labelled with short-lived positron-emitting radionuclides to obtain three-dimensional images of functional processes in animals and/or humans. Within this context, the European Commission, under the H2020 – MSCA-ITN-2015 program (grant agreement No. 675417), financed the PET3D project aimed to train 15 early-stage researchers (ESR) in PET imaging and drug development. One of the partners of the consortium was the Radiochemistry and Nuclear Imaging Group at CIC biomaGUNE, in which this PhD thesis has been carried out.

The final goal of this PhD thesis was the pharmacokinetics evaluation of new drugs with potential application in Duchenne muscular dystrophy using PET and complementary techniques. Because of this, the first part of the work consisted of developing radiolabelling strategies to incorporate, in different positions, either positron or beta emitters into two molecules of interest, AHK-1 and AHK-2. Both approaches did not modify the chemical structure of compounds to be investigated, resulting in a formal substitution of CH_3- group by a $[^{11}C]CH_3$- group, in the case of the positron emitters incorporation, or -H by a $-H^3$ atom, in the case of the beta emitters incorporation. Additionally, this multi-radionuclide/multi-position labelling approach was expected to provide information about the metabolic rate, together with basic information about the chemical structure of the metabolites.

Moving forward towards the feasibility of nuclear imaging techniques to facilitate the investigation of pharmacokinetics of new drugs, we focused on the delineation of the appropriate experimental setting and processing data method. In this second part of the PhD thesis, two scenarios to get reliable and quantitative data were investigated and compared in terms of simplicity and accuracy. These studies provided evidence about the adequacy of an in-

house developed system and a procedure implemented in our group for the quantitative PET studies. The system enables the extracorporeal circulation of arterial blood and the possibility to withdraw blood samples, which were further processed and analysed to get the indispensable data for the pharmacokinetics evaluation.

Once the radiolabelling strategies and the experimental setting have been established, we finally tackled an exhaustive evaluation of the ADME (Absorption, Distribution, Metabolism and Excretion) processes. With that aim, the radiolabelled derivatives were administrated to experimental animals (rats and mice) through intravenous (IV) injection and oral (OR) administration at two different doses. PET imaging studies were conducted to determine the biodistribution after the IV and OR administration of the positron emitter compounds to determine the biodistribution within the organ of interest. PET imaging studies were combined with determination of arterial blood time-activity curves (TACs) and analysis of plasma samples by high performance liquid chromatography (HPLC) to quantify radioactive metabolites. Arterial TACs were obtained in continuous mode by using an in-house developed system which enables extracorporeal blood circulation and continuous measurement of radioactivity in the blood. The most important pharmacokinetic parameters such as volume of distribution (V_d), plasma clearance (Cl), elimination half-life ($t_{1/2}$), area under the curve (AUC), mean residence time (MRT) and bioavailability (F), were determined by analysis of the metabolite-corrected arterial plasma TACs.

RESUMEN

El desarrollo de fármacos es un proceso complejo destinado a evaluar la seguridad, la toxicidad y la eficacia de los nuevos medicamentos. A pesar del esfuerzo constante para mejorar todo el proceso, éste sigue requiriendo mucho tiempo y dinero. Con el objetivo de aumentar los casos de éxito y facilitar un desarrollo más inteligente de los medicamentos, se han incorporado las técnicas de imagen en diferentes estadios del proceso de desarrollo de fármacos. Entre las distintas técnicas de imagen disponibles, la tomografía por emisión de positrones (PET, de sus siglas en inglés; *Positron Emission Tomography*) ha desempeñado un papel importante a la hora de proporcionar datos valiosos para la identificación temprana de moléculas con características prometedoras. La PET es una técnica ultrasensible, y se basa en la administración de compuestos marcados con radioisótopos emisores de positrones de vida media corta, con el fin de obtener imágenes tridimensionales de los procesos funcionales en animales y/o humanos. En este contexto, la Comisión Europea, en el marco del programa H2020 - MSCA-ITN-2015 (acuerdo de subvención nº 675417), financió el proyecto PET3D, cuyo objetivo era formar a 15 jóvenes investigadores (ESR, de sus siglas en inglés; *Early Stage Researchers*) en la técnica de imagen PET y su aplicación al desarrollo de fármacos. El consorcio estaba formado por 8 socios de 7 países europeos diferentes (España, Alemania, Bélgica, Noruega, Suecia, Países Bajos y Inglaterra) especializados en el sector. Uno de los socios del consorcio fue el Grupo de Radioquímica e Imagen Nuclear del CIC biomaGUNE, en el que se ha realizado esta tesis doctoral.

El trabajo llevado a cabo en este doctorado se ha dividido en tres partes, que corresponden a los capítulos 3, 4 y 5 del presente documento.

En la primera parte del trabajo (Capítulo 3), se presenta el desarrollo de métodos de marcaje de las moléculas de interés, AHK-1 y AHK-2. Uno de los aspectos a tener en cuenta cuando se quiere abordar estudios con compuestos marcados radioactivamente, es la selección de radioisótopo adecuado. En primer lugar, su vida media debe ser lo suficientemente larga como para llevar a cabo el proceso de marcaje, purificación, formulación y control de calidad del producto final. En segundo lugar, la incorporación del radioisótopo no debe modificar la estructura química del compuesto a investigar. Esto es especialmente relevante cuando se trata de moléculas pequeñas, en las cuales mínimas modificaciones en la estructura química pueden provocar

cambios drásticos en las propiedades fisicoquímicas y biológicas. La posición del marcaje también es fundamental puesto que las técnicas radio-analíticas sólo detectan el radionúclido. Por lo tanto, si una molécula se descompone o sufre un metabolismo, sólo se detectará el fragmento que contiene el radionúclido. Por ello, incorporar el/los radioisótopo/s en diferentes posiciones es una estrategia interesante para obtener datos cuantitativos sobre la formación de diferentes metabolitos a lo largo del tiempo. Teniendo en cuenta la estructura química de las moléculas a investigar (ver Fig. 1a) y las tecnologías disponibles, se decidió utilizar una estrategia de marcaje multi- radioisótopo/multi-posición para poder obtener, en una primera etapa, información sobre la tasa metabólica junto a una información básica sobre la estructura química de los metabolitos. Inicialmente, aprovechando de la presencia de grupos metilo (CH_3-) directamente unidos a heteroátomos, ambos compuestos fueron radiomarcados en dos posiciones diferentes, vía ^{11}C-metilación, utilizando [^{11}C]CH_3I como agente de marcaje (ver Fig. 1b). El marcaje resultó en una sustitución formal de un grupo CH_3- por un grupo [^{11}C]CH_3-, lo que significa que la estructura química permanece inalterada. Posteriormente, y aprovechando la posibilidad de efectuar una estancia en el laboratorio dirigido por el Dr. Charles S. Elmore en el Early Chemical Development, Pharmaceutical Sciences R&D de AstraZeneca, se marcaron los mismos compuestos (ver Fig. 1b).

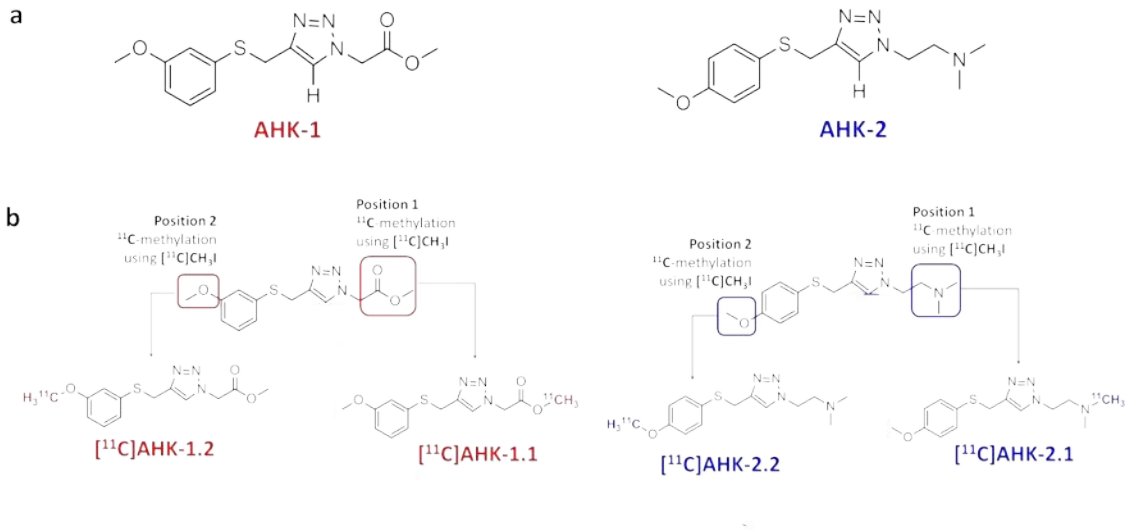

Fig. 1: a) Estructura química de las moléculas a investigar AHK-1 y AHK-2. b) Estructura química de AHK-1 y AHK-2. En ellas se marcan las posiciones en las cuales se realizó la metilación con ^{11}C y la reducción con gas ^{3}H. La estructura química de los compuestos resultantes radiomarcados está ilustrada.

Tras el proceso de desarrollo y optimización de las condiciones para el marcaje mediante la metilación con $_{11}C$, los compuestos [$_{11}C$]AHK-1.1, [$_{11}C$]AHK-1.2, [$_{11}C$]AHK-2.1 y [$_{11}C$]AHK-2.2 se obtuvieron con rendimientos radioquímicos no corregidos por decaimiento en el rango del 5-15% y en tiempos de producción globales de unos 30 minutos desde el final del bombardeo. La pureza radioquímica fue superior al 95% en todos los casos y los valores de actividad específica al final de la síntesis estaban entre 40-140 GBq/µmol.

Una vez establecido el proceso de radiomarcado para la preparación de [$_{11}C$]AHK-1.1, [$_{11}C$]AHK-1.2, [$_{11}C$]AHK-2.1 y [$_{11}C$]AHK-2.2, se abordó la investigación *in vitro* de la estabilidad metabólica utilizando microsomas de rata, que son una fracción subcelular de los hepatocitos que contienen enzimas responsables del metabolismo de más del 90% de los fármacos comerciales. Con estos estudios, se consiguió una estimación del metabolismo, y pudieron identificarse algunos de los metabolitos. Los resultados mostraron que, para el compuesto AHK-1, la hidrólisis del residuo -COOCH $_{3}$es la principal vía metabólica. El éster podría

ser una especie de profármaco que, tras su administración, podría convertirse inmediatamente en el ácido libre, que se metaboliza posteriormente. Para el compuesto AHK-2, la principal vía metabólica fue la desmetilación del residuo CH_3O-Ar, seguida de la oxidación del grupo tioéter en sulfóxido y la desmetilación de -$N(CH_3)_2$ (ver Fig. 2).

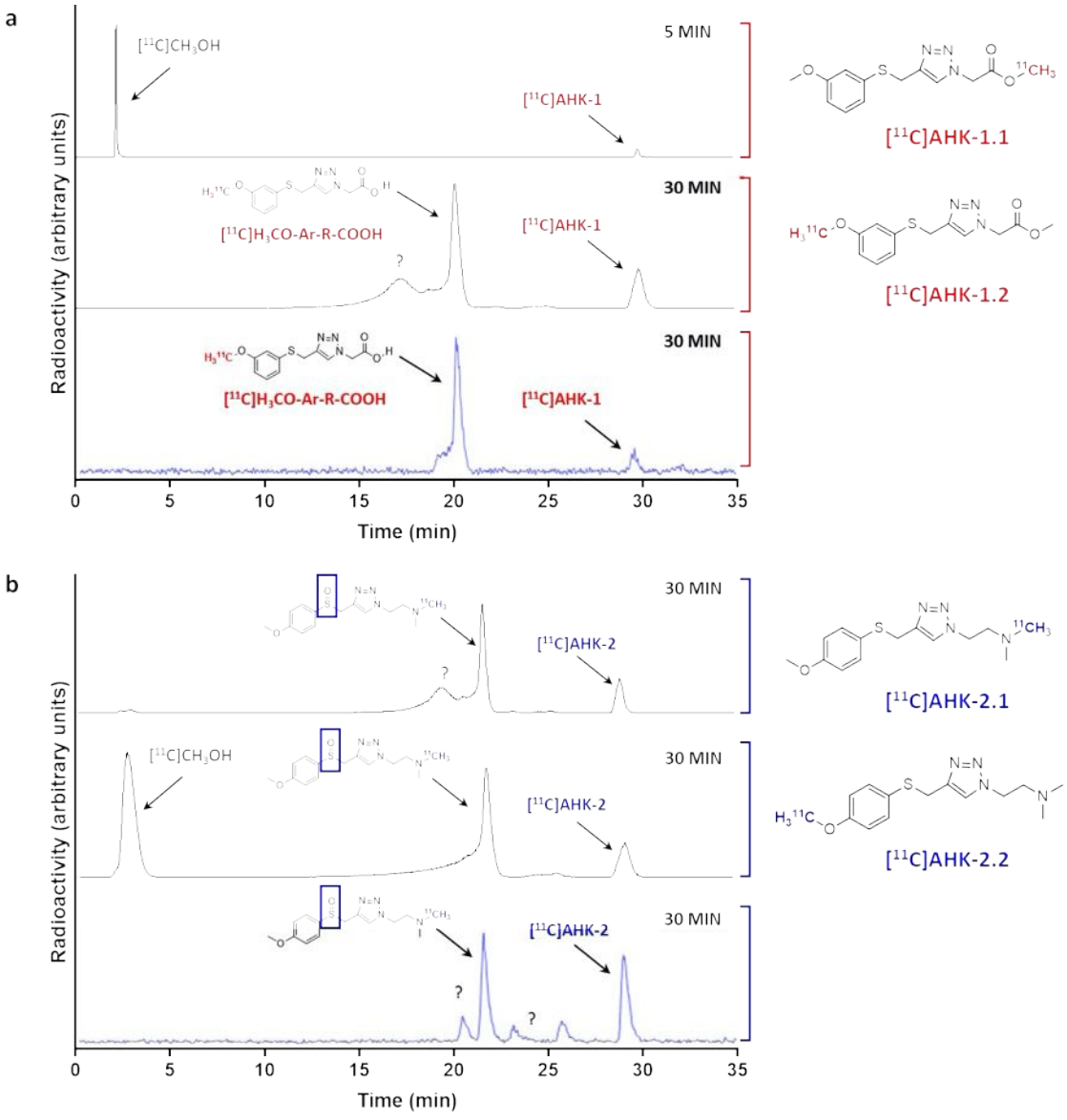

Fig. 2: Cromatogramas representativos correspondientes al estudio del metabolismo *in vitro* (detector de radiactividad) de los derivados radioactivos del compuesto AHK-1 (a) y AHK-2 (b). La posición de los picos correspondientes a los metabolitos identificados está indicada.

En la segunda parte del trabajo (Capítulo 4), se abordó el estudio para la determinación de la función de entrada (IF, de sus siglas en inglés; *input function*). La determinación de la función de entrada representa un punto clave en los estudios PET, especialmente cuando se aborda el desarrollo de nuevos radiotrazadores. La concentración del compuesto no metabolizado en el plasma arterial (o en la sangre, dependiendo del trazador) es la función de entrada de referencia para el análisis cuantitativo de datos PET. En los últimos años, se han desarrollado varias maneras de determinar la IF, como por ejemplo mediante: la función de entrada derivada de la imagen (IDIF, de sus siglas en inglés *Image derived input function*); la medición en tiempo real mediante cateterismo vascular; la función de entrada basada en las venas y la función de entrada basada en la población. Con el fin de concretar el entorno experimental y el método de procesamiento de datos más adecuado, se decidió determinar la IF a partir de imágenes PET dinámicas (IDIF) y de un detector gamma externo (medición de la IF en tiempo real). Para esta última, se practicó una circulación extracorpórea de la sangre arterial mediante un *by-pass* externo de la arteria y la vena femorales, utilizando un sistema desarrollado por el Grupo de Radioquímica e Imagen Nuclear en CIC biomaGUNE. Como radiotrazador, se seleccionó [^{18}F]FDG ya que después de la administración intravenosa, permanece como la única especie radiactiva en la sangre, simplificando así el procesamiento de los datos. Como principales estructuras vasculares visibles en las imágenes PET, se seleccionaron el ventrículo izquierdo y la vena cava inferior (ver Fig. 3). En comparación con la medición en tiempo real de la sangre arterial, los IDIF resultaron ser más fáciles de determinar y menos invasivos, aunque hubo variabilidad en los resultados dependiendo de la estructura vascular seleccionada (vena cava, ventrículo izquierdo) e incluso en la posición donde se dibujó el volumen de interés (VOI). Estos resultados proporcionaron pruebas suficientes para establecer la medición de la IF en tiempo real como abordaje experimental adecuado puesto que permite el acceso a la sangre arterial y la posibilidad de extraer muestras de sangre para su posterior análisis. A pesar de que el método es bastante invasivo y técnicamente desafiante, se decidió aplicar esta alternativa para estudios posteriores ya que la información proporcionada es muy valiosa especialmente en el desarrollo de nuevos radiotrazadores.

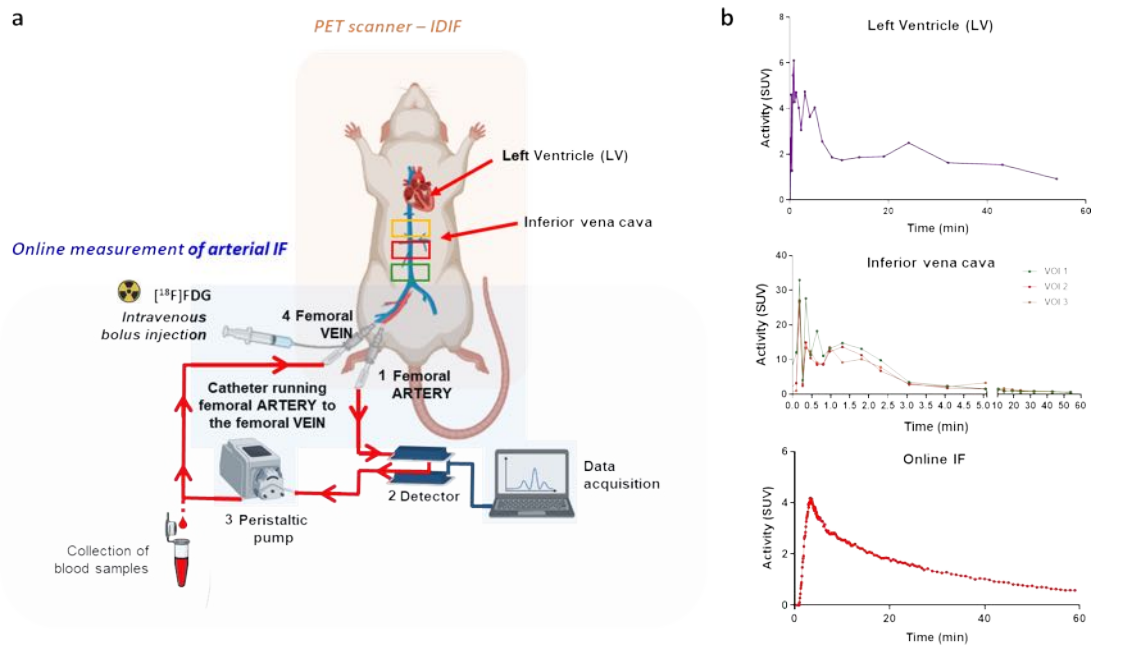

Fig. 3: a) Representación esquemática de la configuración experimental utilizada para la determinación de la función de entrada derivada de la imagen (IDIF) y la función de entrada arterial mediante la medición continua de la radiactividad en la sangre. En primer lugar, se introdujeron dos catéteres en la arteria y la vena femorales, respectivamente. La sangre se bombeó a través de un detector radiactivo mediante una bomba peristáltica y se creó un sistema de circulación extracorpórea. El animal permaneció en el escáner PET, donde se adquirieron imágenes dinámicas y se determinaron las IDIF en el ventrículo izquierdo y en la vena cava inferior. b) Ejemplo de IF obtenidas en función de la estructura vascular seleccionada en la imagen (ventrículo izquierdo y vena cava) y mediante medición en tiempo real de la sangre arterial (online IF).

Una vez establecidas las estrategias de radiomarcaje y el método para determinar la IF, se abordó finalmente la evaluación de la farmacociné=ca (ADME: Absorción, Distribución, Metabolismo y Excreción) de los compuestos AHK-1 y AHK-2. Para ello, se administraron los derivados radiomarcados a animales de experimentación (ratas y ratones) mediante inyección intravenosa (IV), oral (OR) a dos dosis diferentes. Se realizaron estudios de imagen PET para determinar la biodistribución tras la administración IV y OR de los compuestos marcados con ^{11}C (ver Fig. 4).

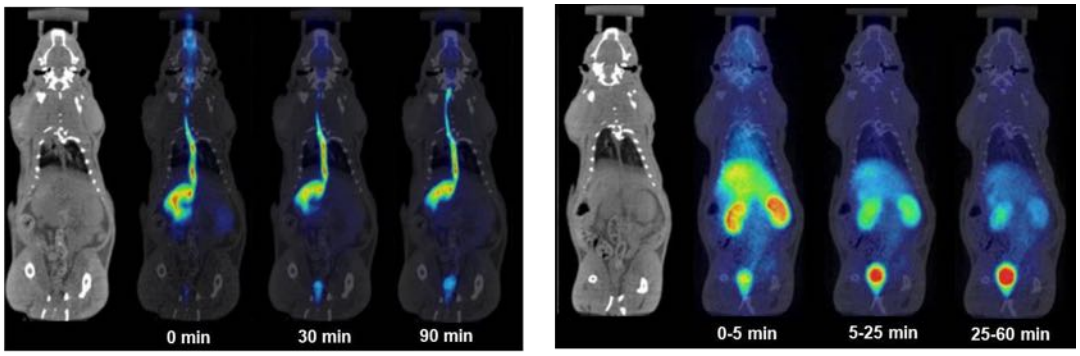

Fig. 4: Imágenes PET (vista coronal) representativas de todo el cuerpo (proyecciones) obtenidas en diferentes momentos tras la administración oral (izquierda) e intravenosa (derecha) del compuesto [$_{11}$C]AHK-1.1 como ejemplo. Las imágenes PET se muestran corregistradas con cortes representativos de imágenes CT correspondientes al mismo animal para facilitar la localización de la señal radioactiva.

Los estudios de imagen PET se combinaron con la determinación de las funciones de entrada en sangre arterial (TAC) y el análisis de muestras de plasma mediante cromatografía líquida de alta resolución (HPLC) para cuantificar los metabolitos radiactivos (ver. Fig. 5). Los parámetros farmacocinéticos más importantes, como el volumen de distribución (Vd), el aclaramiento plasmático (Cl), la semivida de eliminación ($t_{1/2}$), el área bajo la curva (AUC), el tiempo medio de residencia (MRT) y la biodisponibilidad (F), se determinaron mediante el análisis de los TAC plasmáticos arteriales corregidos por metabolitos.

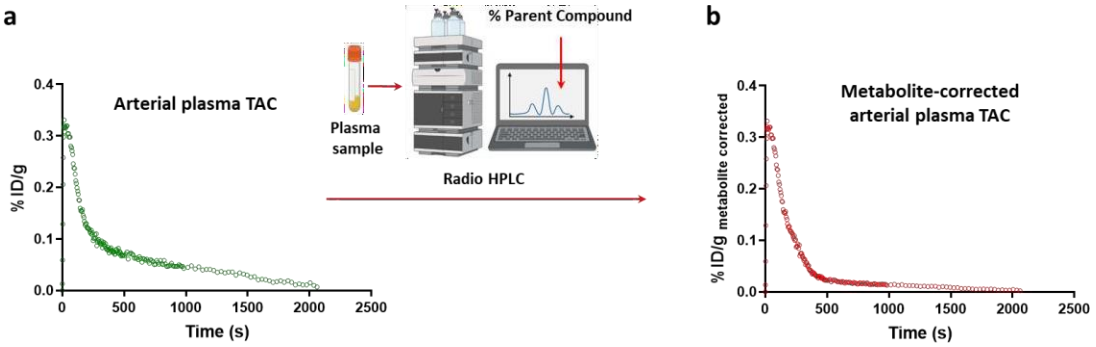

Fig. 5: Ejemplo de TAC obtenida mediante la circulación extracorpórea de la sangre y la medición continua de la radiactividad para la determinación de los parámetros farmacocinéticas más importantes. Tras la conversión de la TAC original en porcentaje de dosis administrada por gramo (a) esta ha sido corregida por metabolismo (b) gracias a la extracción de muestras de sangre arterial que han sido procesadas y analizadas mediante HPLC equipado con detector de radioactividad.

CHAPTER 1: GENERAL INTRODUCTION

1.1 DRUG DEVELOPMENT: AN OVERVIEW

Drug development is a complex process typically divided into three major steps: discovery, preclinical development, and clinical trials (Fig. 1.1), focused on the evaluation of safety, toxicity, and efficacy of new drugs. It takes in general 10 to 15 years with an average cost of US $ 500-1000 million[1].

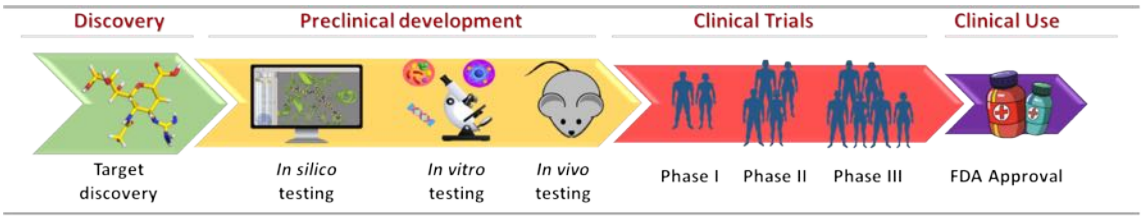

Fig. 1.1: Schematic representation of the main steps in the drug development process.

The first step in drug development is to discover the best target for treating or preventing a disease. Targets are usually proteins in the patient body, which are associated with the disease, or proteins in microorganisms causing a disease. The challenges are to identify which proteins are relevant and, more important, to confirm their role in a disease. Once the target has been identified, rational design of the adequate chemical entity based on structural biology and high throughput screening of libraries of compounds is used to select the best ligand/s. The chemical entities that show promising results during *in vitro* assays are selected for preclinical *in vivo* studies, the bottleneck before reaching clinical trials, which involve human subjects. Clinical trials are divided in three phases, and transition to the following phase only occurs when results in the current phase are satisfactory. Phase I trials generally enrol less than 30 volunteers and are designed to investigate if the drug is safe, to evaluate pharmacokinetics and to obtain preliminary data on pharmacodynamics. Different types of phase I trials can be distinguished: (I) single ascending dose studies, in which small groups of subjects receive a single dose of the test drug that is scaled up until the pre-calculated pharmacokinetics are achieved or side effects occur; (II) multiple ascending dose studies, characterized by repeated administration of the same dose of the test drug; and (III) trials designed to investigate variations in the absorption of the new drug

[1] Di Masi, J.A., Grabowski, H.G., Hansen, R.W. Innovation in the pharmaceutical industry: new estimates of R&D costs. *J. Health. Econ*. (2016) doi:10.1016/j.jhealeco.2016.01.012.

following its oral administration in the presence of food. If the safe dose is found, the new drug goes to phase II. In this phase, more subjects, usually around one hundred including patients, are enrolled and the efficacy and side effects of the drug candidate are investigated. If the new treatment is found to be safe and has some therapeutic effect, it goes to phase III. Phase III is where more participants are involved, typically ranging from a few hundreds to a few thousands. Phase III clinical trials are designed to compare the efficacy of the new treatment with existing treatments (if available) and to monitor eventual adverse reactions. Despite various efforts to improve the entire process, the success rates, in both public and private sectors, are 64.5% for phase I, 20.5% for phase II and 12.3% for phase III[2].

1.2 PRECLINICAL STUDIES

Preclinical studies aim at providing information about pharmacokinetics, safety, and efficacy of a drug candidate before being tested in humans. Preclinical studies need to comply with the guidelines dictated by Good Laboratory Practices (GLP) to ensure reliable results. Fulfilment of GLPs is required by authorities such as the Food and Drug Administration (FDA) or the European Medicines Agency (EMA) for final approval. Information on the dosage and toxicity levels of the compound is essential to determine whether it is justified and safe to proceed with clinical studies, and this information is obtained by conducting pharmacokinetics, pharmacodynamics, and toxicology studies. Animals play a critical role in preclinical studies. Although *in vitro* studies, which typically precede animal experimentation, are relatively fast, simple, and cost-efficient, complex disease mechanisms can only be understood by using experimental animals. Animal tests are avoided if possible, and when required, they are conducted under strict regulation and the 3 R's principle: Replacement, Reduction and Refinement.

1.3 PHARMACOKINETICS – WHAT DOES THE BODY DO TO THE DRUG?

The effect of a drug depends on the fraction of the administered dose that reaches the systemic circulation. Pharmacokinetics (PK) describes changes in drug plasma concentrations over time because of absorption (if the administration is not intravenous), distribution, metabolism, and excretion (ADME). ADME profiling is critical for establishing dose ranges and enter clinical trials. Most drugs are administered orally and need to be absorbed in the gastrointestinal tract to enter

[2] Hay, M., Thomas, D. W., Craighead, J. L., Economides, C. & Rosenthal, J. Clinical development success rates for investigational drugs. *Nat. Biotechnol.* (2014) doi: 10.1038/nbt.2786.

the circulatory system and reach their target. On its way to the target, the drug concentration in plasma, and thus its bioavailability, is reduced because of first-pass metabolism that takes place in the liver. Intravenous drug administration bypasses absorption, resulting in higher bioavailability. Once in the circulation, the drug is transported to different tissues. Distribution of the compound throughout the body is determined by: (I) the affinity of the drug for plasma proteins; (II) the molecular properties of the drug; and (III) tissue vascularisation.

To facilitate elimination, drugs are metabolised. Metabolism refers to the chemical alteration of the parental drug into pharmacologically active or inert metabolites. To ensure an appropriate concentration of the drug over time, it is critical to obtain information about clearance, the drug elimination from the body. Clearance is mainly achieved via the renal and hepatic routes; however, pulmonary clearance plays a major role for volatile drugs such as anaesthetics. Diseases, lifestyle factors, and age can affect clearance, and these are frequently studied in later stages of the clinical trial. When the rate of clearance equals the rate of absorption, a so-called steady state is reached. Typically, maintaining a stable steady state level is desirable and can be achieved through repeated dosing. Finally, the drug and its metabolites are excreted from the body mainly through urine or faeces.

1.3.1 PRECLINICAL PHARMACOKINETICS TECHNOLOGY – CURRENT AND FUTURE PERSPECTIVES

Appropriate pharmacokinetic profiling is a critical step to achieve an efficacious and safe clinical dose range. Human pharmacokinetic parameters can be predicted from preclinical pharmacokinetic data. Pharmacokinetics studies at preclinical level are basically conducted with *in silico*, *in vitro* or *in vivo* models[3].

In silico model

In silico models predict drug behaviour based on physicochemical properties of drug candidates in combination with crystal structures of a protein (target) and database of ADME properties generated in laboratories. These studies are often capable to faithfully predict absorption, target

[3] Zhang, D., Luo, G., Ding, X., & Lu, C. Preclinical experimental models of drug metabolism and disposition in drug discovery and development. *Acta Pharmaceutica Sinica B,* (2012) doi:10.1016/j.apsb.2012.10.004.

organ concentration, clearance or efficacy, and toxicity or other adverse effects, early in the drug discovery and development process[4].

In vitro models

In vitro assays play an important role especially in screening of new compounds in the discovery stage. These assays are fast, robust, and simple, and require just a limited amount of compound. They can be designed to answer specific questions about properties that are known to have species-related differences. Generally speaking, *in vitro* pharmacokinetics assays include permeability, metabolic stability, and cytotoxicity. Permeability is a key factor for the biodistribution of the drug when administered orally and represents the capacity of the gastrointestinal tract to be permeated or not by a drug. It can be characterized *in vitro* by using cells and membrane vesicles from organs that usually express a high concentration of transporters. The use of human colon cancer derived Caco-2 cell line and Madin Darby canine kidney cells with the MDR1 gene (MDCK-MDR1), the gene encoding for the efflux protein, P-glycoprotein (P-gp), is widely established to predict *in vivo* absorption[5,6]. Metabolic stability generally comprises studies using primary hepatocyte cultures or sub-cellular fractions isolated from them[7]. Hepatocytes are the primary liver cells where drug metabolism occurs thanks to the high concentration of P450 cytochromes (CYPs), a superfamily of enzymes involved in 75% of the total metabolism of a drug. The cell membrane of hepatocytes contains various uptake or efflux transporters. Drugs could passively diffuse through the hepatocyte membrane or be taken up by transporters. The primary cultures of hepatocytes carry enzymes and co-factors at physiological concentrations and provide the most complex model for drug metabolism studies. However, the culture is not always easily accessible. To overcome this limitation, the use of different sub-cellular fractions represents the most widely used alternative. The cytosol fraction contains a

[4] van de Waterbeemd, H. & Gifford, E. ADMET in silico modelling: towards prediction paradise?. *Nat. Rev. Drug Discov.* (2003) doi:10.0138/nrd1032.

[5] Sambuy, Y., De Angelis, I., Ranaldi, G., Scarino, M.L., Stammati, A., Zucco, F. The Caco-2 cell line as a model of the intestinal barrier: influence of cell and culture related factors on Caco-2 cell functional characteristics. *Cell Biol. Toxicol.* (2005) doi:10.1007/s10565-005-0085-6.

[6] Pastan, I., Gottesman, M. M., Ueda, K., Lovelace, E., Rutherford, A. V., Willingham, M. C., A retrovirus carrying an MDR1 cDNA confers multidrug resistance and polarized expression of P-glycoprotein in MDCK cells. *Proc Natl Acad Sci USA* (1988) doi: 10.1073/pnas.85.12.4486.

[7] Jia, L., Liu, X. The conduct of drug metabolism studies considered good practice (II): *in vitro* experiments. *Curr. Drug Metab.* (2007) doi: 10.2174/138920007782798207.

group of soluble drug-metabolizing enzymes and represents the simplest system. The S9 fraction contains both cytosol and microsomal enzymes and represents a nearly complete collection of the metabolizing system; finally, microsomal fraction contains CYPs and primary conjugation enzymes such as UDP-glucuronosyltransferase (UGTs). Among the enzyme systems mentioned, the microsomal fraction, containing enzymes responsible for the metabolism of over 90% of commercial drugs, is the most used. Finally, cytotoxicity and therefore cell death detection studies are generally performed by measuring changes in the expression levels of enzymes or any biomarker during drug ensure[8].

In vivo models

In silico and *in vitro* models have a limited value as they reflect only one aspect of a complex behaviour. Contrarily, *in vivo* models provide a unique opportunity to obtain a combination of information about the complex interactions existing in living systems. Animal models may faithfully predict the behaviour of a drug in a human subject. Unfortunately, this is not always the case, and hence especial attention needs to be paid when translating data obtained in experimental animals to humans. Many drugs that are safe and effective in animal studies may have limited therapeutic benefits or could show toxicity or side effects in humans. The selection of the species and the model will depend on the investigated drug and the disease area, and often the combination of different species and/or models is required to gather accurate data.

Pharmacokinetic studies in animals usually involve the use of high-performance liquid chromatography combined with mass spectrometry (HPLC-MS) as the analytical technique. After the administration of the drug to the animal, body fluids (*i.e.* blood, urine) or organs (these after animal sacrifice) are extracted and, after appropriate processing, the resulting samples are analysed to get information about the concentration of the test compound and/or metabolites in order to gather pharmacokinetic information [9, 10]. This approach provides accurate and

[8] Riss, T. *et al*. Cytotoxicity Assays: *In Vitro* Methods to Measure Dead Cells. Assay Guidance Manual [Internet]; Eli Lilly & Company and the National Center for Advancing Translational Sciences (2019).

[9] Sandhu, P. *et al.* Evaluation of microdosing strategies for studies in preclinical drug development: demonstration of linear pharmacokinetics in dogs of a nucleoside analog over a 50-fold dose range. *Drug Metabolism and Disposition* (2004) doi:10.1124/dmd.104.000422.

[10] Kamath, A. V., Wang, J., Lee, F. Y., & Marathe, P. H. Preclinical pharmacokinetics and *in vitro* metabolism of dasatinib (BMS-354825): a potent oral multi-targeted kinase inhibitor against SRC and BCR-ABL. *Cancer Chemotherapy and Pharmacology.* (2007) doi:10.1007/s00280-007-0478-8.

exhaustive information. However, the main drawback is that it is invasive and requires the use of a large number of animals, with the consequent economic and ethical burden.

As an alternative to HPLC-MS, the use of radiolabelled drugs can be applied for ADME studies, especially when in addition to the parent compound, a good understanding of metabolites is necessary. Radioactive labelled drugs play an increasing role in drug discovery, [11]and this is because the ultra-sensitivity of detection methods allow the identification and quantification of all drug-related substances in systems as complex as experimental animals or humans.

Molecular imaging techniques have also gained increased attention in preclinical assessment of new drug candidates, as they can aid in refining and accelerating the process of drug discovery and development. Molecular imaging can be defined as a set of techniques that allow the non-invasive visualization of biological processes at molecular or cellular level in living organisms. Among molecular imaging techniques, Positron Emission Tomography (PET) has positioned as a key tool in the process of drug development, due to its superb sensitivity, sufficient spatiotemporal resolution, and minimal invasiveness. In the following sections, the principles of PET imaging and the application of this emerging technology in the drug development process will be covered, as this is the main tool used in this PhD thesis.

1.4 Positron Emission Tomography (PET)

1.4.1. General aspects

Positron Emission Tomography (PET) is the most sensitive nuclear imaging technique. It is based on the administration of compounds labelled with short-lived positron-emitting radionuclides to obtain three-dimensional images of functional processes in animals and/or humans. The positron-emitting radionuclides are incorporated into biologically active compounds that play a specific role in living organisms. The radioactive atom defines the physical properties, while the chemical structure of the molecule attached to the radioisotope defines the biological properties. The radiolabelled probes, so called radiotracers, are administrated at tracer amount (*ca.* < 1 µg in humans; 10-100 times lower in small animals) and hence do not perturb the physiology of the investigated subject. Therefore, PET allows for the investigation of

[11] Isin, E. M., Elmore, C. S., Nilsson, G. N., Thompson, R. A. & Weidolf, L. Use of Radiolabeled Compounds in Drug Metabolism and Pharmacokinetic Studies. *Chemical Research in Toxicology* (2012) doi:10.1021/tx2005212.

physiological and molecular processes without the need of administering pharmacologically active doses, contrarily to classical pharmacological investigations.

When a positron emitter disintegrates by spontaneous radioactive decay, a positron is emitted (Fig. 1.2a). The positron is the anti-particle of the electron and has the same mass of the electron but positive charge. The positron is emitted with a certain energy, and hence with a certain speed. The positron interacts with surrounding particles following a random path, while losing its kinetic energy. When it is almost at rest, the positron annihilates with an electron. In this process, the combined mass of the two particles is converted into energy, and two gamma rays with energy = 511 keV each are emitted, 180° apart from each other (Fig. 1.2a). These high-energy photons, which have a high penetration power, escape from the body and are detected by an external ring of detectors, which are installed into the PET camera (Fig. 1.2b). When two detectors detect one photon each simultaneously (Fig. 1.2c), this is considered as a coincidence event, and the straight line between the two detectors defines the *line of response* (LOR). The annihilation occurred at some spot within the LOR, although the precise position is not known. Still, the detection of millions of coincidence events, which results in the generation of millions of LORs, allows for the reconstruction of 4D-images containing quantitative spatiotemporal information of the concentration of the radionuclide over time.

It is worth mentioning that the line of response identifies the position where the annihilation occurred, and not the position in which the positron is emitted. The linear distance between the points where the disintegration and the annihilation occur is called positron range and is determined by the energy of the emitted positron (which is an intrinsic property of the radionuclide) and the media. Positrons emitted with a high energy result in a high positron range, and vice-versa. The positron range has a negative effect on image resolution: the larger the positron range, the lower the spatial resolution that can be achieved. Positron emitters typically used in nuclear medicine have positron ranges ranging from a few mm to a few cm in water.

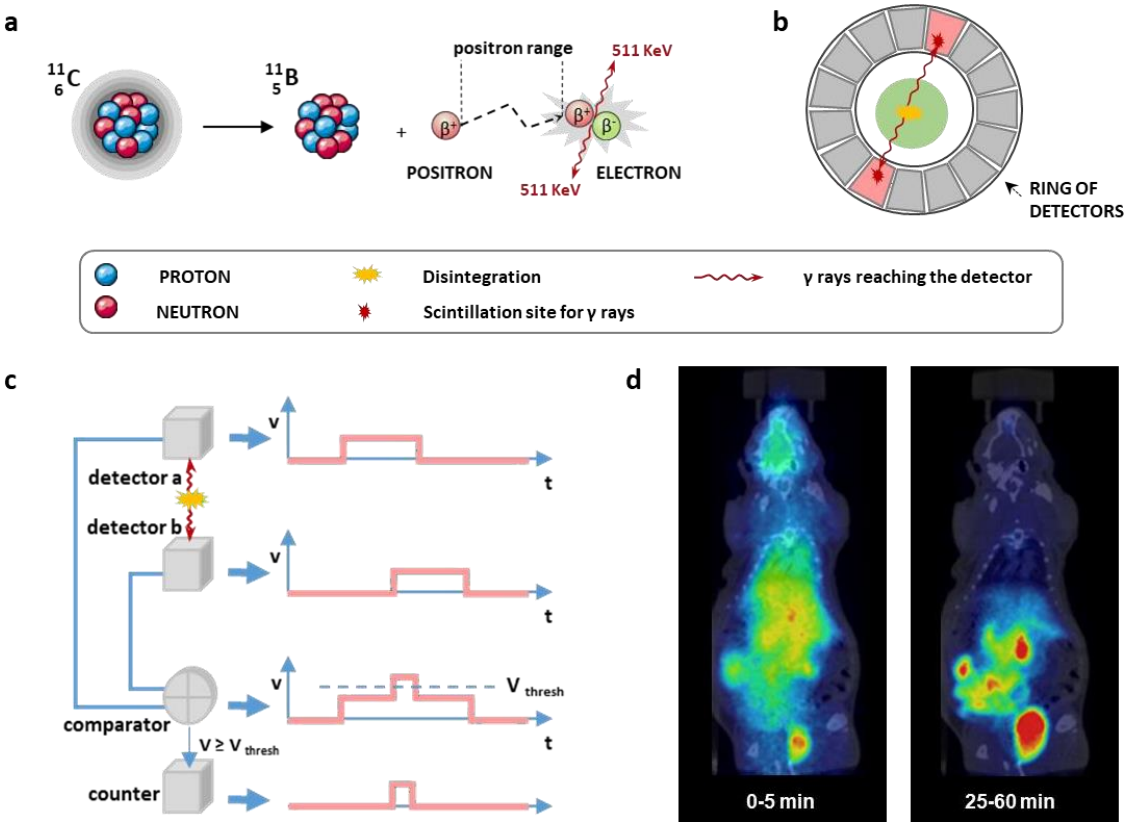

Fig. 1.2: a) Schematic representation of the positron annihilation process. Spontaneous radioactive decay of positron emitters (carbon-11 converted into boron-11 in the example) produces the emission of a positron. After travelling a certain distance, the annihilation with an electron results in the formation of two anti-parallel gamma rays, with energy of 511 KeV each. b) Schematic representation of the detection of gamma rays using a PET scanner. The two gamma rays generated during the annihilation process escape from the body and hit the external ring of detectors. c) Coincidence detection: when two signals overlap in time, the pulse amplitude is doubled. The resulting voltage is higher than the threshold voltage and the event will be registered as a true coincidence event. d) Example of 4D reconstructed PET images.

In the recent years, the concept of Time of Flight (TOF), originally developed by Brownell *et al.* in 1969[12], has gained relevance. Indeed, when the annihilation occurs in a position that is not located at the geometrical centre of the ring of detectors, the photons reach the detectors with a very small, but measurable, time difference. This time difference is used to define the probability of the annihilation to have occurred along the line of response. If no TOF information

[12] Brownell, G. L., Burnham, C. A. *et al.* New developments in positron scintigraphy and the application of cyclotron produced positron emitters. *Medical Radioisotope Scintigraphy* (1969).

is used, the probability of annihilation at a certain point along the LOR is uniformly distributed. If TOF information is used, the probability profile along the LOR is a Gaussian distribution (Fig. 1.3).

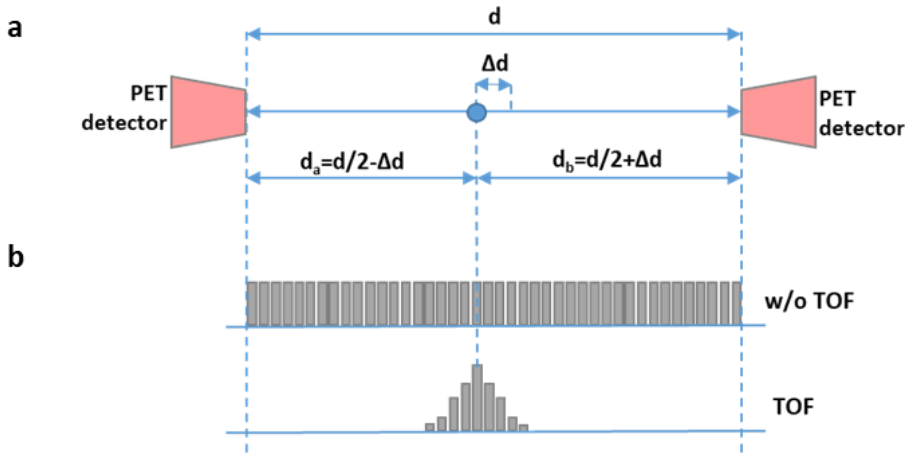

Fig 1.3: Time of flight (TOF) information for PET reconstruction. a) For annihilation not occurring at the centre of the scanner, the two photons reach the PET detectors with a time delay Δt. Measurement of Δt allows estimation of Δd. b) Probability distribution of annihilation event along the LOR when no TOF information (top histogram) or TOF information is used (bottom histogram).

The TOF principle localizes the events and reduces the noise in the image. In each spatial position, only coincidence events with TOF differences consistent with such positions are accumulated. Noise and random events with inconsistent time information are filtered out [13]. It is worth mentioning that the application of TOF is limited by the speed of the electronic components currently available. At the moment, state of the art detectors enable the discrimination of events with a time resolution of *ca.* 500 ps, which means that the localization of the disintegration event using TOF can be determined within a range of *ca.* 15 cm. Because of this, TOF finds application in clinical scanners, where the diameter of the ring of detectors is close to 1 m. However, preclinical small-rodent scanners, which have rings of detectors with diameters close to 10-20 cm, do not profit from the TOF principle. This is, however, an option for the future, if development in electronics allows for time resolution in the range of less than 10 ps.

[13] Conti, M., Bendriem, B. The new opportunities for high time resolution clinical TOF PET. *Clinical and Translational Imaging* (2019) doi:10.1007/s40336-019-00316-5.

1.4.2. PET RADIONUCLIDES – GENERAL ASPECTS

One key aspect in PET imaging is the selection of the positron emitter. Typical positron emitters used at the pre-clinical and clinical levels include fluorine-18 (F-18), carbon-11 (C-11), nitrogen-13 (N-13), oxygen-15 (O-15), zirconium-89 (Zr-89) and galium-68 (Ga-68). In table 1.1, half-life values (time required to decrease the number of radioactive atoms to one half) and the energies of the emitted positrons are shown for these radionuclides.

Table 1.1 Physical characteristics of Fluorine-18, Carbon-11, Nitrogen-13 and Oxygen-15.

Radionuclide	Half-life	Decay mode / decay product	Max. positron Energy (MeV)	Most Probable positron Energy (Mev)	Max. Range in water (mm)
Fluorine-18	109.8 min	97% β^+ 3% EC* Oxygen-18	0.69	0.202	2.4
Carbon-11	20.4 min	100 % β^+ Boron-11	0.96	0.326	4.1
Nitrogen-13	9.98 min	100 % β^+ Carbon-13	1.19	0.432	4.5
Oxygen-15	2.05 min	100 % β^+ Nitrogen-15	1.70	0.650	8.0
Zirconium-89	78.4 hours	22.3% β^+ 76.6% EC* Yttrium-89	0.90	0.4	3.8
Galium-68	67.7 min	89.1% β^+ 10.9% EC* Zinc-68	1.90	0.829	13.6

EC*: Electronic capture. Obtained from: Welch, M.J., Redvanly, C.S., Handbook of radiopharmaceuticals: Radiochemistry and applications. *Wiley*, 2005.

The physical and chemical properties of the radionuclide will define the applicability of the labelled specie. The first aspect to take into consideration when selecting the radionuclide for the preparation of a labelled compound is the half-life. This should be long enough to perform the radiolabelling, purification, formulation, and quality control of the final product, before being administered to the living subject. Moreover, the physical half-life of the radionuclide should match the biological half-life of the molecule to be investigated. If the physical half-life is too short, only partial information about the pharmacokinetics will be obtained. If the half-life is too long, a high (and unnecessary) radiation dose will be imposed on the subject under investigation. The latter is especially relevant in clinical studies, and when repeated administration is required.

Another aspect is, as mentioned above, the positron range. If the positron range is very high, the resolution of the images can be compromised.

The third critical aspect is the availability. Positron emitters have relatively short half-lives, and hence they require *in situ* production, which is carried out using particle accelerators (see section 1.4.3). The infrastructure required to produce positron emitters and the preparation of the radiotracers has a huge cost and requires trained personnel. This has historically limited the consolidation of PET imaging, especially at the preclinical level and in the process of drug development. Using radionuclides with relatively long half-life (*e.g.* F-18) enables the centralized production of the radiotracer and distribution to end users.

Finally, besides the physical properties, one key aspect in the selection of the radionuclide is the chemical compatibility with the molecule to be investigated. In other words, the radionuclide needs to be attached to/incorporated in the molecule under investigation. A thorough discussion covering PET radiochemistry is beyond the scope of this introduction. However, the main radiochemical aspects of C-11, the radionuclide used in this PhD thesis, and other PET radionuclides commonly employed in the clinical arena are discussed below.

1.4.3. PET RADIONUCLIDES – PRODUCTION

Clinically used positron-emitters, with the exemption of Ga-68, this is, F-18, C-11, N-13, O-15, and Zr-89, are generated in a cyclotron. A cyclotron (Figs. 1.4 and 1.5) is a particle accelerator in which an electric field is used to accelerate ions, such as H^- or D^-, which are guided with a magnetic field. The electric field is generated by the application of an electric potential between two electrodes (do called “dees” and “counter-dees”), connected to an alternating current source. Negative ions are generated in the ion source (placed in the centre of the cyclotron) by applying a high voltage to hydrogen or deuterium gas. When the “dee” is positively charged, the “counter-dee” is negatively charged, and vice versa. When the “dee” is positively charged, the negative ions, which are extracted from the ion source using an electric field, are accelerated towards the “dee” by the electric field. Due to the presence of the magnetic field, the charged particles describe a curved trajectory. When the ion leaves the “dee”, the polarity on the “dees”/”counter dees” is reversed, and the ion is accelerated again towards the “counter dee”. The same process is repeated, and the orbit radius becomes larger as the speed of the ion is higher. The ion describes a spiralling outward trajectory towards the border of the magnetic field,

and when the radius is sufficient, the two electrons of the accelerated particle are sequestrated with a carbon foil (named stripper). The accelerated particle becomes positively charged (proton or deuteron, depending on the accelerated particle) and the direction of rotation is inversed. As a result, the accelerated ion escapes from the cyclotron and impacts in one of the targets, which are situated in the periphery of the cyclotron. In the target, a stable material is irradiated with the high energy protons or deuterons to produce the nuclear reaction and generate the radioisotopes.

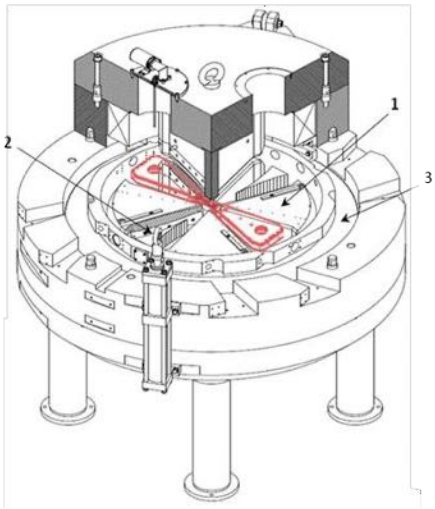

Fig. 1.4: General view of the main body of an IBA Cyclone 18/9 cyclotron. Some parts have been removed from the drawing for clarity. The electrical current in the coils (3) that surround the four wedge-shaped steel sectors (1) creates the magnetic field. "Dees" (highlighted in red) are placed between the steel sectors, and "counter dees" (not shown in the drawing) are placed on the edges of the four steel sectors close to the "dees". For dual particle cyclotrons (acceleration of H^- and D^-), small steel sectors called flaps (2) can be introduced or removed to modulate the magnetic field when particle is changed from H^- to D-. Adapted from the PhD Thesis: Gómez-Vallejo, V., Synthesis of Radiotracers Labeled with Short-Lived Isotopes: Application to ^{11}C and ^{13}N. Universitat Ramon Llull, 09.07.2010.

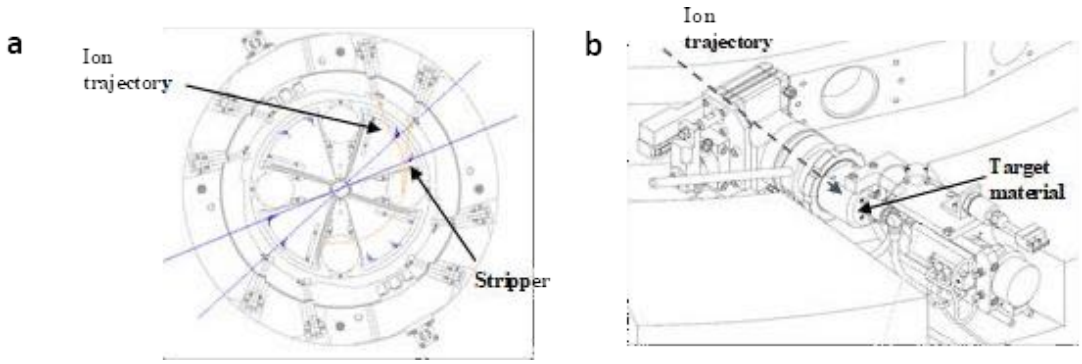

Fig. 1.5: a) Negative ions are accelerated until they hit a stripping foil (stripper), which removes the electrons. The ion charge, now positive, escapes from the cyclotron and hits the selected target; b) disposition of a target in an IBA Cyclone 18/9 cyclotron. Positive ions deflected by the stripper collision with the target material to produce the radioisotope. Adapted from the PhD Thesis: Gómez-Vallejo, V., Synthesis of Radiotracers Labeled with Short-Lived Isotopes: Application to ^{11}C and ^{13}N. Universitat Ramon Llull, 09.07.2010.

1.4.4. PET RADIONUCLIDES – RADIOCHEMISTRY

Radioactive labelling is a chemical reaction in which a radionuclide is incorporated into the desired molecule to produce a radiotracer. There are two main strategies for the incorporation of the radionuclide into a molecule: (I) in the case of small organic molecules, radiolabelling can be achieved by preparing a precursor which enables direct incorporation of the radionuclide by a chemical reaction; and (II) in the case of large molecules such as peptides, proteins, antibodies, polymers or nanoparticles, radiolabelling is usually achieved by attaching a functional group that contains the radioactive atom. Radiochemistry laboratories use "hot cells" (Fig. 1.6b), which are basically lead-shielded versions of a classical chemical hood. The radionuclide is transferred from the cyclotron to the hot cell (Fig. 1.6), where is transformed into the desired radioactive chemical species after a series of reactions. Usually computer-controlled robotic modules are used to minimise exposure to radioactivity by the user.

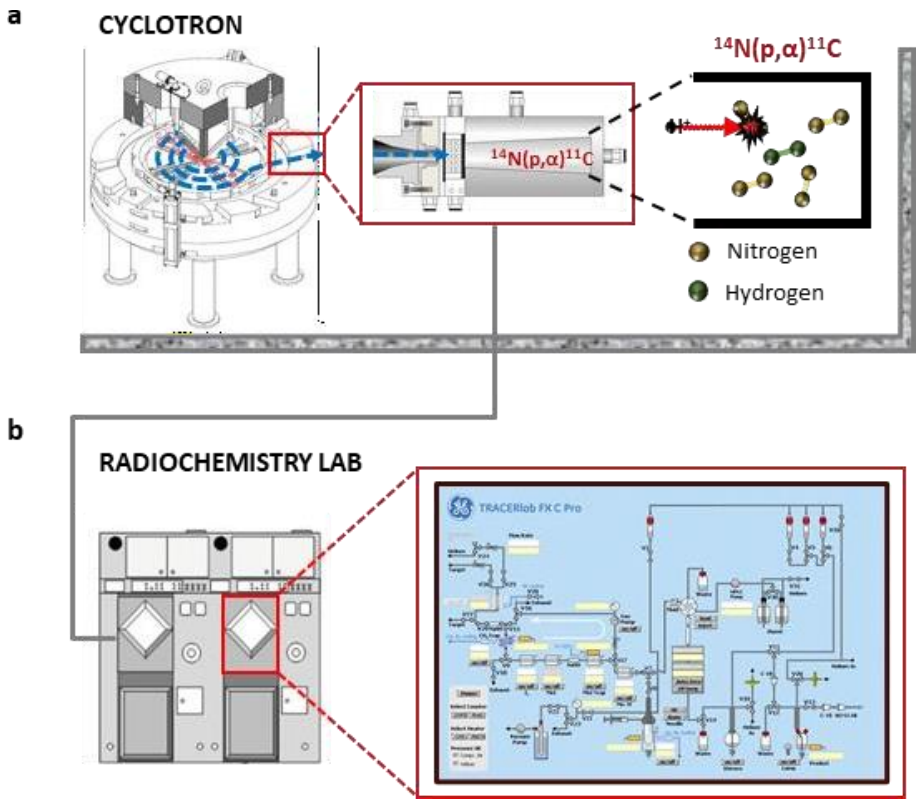

Fig. 1.6: Schematic representation of the radiolabelling process. a) The positron-emitter (carbon-11 in the example) is produced in the cyclotron by proton irradiation of a gas (N_2/H_2 mixture in this case, to generate $[^{11}C]CH_4$). b) The radionuclide is transferred from the cyclotron to "hot-cell" in the radiochemistry laboratory, where it is transformed in the desired chemical specie by computer-controlled chemical reactions.

In radiochemistry, classical chemical reactions are usually employed. However, there are three major considerations that need to be considered: (I) PET radionuclides have a short half-life, and hence the chemical reactions must be fast and efficient; (II) radionuclides emit ionizing radiation. This means that protection equipment (*e.g.* hot cells as described above) has to be used, and all processes need to be automated and conducted using remote-controlled systems to avoid personnel exposure; and (III) only a few labelling agents can be produced in the cyclotron. For example, C-11 can be produced as $[^{11}C]CH_4$ or $[^{11}C]CO_2$. This, ultimately, severely limits the catalogue of chemical reactions that can be applied to produce the radiotracers. In addition, the mass amount of radioactivity that is produced in the cyclotron is extremely low, typically in the order of picomol to nanomol. Hence, the labelling agent is always the limiting reagent. This has an impact on reaction kinetics that will be discussed when appropriate in the following chapters.

Another important consideration is that the reaction yield in radiochemistry (so called radiochemical yield; RCY) is calculated based on the labelling agent. It is generally expressed as a percentage of the amount of radiotracer obtained relative to the initial amount of radionuclide. The value can be decay-corrected to the start of the synthesis process, although in this case it is paramount to provide information regarding the overall production time.

It is important to mention that a radiotracer is always obtained as a mixture of the "labelled" and the "non-labelled" molecule of interest. Because of this, it is critical to determine the Molar activity (MA) or the Specific Activity (SA) of the final radiotracer. The MA is defined as the ratio between the amount of radioactivity and the mass amount of the compound, expressed in mol[14]. The SA responds to the same definition, but the mass amount is expressed in grams. Both MA and SA depend on a variety of factors, including the production process of the radionuclide, the synthesis time, the purity of the non-labelled precursor, etc. After administration to a living system, both the labelled and the non-labelled species have the same biological activity, and hence competition between them may have a negative effect on the concentration of the radioactivity in the target tissue, thus resulting in a low image quality or preventing the visualization of biological or physiological processes. In addition, the lower the SA the higher the mass amount of radiotracer that needs to be injected, with potential pharmacological and/or toxicological effects. A high specific activity should provide a sufficient contrast in images between the target tissue and its surrounding. However, in the case of dosimetry studies, a selective use of different specific radioactivity values can help in finding an optimal value[15]. The molar activity is usually given in units of Bq/mol while the specific activity in units of Bq/g.

As mentioned above, typical cyclotron-generated positron emitters used at the pre-clinical and clinical levels include F-18, C-11, N-13, O-15 and Zr-89. A brief description of the production process of these radionuclides and the chemical reactions used for the preparation of radiotracers is included below.

[14] Gmez-Vallejo, V., Gaja, V., Koziorowski, J., Llop, J. Specific Activity of ^{11}C-Labelled Radiotracers: A Big Challenge for PET Chemists. *Positron Emission Tomography - Current Clinical and Research Aspects.* (2012) doi:10.5772/31491.

[15] Velikyan, I., Beyer, G.J., Bergström-Pettermann, E., Johanse, P., Bergström, M., Langström, B. The importance of high specific radioactivity in the performance of ^{68}Ga-labeled peptide *Nuc. Med. Biol*. (2008) doi: 10.1016/j.nucmedbio.2008.03.002.

Fluorine-18

Fluorine-18 is probably the most widely used positron emitter, especially in clinical applications. Fluorine-18 forms strong covalent bonds with carbon atoms and can be incorporated into a wide variety of organic molecules; moreover, the replacement of a hydrogen atom with a fluorine atom only causes small steric alterations in the molecule. In some particular cases the biological properties of the radiotracer are even improved with respect to the original molecule, as it is the case for 2-[^{18}F]fluoro-2-deoxy-D-glucose ([^{18}F]FDG), a radiotracer used in the clinical-care setting for the diagnosis of certain types of cancer. Fluorine-18 can be generated in biomedical cyclotrons in two chemical forms ([^{18}F]F^- and [^{18}F]F_2) by using different nuclear reactions, although the most commonly used is ^{18}O(p,n)^{18}F. Currently, the production of [^{18}F]F^- is achieved by proton irradiation of ^{18}O-enriched water, while the production of [^{18}F]F_2 is achieved following a 2-step procedure[16]. The most common reaction for the preparation of ^{18}F-labelled radiotracers, uses $^{18}F^-$ as the labelling agent and starts with a nucleophilic substitution reaction using a precursor bearing a good leaving group[17,18]. Fluorine-18 has a reduced positron range and its half-life is relatively long (109.8 min), allowing the synthesis of a wide variety of complex molecules with acceptable radiochemical performance. Its relatively long half-life allows the commercialization of radiotracers as diagnostic tools in clinical. Because of its versatility, a large range of labelling strategies can be found in the literature[19].

Nitrogen-13

The short half-life of Nitrogen-13 (9.97 min) limits its utilization to fast transformations that do not require time-consuming purification and reformulation steps before injection. Nitrogen-13 can be efficiently produced *via* the ^{16}O(p,α)^{13}N nuclear reaction. If pure water is irradiated, the major radioactive species produced is [^{13}N]NO_3^-, which can be reduced to [^{13}N]NO_2^- and further

[16] Roberts, A. D., Oakes, T. R., Nickles, R. J. Development of an improved target for [^{18}F]F_2 production. *Applied radiation and isotopes.* (1995) doi: 10.1016/0969-8043(94)00111-C.

[17] Yu, S. Review of ^{18}F-FDG synthesis and quality control. *Biomed. Imaging Interv. J.* (2006) doi:10.2349/biij.2.4.e57.

[18] Lee, S. J., Oh, S. J., Moon, W. Y., Choi, M. S., Kim, J. S., Chi, D. Y., Moon, D. Y., Ryu, J. S. New automated synthesis of [^{18}F]FP-CIT with base amount control affording high and stable radiochemical yield: a 1.5-year production report. *Nucl. Med. Biol.* (2011) doi:10.1016/j.nucmedbio.2010.11.012.

[19] Nerella, S. G., Raman, K. J., Rose, D., B., Pardeep, K. Fluorine-18: A radionuclide with diverse range of radiochemistry and synthesis strategies for target based PET diagnosis. *Eur. J. Med. Chem.* (2020) doi:10.1016/j.ejmech.2019.111979.

incorporated into organic molecules[20, 21]. By using 5 mM ethanol in water as the irradiated material, [^{13}N]ammonia is produced as the major species, which can directly be used as very effective perfusion marker[22] or further incorporated into organic molecules. Despite its use has been poorly explored compared to other positron emitters, different production methods for the preparation of nitrogen-13 labelled compounds have been reported[23].

Oxygen-15

Oxygen-15 is the shortest-lived positron emitting isotopes of oxygen. Because of its short half-life (2 min) it does not have many applications and is mainly used directly as produced (inhaled) or to produce [^{15}O]H_2O. Despite several nuclear reactions can be used for the production of oxygen-15, the most commonly used reaction is ^{14}N(d,n)^{15}O. In this case, N_2/O_2 mixtures are irradiated with high energy protons [24] . When these mixtures of nitrogen and oxygen are irradiated with high energy protons, nitrogen oxides can be produced directly, but [^{15}O]O_2 is the most abundant specie. Further reaction with hydrogen under catalytic conditions (e.g., palladium) yields [^{15}O]H_2O, a blood flow marker[25].

Zirconium-89

Zirconium-89 (^{89}Zr) is a positron emitter (23% positron branching) with a relatively long half-life (78.4 hours). It can be effectively obtained by irradiation of natural yttrium foils with protons *via* the ^{89}Y(p,n)^{89}Zr reaction followed by purification in a functionalized hydroxamate column[26]. The

[20] Joishi, S. M., Gómez-Vallejo, V., Salinas, V., Llop, J. Synthesis of ^{13}N-labelled polysubstituted triazoles: Via Huisgen cycloaddition. *RSC Advances.* (2016) doi: 10.1039/C6RA24670B.

[21] Joishi, S. M., de Cozar, A., Gómez-Vallejo, V., Koziorowski, J., Llop, J., Cossío, F. P. Synthesis of radiolabelled aryl azides from diazonium salts: experimental and computational results permit the identification of the preferred mechanism. *Chem Commun.* (2015) doi: 10.1039/C5CC01913C.

[22] Martín, A., San Sebastián, E., Gómez-Vallejo, V., Llop, J. Positron emission tomography with [^{13}N]ammonia evidences long-term cerebral hyperperfusion after 2h-transientfocal ischemia. *Neuroscience.* (2012) doi: 10.1016/j.neuroscience.2012.03.050.

[23] Gómez-Vallejo, V., Gaja, V., Gona, K. B., Llop, J. Nitrogen-13: historical review and future perspectives. *J. Label. Compd. Radiopharm.* (2014) doi:10.1002/jlcr.3163.

[24] Clark, J. C., Crouzel, C., Meyer, G. J., & Strijckmans, K. Current methodology for oxygen-15 production for clinical use. *Int. J. Rad. Appl. Instrum.* (1987) doi:10.1016/0883-2889(87)90122-5.

[25] Weber, B., Westera, G., Treyer, V., Burger, C., Khan, N., Buck, A. Constant-Infusion $H_2{}^{15}O$ PET and Acetazolamide Challenge in the Assessment of Cerebral Perfusion Status. *J. Nucl. Med.* (2004).

[26] Fadeeva, V. I., Tikhomirova, T. I., Yuferova, I. B., Kudryavtsev, G. V. Preparation, properties and analytical application of silica with chemically grafted hydroxamic acid groups. *Analytica Chimica Acta.* (1989) doi:10.1016/S0003-2670(00)80351-7.

most common reaction for the radiolabelling with Zr-89 is the formation of a chelator-radiometal complex of protein scaffold such as antibodies[27].

Carbon-11

Carbon-11 can be considered an ideal radionuclide. Since all organic molecules contain carbon atoms in their structure, C-11 constitutes an opportunity to produce a labelled molecule with the same chemical structure as the compound under evaluation. However, due to its short half-life (20.4 min), transport from manufacturing centres to surrounding hospitals is not possible, thus limiting its application to centres with a cyclotron on site. Carbon-11 can be efficiently produced via the $^{14}N(p,\alpha)^{11}C$ nuclear reaction using nitrogen gas as the irradiated material. By introducing a small amount of hydrogen or oxygen in the target gas, $[^{11}C]CH_4$ or $[^{11}C]CO_2$ can be obtained, respectively[28]. These primary radioactive precursors can be directly used for the preparation of ^{11}C-labelled radiotracers. For example, 1-^{11}C-carboxylic acids can be prepared via Grignard type reactions starting from $[^{11}C]CO_2$ [29]. However, both $[^{11}C]CH_4$ and $[^{11}C]CO_2$ are typically converted into other radioactive precursors better suited to undergo subsequent reactions efficiently (Scheme 1.1). $[^{11}C]CO$ is an attractive radioactive precursor. Cyclotron produced $[^{11}C]CO_2$ can be easily converted into $[^{11}C]CO$ by reduction over zinc or molybdenum[30]. Despite the high efficiency of this conversion, the use of $[^{11}C]CO$ in radiochemistry has been hampered by the difficulties associated with its trapping at atmospheric pressure. Additionally, treatment of $[^{11}C]CO$ with chloride results in the formation of [^{11}C]phosgene that also acts as a good source of electrophilic $[^{11}C]CO$ moiety, which is sometimes a preferred option due to a less problematic trapping[31].

By far the most commonly used secondary radioactive precursor is $[^{11}C]CH_3I$, which can undergo nucleophilic substitution reactions with amines, amides, alcohols or thiols to yield the

[27] van de Watering, F. C. J., Rijpkema, M., Perk, L., Brinkmann, U., Oyen, W. J. G., Boerman, O. C., Zirconium-89 Labeled Antibodies: A New Tool for Molecular Imaging in Cancer Patients. *Biomed. Res. Int.* (2014) doi: 10.1155/2014/203601.

[28] Christman, D. R., Finn, R. D., Karlstrom, K. I., Wolf, A. P. The production of ultra high activity ^{11}C-labeled hydrogen cyanide, carbon dioxide, carbon monoxide and methane via the $^{14}N(p,\alpha)^{11}C$ reaction (XV). *The International Journal of Applied Radiation and Isotopes.* (1975) doi: 10.1016/0020-708X(75)90057-5.

[29] Le Bars, D., Malleval, M., Bonnefoi, F., Tourvieille, C., Simple synthesis of [1-^{11}C]acetate. *Journal of Labelled Compounds and Radiopharmaceuticals.* (2006) doi: 10.1002/jlcr.1024.

[30] Zeisler, S. K., Nader, M., Theobald, A., Oberdorfer, F. Conversion of No-carrier-added [^{11}C]carbon dioxide to [^{11}C]carbon monoxide on molybdenum for the synthesis of ^{11}C-labelled aromatic ketones. *Applied Radiation and Isotopes.* (1997) doi: 10.1016/S0969-8043(97)00109-7.

[31] Fukumura, T., Mori, W., Ogawa, M., Fujinaga, M., & Zhang, M.-R. [^{11}C]phosgene: Synthesis and application for development of PET radiotracers. *Nucl. Med. Biol.* (2020) doi:10.1016/j.nucmedbio.2020.04.007.

corresponding [^{11}C]methylated derivatives. As an alternative the [^{11}C]CH_3OTf can be used as labelling agent when the methylation reaction is slow [32] . In this PhD thesis, the carbon-11 methylation using [^{11}C]CH_3I as radiolabelled agent has been the strategy of choice to run nuclephilic substitution reactions on primary alcohols, carcoxylic acid and amine groups (see Chapter 3).

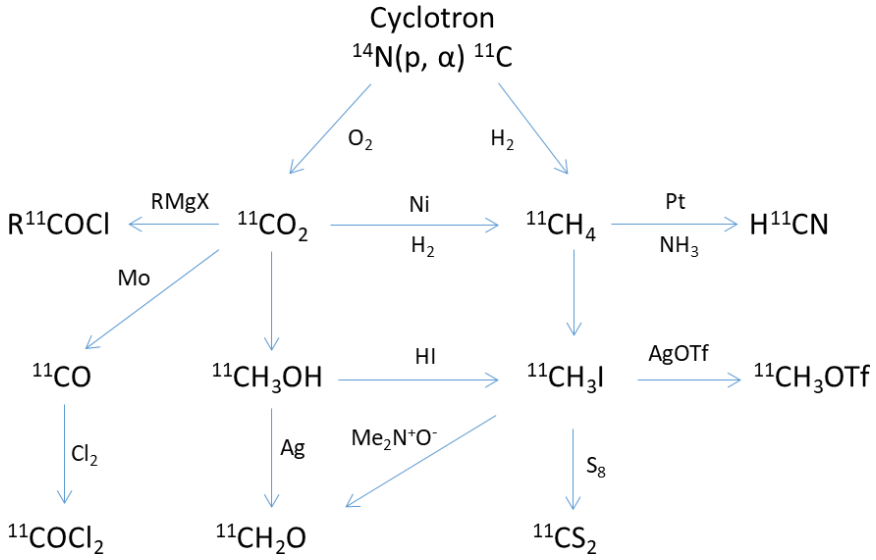

Scheme 1.1: Most important ^{11}C precursors used in the synthesis of ^{11}C-labelled compounds produced from either [^{11}C]CO_2 or [^{11}C]CH_4.

1.5 CRITICAL PARAMETERS IN SMALL ANIMAL PET SCANNERS

The extensive use of PET technique in pre-clinical research has increased the need for the development of sophisticated small animal scanners. In small animal PET, resolution and sensitivity are critical. Due to the low body weight of small animals, the amount of radioactivity that can be injected is low. Therefore, the number of events to be detected is significantly lower than those detected in human scans, thus compromising the sensitivity. In addition, the size of the animal is much smaller than a human subject, especially in the case of small rodents. As a consequence, improved spatial resolution is required.

The most commonly used PET detector consists of an array of scintillation crystals optically coupled to several photomultipliers (Fig. 1.7). The incident high-energy photons interact with the

[32] Jewett, D. M., A simple synthesis of [^{11}C]methyl triflate. *International journal of radiation applications and instrumentation. Part A, Applied radiation and isotopes.* (1992) doi: 10.1016/0883-2889(92)90012-4.

scintillation crystal removing electrons from the valence band. These electrons return to the stationary phase dissipating energy in the form of light, that is finally amplified by a photon-sensitive photomultiplier.

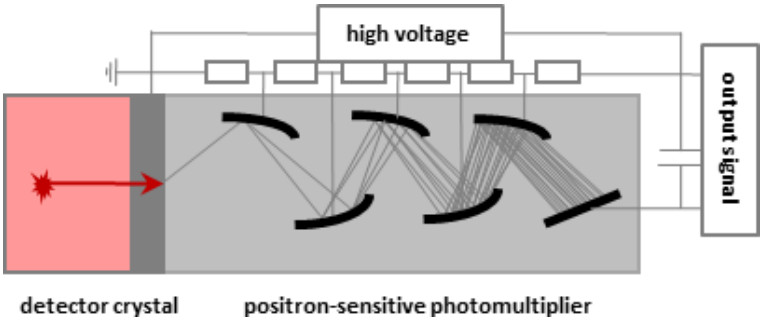

Fig 1.7: Detector system of a PET scanner: Scintillation crystals are optically coupled to several photomultiplier. The photon emitted from annihilation hit the crystal, exciting an electron from the valence band. The electron returns to the valence band dissipating energy as light photon. The signal is then amplified by the photon-sensitive photomultiplier.

The spatial resolution of PET is generally determined by the crystal size and the diameter of the ring of detectors of the scanner, as well as by physical parameters such as the positron range, the non-linearity of the annihilation photons and parallax error[33]. These effects, illustrated in Fig. 1.8, result in a limitation of the detectability and quantification of small regions in a PET image, especially for animal scanners. For clinical scanners the positron range is significantly smaller than the spatial resolution determined by the geometry of the scanner. However, for animal scanners this factor may become relevant. Currently, small animal PET scanners can achieve resolution close to 0.8 mm in the centre of the field of view,[34] while resolution of clinical scanners is *ca.* 3mm.

[33] Levin, C. S., & Hoffman, E. J. Calculation of positron range and its effect on the fundamental limit of positron emission tomography system spatial resolution. *Physics in Medicine and Biology* (1999) doi:10.1088/0031-9155/44/3/019.
[34] Moses, W. W. Fundamental limits of spatial resolution in PET. *Nucl. Instrum. Methods Phys. Res*. (2011) doi:10.1016/j.nima.2010.11.092.

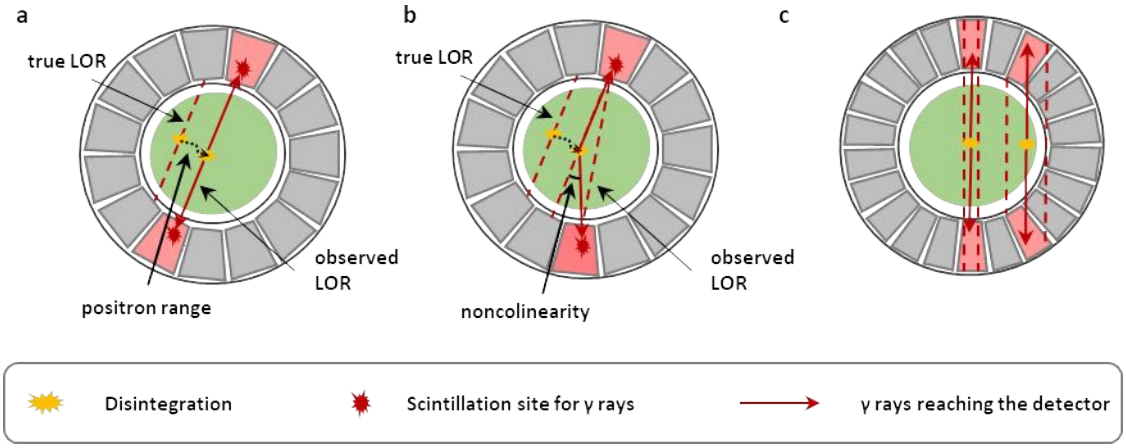

Fig. 1.8: Schematic representation of the physical parameters that limit the spatial resolution. a) The positron travels a certain distance before annihilation depending on the kinetic energy of the positron and the density of the material it travels through. b) Because positrons are emitted with a range of energy, small deviation from collinearity in the two annihilation photons occurs as a result of the residual kinetic energy. c) The parallax error is an effect due to the fact that it is not know where in the crystal element the interaction occurred.

High-resolution results to be important to quantify the concentration of radioactivity in small structures. If the resolution is not high enough, the quantification of radioactivity in these small regions might be subjected to error due to spillover and/or partial volume effects. The latter is especially important if the size of the object is less than twice the spatial resolution of the system[35]. The spillover effect is defined as the spill-in of radioactivity into volume of interest (VOI) from surrounding high-activity regions, leading to overestimation of radiotracer uptake; while the partial volume effect is defined as the spill-out of radioactivity into surrounding tissue from a high activity region, leading to underestimation of tracer uptake (Fig. 1.9). To overcome these limitations different correction methods such as software and mathematical tools are available[36, 37].

[35] Hoffman, E. J., Huang, S. C., Phetps, M. E., Quantitation in positron emission tomography: 1. Effect of object size. *J. Comput. Assist. Tomogr*. (1979) doi:10.1097/00004728-197906000-00001.

[36] Van der Weerdt, A. P., Kelin, L. J., Boellaard, R. *et al.* Image-derived input functions for determination of MRGlu in cardiac ^{18}F-FDG PET scans. *J. Nucl. Med.* (2001).

[37] Patlak, C. S., Blasberg, R. G., & Fenstermacher, J. D. Graphical Evaluation of Blood-to-Brain Transfer Constants from Multiple-Time Uptake Data. *Journal of Cerebral Blood Flow & Metabolism*. (1983) doi:10.1038/jcbfm.1983.1.

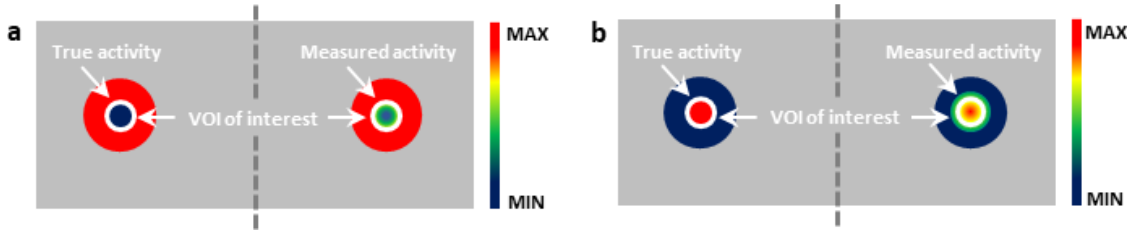

Fig. 1.9: a) Spillover effect: If the surrounding area has higher radioactivity concentration, a spill-in into VOI occurs, leading to overestimation of radiotracer uptake. b) Partial volume (Spill out) effect: If the surrounding area has lower radioactivity concentration than the area of interest, the spill-out leads to underestimation of radiotracer uptake.

The sensitivity, defined as the fraction of events effectively detected as a coincidence, is the second important factor to be considered. Minimizing the crystal size in the axial and transaxial directions can improve the spatial resolution, while increasing the length can improve the sensitivity of the scanner, as the probability of the incident photon to interact with the crystal increases. However, reducing the dimension of the detector crystals can cause an insufficient statistics for the reconstruction if the scan time is short and/or the amount of radioactivity is low. While with increasing crystal length parallax errors will be larger, resulting in the degradation of spatial resolution outside the centre of the field of view (FOV)[38]. Thus, designing a PET scanner is always a compromise between spatial resolution and sensitivity.

Besides the factors just discussed, there are a few others that could limit the quality of PET images and which need to be corrected in order to obtain accurate quantitative images. These are the presence of scattered and random coincidences, the attenuation effect and the dead time of the detector (Fig. 1.10).

Scattered coincidence: The 511 keV photons can interact with tissue through Compton scattering, through an interaction with electrons in the outer-shell of tissue atoms. This leads both to change the photon direction and energy loss. The probability that the emitted photons will be scattered depends on the density and thickness of the object and the scanner geometry. Detection of one or both photons following a scattering event results in events assigned to a wrong LOR, which results in a low contrast image and incorrect quantification. Since energy is lost during the

[38] St James, S., Yang, Y., Bowen, S. L., Qi, J., & Cherry, S. R. Simulation study of spatial resolution and sensitivity for the tapered depth of interaction PET detectors for small animal imaging. *Physics in Medicine and Biology*. (2009) doi:10.1088/0031-9155/55/2/n04.

Compton interaction, an energy threshold allows rejection of a significant amount (typically 90%) of the scattered events, improving the scatter correction.

Random coincidence: A further consequence of Compton scattering is accidental coincidence. If two single events are detected within the same coincidence-timing window, they are detected as a pair, defining the site of annihilation on the corresponding LOR. The number of random events can be reduced by using smaller coincidence windows; however, the reduction of this window is limited by the temporal resolution of the detectors and, ultimately, by the time it takes a photon to travel through the FOV.

Attenuation: It is the loss of counts when one or more photons do not reach the detector because of their absorption in the body. The probability of absorption results to be less in the body surface and soft tissue, and higher deep in the body and in dense tissue, leading to severe artefacts in PET image. Attenuation in PET image data scanned with PET-CT scanners is corrected using data from CT (computed tomography)[39].

Dead time: It is defined as the time after a detection that a detector in unable to process a new event. Any event that hits the detector during this time cannot be processed, and can even cause the exclusion of the previous detected event if the upper limit of the energy window is exceeded due to the pulse amplitude. The effect is more important as the activity in the FOV increases.

Data from PET cameras are obtained as sinograms that are reconstructed into tomographic images after correction for attenuation, scattered and random coincidences and detector efficiency by using different methods that have been developed over time[40].

[39] Kinahan, P. E., Townsend, D. W., Beyer, T. & Sashin, D. Attenuation correction for a combined 3D PET/CT scanner. *Medical Physics* (1998) doi:10.1118/1.598392.

[40] Lewitt, R. M. & Matej, S. Overview of methods for image reconstruction from projections in emission computed tomography. *Proceedings of the IEE* (2003) doi:10.1109/jproc.2003.817882.

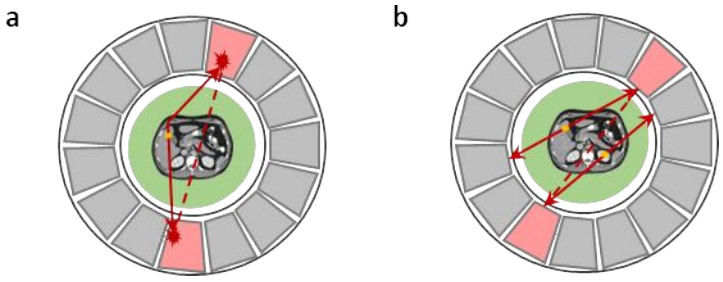

Fig. 1.10: Phenomena that degrade the quality of PET images. a) Scatter coincidences: as a result of interaction with outer-shell electrons of the atoms of the tissue, the photon changes its direction and loses part of its energy resulting in the possibility of a wrong assignment of the line of response (LOR). b) Random coincidences: two single events are recorded as a pair if detected within the same coincidence-time window, defining the site of annihilation on the corresponding LOR connecting the two hit detectors.

1.6 What is the role of Positron Emission Tomography in Drug Development?

Since its introduction in the early nineties as a promising functional imaging technique, PET has become an important tool especially in several oncologic procedures such as tumour staging, evaluation of treatment efficacy and radiotherapy planning. 2-deoxy-2-(^{18}F)fluoro-D-glucose ([^{18}F]FDG), a glucose analogue, is probably the most widely used tracer for PET imaging in oncology, and has been extensively evaluated and established in clinical routine. Besides the classical and widely exploited application in oncology, PET has emerged as an important tool in the early stages of drug development [41] . This technology, along with the array of diverse radioligands, can be used to address several questions of drug development, including:

- Does the drug reach the desired target? (Proof of Target, POT)
- Is a downstream component of the biochemical pathway affected? (Proof of Mechanism, POM)
- Does the drug have any effect? (Proof of efficacy, POE)

The answer to these questions is possible because in PET, and in general in any molecular imaging, biomarkers (which interact with the surrounding, being the resulting image a representation of the molecular changes taking place) are used. According to FDA, biomarker is a defined characteristic that is measured as an indicator of normal biological processes,

[41] Matthews, P. M., Rabiner, E. A., Passchier, J., & Gunn, R. N. Positron emission tomography molecular imaging for drug development. *British Journal of Clinical Pharmacology* (2012) doi:10.1111/j.1365-2125.2011.04085.x.

pathogenic processes or responses to an exposure or intervention[42]. The use of biomarkers as biological indicators for progress of disease, effect of therapeutic interventions and/or drug induced toxicity has exponentially increased due to the high costs incurred when drugs fail during clinical trials[43]. Its role in fact results to be fundamental in guiding decision in every phase of drug development, from drug discovery and preclinical evaluation through each phase of clinical trials and into post-marketing studies. In early phase of drug development, PET plays an important role in providing information around the distribution of a drug and the ability of compounds to reach the target (POT). One of the most valuable contributions of PET-based target biomarkers is to provide sufficient data to stop a research program early. By confirming that a molecule does not reach its target in sufficient concentrations to likely have a therapeutic effect, an alternative chemical can be identified and further developed. Instead, if the interaction of the drug with its target is demonstrated, PET can be used to assess activity in animal models, demonstrate the mechanism of action of an investigational entity (POM) and the safety of compounds. Finally, in the late stages of drug development, PET can be used for the evaluation of desired pharmacological effect (POE).

Another application of PET in drug development that is not adequately identified in this biomarker paradigm, is the information obtained from the simple radiolabelling the drug candidate itself. Administering a radiolabelled candidate allows the evaluation of the pharmacokinetic information about the compound itself. The way in which the body absorbs, distributes, metabolizes, and eliminates (ADME) the drug is one of the factors that makes a drug successful, and PET can facilitate a "smarter" identification of the molecule with the optimum ADME characteristics[44,45,46]. Due to the radioactive properties of radiopharmaceuticals, discussed in the previous section, these agents offer a unique opportunity to observe their pharmacokinetics characteristics in animals and/or humans. As can be easily understood, in

[42] FDA-NIH Biomarker Working Group. BEST (Biomarkers, EndpointS, and other Tools) Resource. Silver Spring (MD): Food and Drug Administration (US); Bethesda (MD): National Institutes of Health (US).

[43] Kraus, V. B. Biomarkers as drug development tools: discovery, validation, qualification and use. *Nature Reviews Rheumatology*. (2018) doi:10.1038/s41584-018-0005-9.

[44] Aboagye EO, Price PM, Jones T. *In vivo* pharmacokinetics and pharmacodynamics in drug development using positron-emission tomography. *Drug Discov. Today.* (2001) doi:10.1016/s1359-6446(01)01684-1.

[45] Prentis, R. A., Lis, Y. & Walker, S. R. Pharmaceutical innovation by the seven UK-owned pharmaceutical companies (1964–1985). *Br. J. Clin. Pharmacol*. (1988) doi:10.1111/j.1365-2125.1988.tb03318.x.

[46] Lappin, G., Garner, R. C. Big physics, small doses: the use of AMS and PET in human microdosing of development drugs. *Nat Rev Drug Discov.* (2003) doi:10.1038/nrd1037.

early-phase drug development, a biodistribution study is very important to confirm that the drug molecule reaches the target tissue and does not accumulate in non-target sites, resulting in potential toxicity. For this purpose, dynamic PET imaging can provide information regarding the concentration-time course of the radiotracer within the organism. Moreover, by measuring the concentration of the radiolabelled drug in the blood it is possible to use bio mathematical kinetic models to derive estimates of the rate of drug clearance from plasma to tissue as well as the ratio of the concentration of the labelled drug and drug metabolites in tissue to blood. Analysis of the blood samples by HPLC, equipped with radioactivity detector, provides additional information on any metabolism of the radiolabelled drug. It is necessary to keep in mind that the PET image represents the distribution of the radionuclide, not to the actual drug. Therefore, if the radiolabelling is not stable, or if the drug decomposes *in vivo*, the visible PET image is due to the fragment which contains the radionuclide and misinterpretation of the obtained image is possible. Because of this, the determination of metabolism is paramount for proper image interpretation.

In this PhD thesis, PET and complementary imaging techniques have been widely used for the preclinical pharmacokinetic evaluation of new drugs with potential application in Duchenne muscular dystrophy. The short-lived positron emitter carbon-11 has been used for the radiolabelling of the new drugs under investigation.

CHAPTER 2: MOTIVATION AND OBJECTIVES OF THE THESIS

2.1 JUSTIFICATION OF THE STUDY: THE PET3D PROJECT

At early stages of the process of drug development, there are certain questions that need to be answered, *e.g.*: 'Where is the drug accumulated?', 'How long does it stay in the body?', 'How is it eliminated?'. Positron Emission Tomography (PET) can be used to address all these questions, accelerating the whole process by identifying poor candidates at early stage in the drug development process.

The PET3D project [1] (PET imaging in Drug Design and Development) originated out of this statement. It is a MSCA-ITN (Marie Skłodowska-Curie Actions - Innovative Training Network), funded by the European Commission under the H2020 – MSCA-ITN-2015 program (grant agreement No. 675417) for a duration of 4 years (June 2016 – May 2020). The aim of the project was to train 15 early-stage researchers (ESR), located at 8 different institutions in Europe, to become experts in PET imaging and drug development. The institutions involved were the University of Aberdeen (with Professor Matteo Zanda as project coordinator, later in Loughborough University), the VUmc Amsterdam (now UMC), the Vrije Universiteit Brussel, the University of Bergen, CIC biomaGUNE in Donostia-San Sebastián (host of this PhD), the European Institute for Molecular Imaging in Münster; and two industrial partners, Imanova (now Invicro; UK) in London and AstraZeneca in Mölndal (Sweden). Covering the main diagnostic/therapeutic areas in which PET is used (oncology, cardiovascular and central nervous system) PET3D was coordinated in five research work packages (WP) (see Fig. 2.1).

[1] Pet 3D | PET imaging in Drug Design & Development (pet3dproject.com).

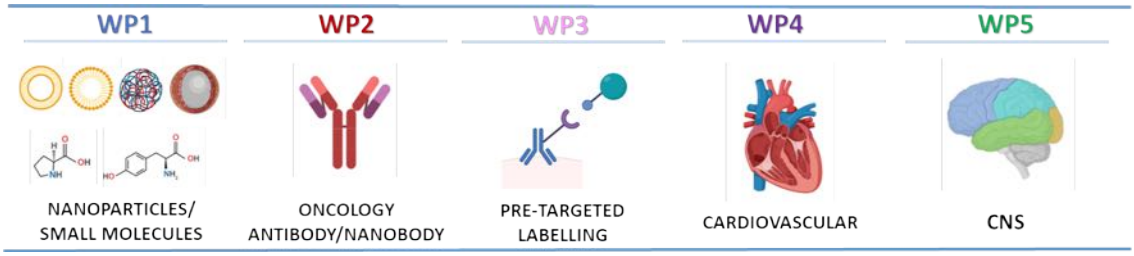

Fig. 2.1: Research work packages of the European project PET3D: WP1: 'Nanoparticles and Small Molecule Tracers in Oncology PET Imaging'; WP 2: 'Biologicals as Tracers in Oncology PET Imaging'; WP 3: 'Pre-targeted Labelling of Biomolecules in Oncology PET Imaging'; WP 4: 'Cardiovascular PET Imaging'; WP 5: 'CNS PET Imaging'.

The work included in this PhD, titled "Pharmacokinetics evaluation of new drugs with potential application in Duchenne muscular dystrophy using Positron Emission Tomography and complementary techniques" was carried out in the frame of WP1, 'Nanoparticles and Small Molecule Tracers in Oncology PET Imaging', and in close collaboration with the Organic Chemistry-I department at UPV/EHU-University of the Basque Country (Prof. Jesús Maria Aizpurua) and Biodonostia Health Research Institute (IIS Biodonostia; Dr. Ainara Vallejo).

Taking advantages of the expertise of the Radiochemistry and Nuclear Imaging Group at CIC biomaGUNE, led by Dr. Llop in developing strategies to radiolabel small molecules, characterize their pharmacokinetic properties, and evaluate their suitability as therapeutic and/or diagnostic agents[2, 3], in this PhD thesis an exhaustive investigation of the pharmacokinetics properties of two drug candidates with potential application in Duchenne muscular dystrophy and developed by UPV/EHU and IIS Biodonostia was carried out using PET imaging and complementary techniques. The selection of the two drug candidates was made based on previous works carried out by our collaborators.

[2] Rejc, L., Gómez-Vallejo, V., Joya, A., Moreno, O., Egimendia, A., Castellnou, P., Ríos-Anglada, X., Cossío, U., Baz, Z., Passannante, R., Tobalina-Larrea, I., Ramos-Cabrer, P., Giralt, A., Sastre, M., Capetillo-Zarate, E., Košak, U., Knez, D., Gobec, S., Marder, M., Martin, A., Llop, J. Longitudinal evaluation of a novel BChE PET tracer as an early *in vivo* biomarker in the brain of a mouse model for Alzheimer disease. *Theranostics* (2021) doi: 10.7150/thno.54589.

[3] Zanda, M., Colombano, A., Dall'Angelo, S., Kingston, L., Grönberg, G., Correia, C., Passannante, R., Baz, Z., Llop, J. 4,4,16-Trifluoropalmitate: design, synthesis, tritiation, radiofluorination and pre-clinical PET imaging studies on myocardial fatty acid oxidation. *ChemMedChem* (2020) doi:10.1002/cmdc.202000610.

CHAPTER 2. MOTIVATION AND OBJECTIVES OF THE THESIS

The work carried out in the context of this PhD thesis has been divided in three main blocks, which constitute the three experimental chapters (chapters 3-5).

In the first part (chapter 3), synthe2c strategies for the incorpora2on of two radioac2ve isotopes, carbon-11 ($_{11}$C), in different posi2ons of the two drug candidates were developed, to enable subsequent *in vitro* and *in vivo* investigation. The work related to $_{11}$C was carried out in the Radiochemistry and Nuclear Imaging Laboratory at CIC biomaGUNE, while the radiolabelling with the beta emitter was carried out in the Early Chemical Development, Pharmaceu2cal Sciences R&D at AstraZeneca, under the supervision of Prof. Chad Elmore. This multi-radionuclide/multi-position labelling approach was expected to provide informa2on about the metabolic rate, together with basic informa2on about the chemical structure of the metabolites both *in vitro* and *in vivo*.

In the second part (chapter 4), different approaches for the determination of the concentration of the non-metabolized compound in arterial plasma, also called input function (IF), which represents the gold standard for a quantitative PET data analysis, were evaluated. Among the different options, we selected the determination of the image-derived input function (IDIF) and the real time measurement of IF, in order to compare them in terms of: (I) simplicity; and (II) accuracy. For the online (real time) measurement of IF we used an in-house developed monitoring system and a procedure implemented by our group[4].

In the third part (chapter 5), we tackled an exhaustive evaluation of the ADME (Absorption, Distribution, Metabolism and Excretion) processes of the new drug candidates. For the study, the radiolabelled drug candidates were administered in experimental rodents using three different routes (intravenous and oral) and two different doses, 1 µg/kg and 5 mg/Kg . To get information about biodistribution, PET imaging studies were carried out, while arterial catheterizaHon and online blood sample sampling enabled the calculation of the most important pharmacokinetics parameters such as volume of distribution (V_d), plasma clearance (Cl), elimination half-life ($t_{1/2}$), area under the curve (AUC), mean residence Hme (MRT) and bioavailability (F).

[4] Guarra, F., Terenzi, A., Pirker, C., Passannante, R., Baier, D., Zangrando, E., Gómez-Vallejo, V., Biver, T., Gabbiani, C., Berger, W., Llop, J., Salassa, L. 124 I Radiolabeling of a Au III -NHC Complex for In Vivo Biodistribution Studies. *Angew. Chem.* (2020) doi:10.1002/ange.202008046.

2.2 OBJECTIVES

The specific objectives of this PhD thesis are:

1. To develop strategies for the radiolabelling of two triazole-based FKBP12-Ryr stabilizers, AHK-1 and AHK-2, and evaluate their metabolism *in vitro*.
2. To compare two different methods to calculate the input function, in terms of: (I) simplicity; and (II) accuracy.
3. To determine the metabolite-corrected arterial plasma Time Activity Curves (TACs) of the ^{11}C-labelled triazole-based FKBP12-Ryr stabilizers AHK-1 and AHK-2 after intravenous and oral administration.
4. To evaluate biodistribution and pharmacokinetics parameters of the triazole-based FKBP12-Ryr stabilizers AHK-1 and AHK-2 after intravenous and oral administration using positron emission tomography.

CHAPTER 3: RADIOLABELLING AND PRECLINICAL *IN VITRO* METABOLISM EVALUATION OF TRIAZOLE-BASED FKBP12-RYR STABILIZERS

3.1 INTRODUCTION

The criteria for the acceptance of new drugs for pharmacological use in humans have become more stringent over years. Before any drug can be accepted and used clinically, knowledge of its metabolism is commonly required by national licensing authorities. Information as to whether a drug is metabolized slowly or rapidly, can furnish a rational basis for establishing dosage schedules needed for initial clinical evaluation. Beside the significant progress achieved in the different steps of the long process of drug development, the percentage of potential drugs that fail due to an inappropriate drug metabolism is up to 40%[1]. To increase the effectiveness of the entire process, identifying poor candidates at early stages is paramount. As radiolabelling is a useful strategy in this context, a wide range of examples reporting the use of radioactive labelled compounds for the evaluation of pharmacokinetic parameters can be found in the literature[2]. Radioactive labelled compounds, particularly those labelled with carbon-14 play an increasing role in pharmacological research[3].

Tritium is one of the three isotopes of hydrogen, and it is radioactive. When an atom of tritium decays, one of its neutrons turns into a proton, and an electron (also called a beta-particle) and a neutrino are emitted (Fig. 3.1a). The β-radiation is emitted with a low energy of about 5.700 KeV. Thus, the energy of this β-particle has a low range of penetration into the matter, reaching a maximum of about 6 mm in air. Because of the low range of penetration, different methods of detection have been implemented. One of them is the liquid β-scintillation measurement. The principle of the method is the conversion of the β-radiation energy into photoelectrons producing charge pulses, which can be amplified and counted. The scintillation process consists of the following steps: (I) the β-energy is transferred to a solute molecule as energy of ionization,

[1] Lappin, G., Garner, R. C., Big physics, small doses: the use of AMS and PET in human microdosing of development drugs. *Nature Reviews Drug Discovery,* (2003) doi:10.1038/nrd1037.

[2] Uhl, P., Fricker, G., Haberkorn, U., Mier, W. Radionuclides in drug development. *Drug Discovery Today,* (2015) doi:10.1016/j.drudis.2014.09.027.

[3] Isin, E. M., Elmore, C. S., Nilsson, G. N., Thompson, R. A. & Weidolf, L. Use of Radiolabeled Compounds in Drug Metabolism and Pharmacokinetic Studies*. Chemical Research in Toxicology,* (2012) doi:10.1021/tx2005212.

dissociation or excitation; (II) the energy of the solute molecule is transferred to a molecule of a primary solute which is a fluorescent compound; and (III) light in the visible or near ultraviolet region are emitted (Fig. 3.1b).

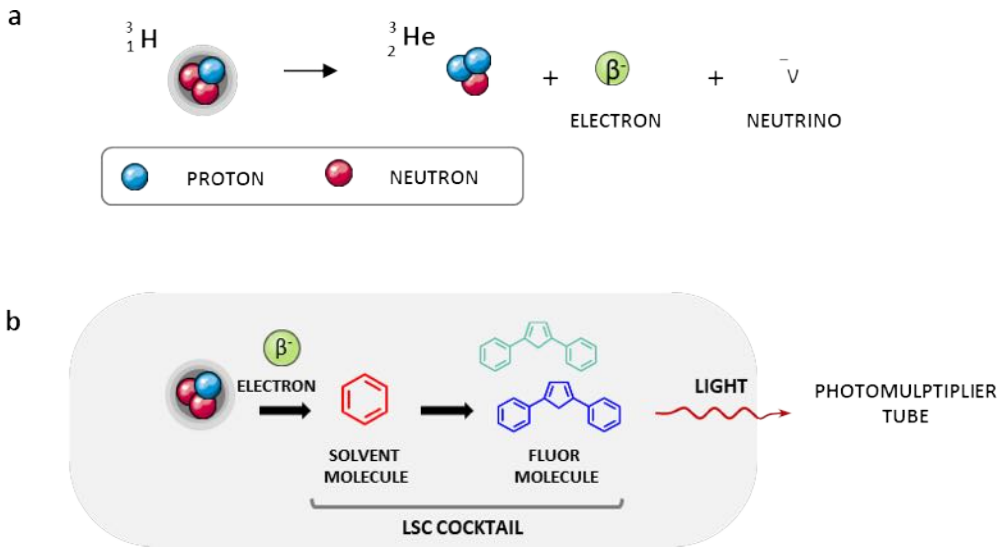

Fig. 3.1: a) Schematic representation of tritium decay. Spontaneous radioactive decay of beta emitters (tritium converted into helium in the example) produces the emission of a beta-particle and a neutrino. b) Schematic representation of liquid β-scintillation measurement. The β-energy is initially transferred to a solute molecule (aromatic molecule), and then to a fluorescent compound in a process called quenching. A quantum of light in the visible or near ultraviolet region is finally emitted and amplified by a photon-sensitive photomultiplier.

Tritium has certain unique advantages. It is one of the least expensive radioisotopes, the half-life of 12.35 years is conveniently long, and the low energy of the β^- particles makes tritium an ideal isotope for use in high-resolution autoradiographic applications[4]. There are, however, important unfavourable properties that need to be considered. Tritium labelling results in just moderately high specific activities since tritium sources are contaminated with non-radioactive hydrogen. Moreover, depending on the stability of the label, hydrogen exchange[5] with water and

[4] Klein, A. B., Bay, T., Villumsen, I. S., Falk-Petersen, C. B., Marek, A., Frølund, B., Clausen, R. P., Hansen, H. D., Knudsen, G. M., Wellendorph, P. Autoradiographic imaging and quantification of the high-affinity GHB binding sites in rodent brain using ^{3}H-HOCPCA. *Neurochemistry International* (2016) doi:10.1016/j.neuint.2016.09.002.

[5] Gold, V. & Satchell, D. P. N. The principles of hydrogen isotope exchange reactions in solution. *Quarterly Reviews, Chemical Society* (1955) doi:10.1039/qr9550900051.

decomposition by self-irradiation can occur [6] . Nonetheless, tritium-labelled analogues are considered as highly convenient to determine binding selectivity, kinetics and metabolic stability as, for practical reasons, this type of experiments requires the use of long-lived isotopes that do not alter the original structure of the molecule under investigation.

In the recent years, as widely described in the previous chapter, PET has emerged as a useful technique to accelerate the whole process of drug development, allowing the quantification of the amount of labelled species at *in vitro*/*in vivo* and preclinical/clinical stages. Among all positron-emitters isotopes, Carbon-11 is very attractive as: (I) it can be produced in relatively high quantities in commercial cyclotrons; (II) it is chemically versatile; and (III) its half-life (20.4 min.) is long enough to allow imaging studies but short enough to minimize the radiological effects after administration to a living organism. In addition, carbon is present in all organic molecules, thus enabling the preparation of radioactive analogues with the same chemical structure of the molecule of interest.

In this chapter, we evaluate the *in vitro* pharmacokinetics properties of new triazole-based FKBP12-RyR stabilizers (AHK-1 and AHK-2[7], Fig. 3.2) with potential application in Duchenne muscular dystrophy (DMD), a severe type of muscular dystrophy with no cure characterized by alteration or absence of dystrophin protein, membrane fragility and increased basal intracellular Ca^{2+} levels[8]. It has been shown that the stabilization of FKBP12-RyR interaction could inhibit sarcoplasmic reticulum Ca^{2+} leak, reduce biochemical and histological evidence of muscle damage, and provide an efficient therapeutic alternative[9,10,11]. Our approach consists of the

[6] Evans, E. A., & Stanford, F. G. *Decomposition of Tritium-Labelled Organic Compounds. Nature* (1963) doi:10.1038/197551a0.

[7] Aizpurua, J. M., Irastorza, A., Ferrón, P., Miranda. J. I., Vallejo, A., López de Munain, A. J., Toral, I., Aldanondo G., Triazoles for regulating intracellular calcium homeostasis. Patent WO2017203083A1.

[8] Allena, D. G., Whitehead, N. P., Duchenne muscular dystrophy – What causes the increased membrane permeability in skeletal muscle? *Int. J. of Biochem. Cell. Biol.* (2011) doi:10.1016/j.biocel.2010.11.005.

[9] O'Reilly, F. M., Robert, M., Jona, I., Szegedi, C., Albrieux, M., Geib, S., De Waard, M., Villaz, M., Ronjat, M., FKBP12 Modulation of the Binding of the Skeletal Ryanodine Receptor onto the II-III Loop of the Dihydropyridine Receptor. *Biophysical Journal* (2002) doi:10.1016/s0006-3495(02)75381-2.

[10] Bellinger, A. M., Reiken, S., Carlson, C., Mongillo, M., Liu, X., Rothman, L., Matecki, S., Lacampagne, A., Marks, A. R. Hypernitrosylated ryanodine receptor calcium release channels are leaky in dystrophic muscle. *Nat Med* (2009) doi.org/10.1038/nm.1916.

[11] Fauconnier, J., Thireau, J., Reiken, S., Cassan, C., Richard, S., Matecki, S., Lacampagne, A. Leaky RyR2 trigger ventricular arrhythmias in Duchenne muscular dystrophy. *Proceedings of the National Academy of Sciences* (2010) doi:10.1073/pnas.0908540107.

radiolabelling of the compounds using radioactive isotope ^{11}C for their *in vitro* metabolism evaluation using rat (Sprague Dawley) microsomes.

Fig. 3.2: Chemical structure of triazole-based FKBP12-RyR stabilizers AHK-1 and AHK-2.

3.2. OBJECTIVES

The specific objectives of this chapter are:

1. To develop synthetic strategies for the radiolabelling of two triazole-based FKBP12-Ryr stabilizers, AHK-1 and AHK-2, in different positions and with ^{11}C radionuclide.

2. To evaluate the metabolism of both compounds *in vitro* using Rat (Sprague Dawley) microsomes.

3.3 RESULTS AND DISCUSSION

The work included in this chapter has been carried out in the Radiochemistry and Nuclear Imaging group at CIC biomaGUNE and Early Chemical Development, Pharmaceutical Sciences R&D at AstraZeneca, Sweden; in collaboration with the Organic Chemistry-I department at UPV/EHU-University of the Basque Country and Biodonostia Health Research Institute, where the compounds were synthetized and tested as FKBP12-RyR stabilizers. For this reason, the information included below is focused on the results related to radiolabelling and *in vitro* metabolism evaluation using Rat (Sprague Dawley) microsomes.

3.3.1 RADIOLABELLING OF FKBP12-RYR STABILIZERS

A key factor to be considered when planning studies using labelled drugs is the selection of the appropriate radionuclide and radiolabelling strategy. The selection of the radionuclide is of outmost importance. First, its half-life should be long enough to perform the radiolabelling, purification, formulation, and quality control of the final product. Second, the incorporation of the radionuclide should not modify the chemical structure of the compound to be investigated.

This is particularly relevant when dealing with small molecules, in which minimal modifications in the chemical structure may lead to dramatic changes in physico-chemical and biological properties. Finally, the physical half-life of the radionuclide should match the biological half-life of the molecule to be investigated.

The position of the radiolabel is also critical. Radioanalytical techniques detect only the radionuclide. Hence, if a molecule decomposes or undergoes metabolism, only the fragment containing the radionuclide will be detected. Because of this, incorporating the radiolabel/s in different positions is an interesting approach to get quantitative data regarding the formation of different metabolites over time.

Here, and considering the chemical structure of the molecules to be investigated (see Fig. 3.2) and the technologies available, we decided to use a multi-radionuclide/multi-position labelling approach to investigate the *in vitro* metabolism of the triazole-based FKBP12-RyR stabilizers (Fig. 3.3).

In a first approach, taking advantage of the presence of methyl units directly attached to heteroatoms, both compounds were radiolabelled in two different positions via ^{11}C-methylation using [^{11}C]CH_3I as the labelling agent (Fig. 3.3). The labelling results in a formal substitution of a CH_3- group by a [^{11}C]CH_3- group, which means that the chemical structure remains unaltered.

This multi-position labelling approach was expected to provide information about the metabolic rate, together with basic information about the chemical structure of the metabolites.

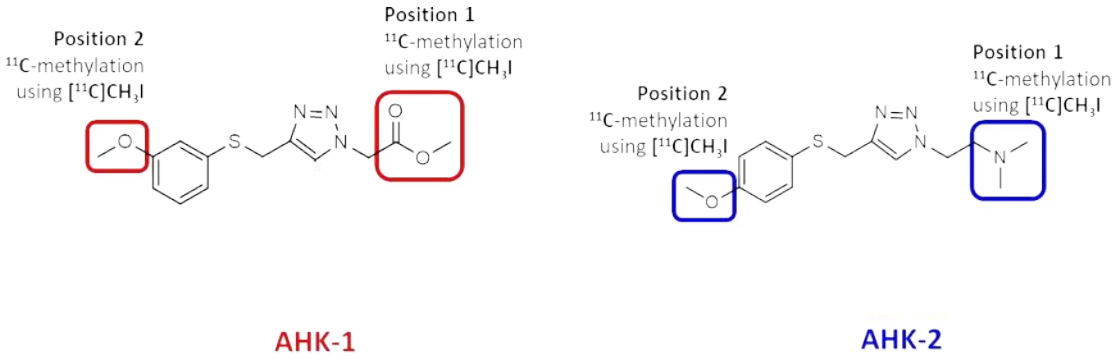

Fig. 3.3: Chemical structure of the drug candidates AHK-1 and AHK-2.

For $_{11}$C-methylation, during optimization of the syntheses processes, different experimental scenarios were assayed by modifying the amount of precursor, the base, the reaction temperature, and the reaction time. The optimization process was discontinued when the amount of activity obtained was considered to be sufficient to approach experiments.

3.3.1.1 ^{11}C-labelling

In all cases, the ^{11}C-labelling was carried out by ^{11}C-methylation of the appropriate precursor using [^{11}C]CH_3I as radiolabelled agent. [^{11}C]CH_3I was produced in a TRACERlab FXC Pro synthesis module (GE Healthcare) using the gas phase method as previously described[12]. Briefly, [^{11}C]CH_4 was generated in a 18/9 MeV cyclotron (IBA) by proton irradiation of a gas N_2/H_2 mixture (99/1), trapped in Carbosphere 60/80 (Alltech Associates, Inc.) at T = -140°C and allowed to react with iodine at 720°C to form [^{11}C]CH_3I in a gas circulating process. At the end of the process, the radioactive gas was distilled into a 2 mL stainless steel loop pre charged with a solution containing the precursor to carry out the ^{11}C-methylation reaction. The reaction mixture was purified by high performance liquid chromatography (HPLC) and the labelled compound was finally reformulated and reconstituted with physiologic solution.

A description of the experimental scenarios explored during process optimisation to achieve ^{11}C-methylation of each compound in each position is included below. In all cases, initial experiments

[12] Gómez-Vallejo, V., Llop, J., Fully automated and reproducible radiosynthesis of high specific activity [^{11}C]raclopride and [^{11}C]Pittsburgh compound-B using the combination of two commercial synthesizers. *Nucl. Med. Commun*. (2011) doi: 10.1097/MNM.0b013e32834b45a3.

were conducted without purification, and the reaction crude was directly analysed by HPLC with radioactive detection to determine the chromatographic yield. The purification step was finally implemented when chromatographic yields were anticipated as sufficient to yield reasonable radiochemical yields.

Synthesis of [^{11}C]AHK-1.1

Amines, carboxylic acids, alcohols, and thiols can be successful labelled with [^{11}C]CH_3I. Methylation reactions, using [^{11}C]CH_3I as radiolabelled agent, are nucleophilic reactions which involve the attack by an electron-rich element (so called nucleophile) on an electron-poor atom, so-called electrophile (Fig. 3.4). When the nucleophilic reaction involves a carboxylic acid group (-COOH) or an alcoholic group (-OH), the first step is an acid-base reaction to form the nucleophilic agent. Hence, the addition of a strong base is needed. In contrast, when amines and thiols are used the methylation proceed without prior deprotonation, due to the intrinsic nucleophilic properties of these functional groups.

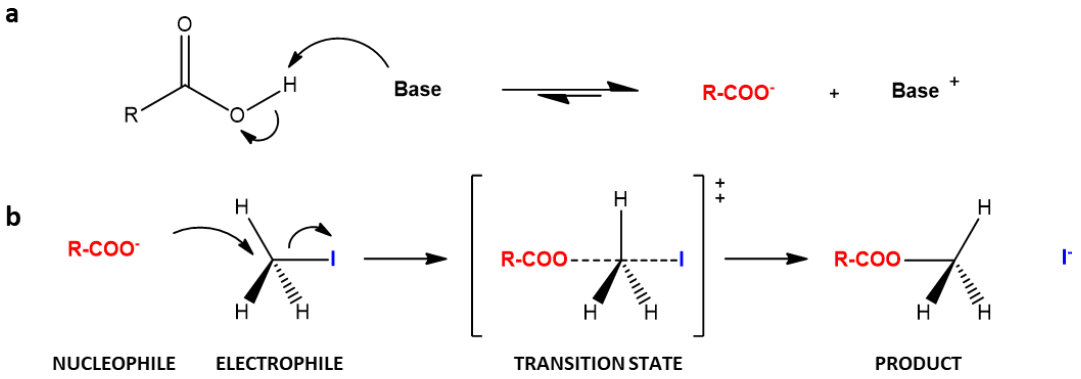

Fig. 3.4: Schematic representation of the nucleophilic reaction. a) Acid-base reaction and formation of the nucleophile. b) The nucleophile, (carboxylate group in the example, R-COO^-), reacts with the electrophile, (methyl iodine in the example, CH_3I), in a process that involves simultaneous bond formation by the nucleophile and bond cleavage by the leaving group (iodide in the example, I^-). The transition state is also represented.

The preparation of [^{11}C]AHK-1.1 (see Fig. 3.5a) was first assayed using different bases covering a wide range of pKa values, from aniline (pKa = 4.6) to sodium hydroxide (NaOH; pKa = 13.8) (Fig. 3.5b). In all cases, the amount of base was fixed to 5 µL (pure base in all cases except NaOH, where a 5M aqueous solution was used), and the reaction time and temperature were fixed at 5 min and room temperature, respectively.

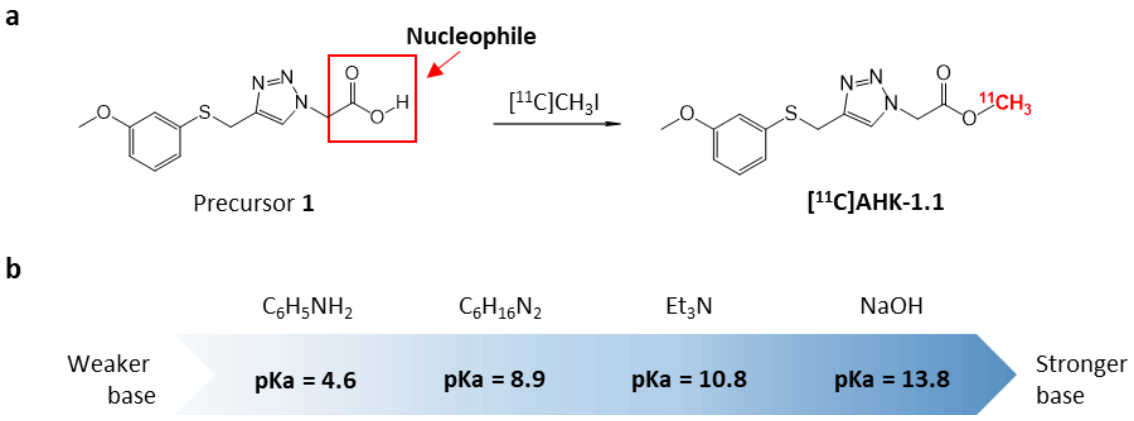

Fig. 3.5: a) Preparation of [^{11}C]AHK-1.1 from the corresponding carboxylic acid (precursor **1**). b) Different bases used for the ^{11}C-methylation reaction and their pKa values.

Under the experimental conditions assayed, trimethylamine (Et_3N) was the only one which led to the formation of the desired labelled compound. The peak with retention time = 10.2 min (Fig. 3.6c) co-eluted with AHK-1 reference standard and accounted for *ca.* 20% of the total radioactivity (Table 3.1, entry 3). Under these conditions, two radiolabelled impurities were identified in the chromatogram (radioactive detector). The first one, with retention time = 1.5 min, accounted for 15% of the total radioactivity. Although not proven, the short retention time suggests strong polarity of this by-product. Hence, we hypothesize that it could be due to the formation of [^{11}C]CH_3OH. A second radioactive peak, with retention time = 8.5, co-eluted with the radiolabelling agent [^{11}C]CH_3I (Fig. 3.6c) and accounted for *ca.* 65% of the radioactivity. These results suggest incomplete reaction, and hence that longer reaction times or higher temperatures may result in increased chromatographic yield.

Table 3.1: Different experimental scenarios for the synthesis of [^{11}C]AHK-1.1.

Entry	N°	Base	Volume (µl)	Time (min)	Temperature (°C)	Chromatographic yields (%)*
1	2	$C_6H_5NH_2$	5	5	RT	0
2	2	$C_6H_{16}N_2$	5	5	RT	0
3	3	Et_3N	5	5	RT	18.3±8.9
4	2	NaOH	5	5	RT	0

* Calculated as the ratio between the area under the peak corresponding to [^{11}C]AHK-1.1, and the sum of the areas under all peaks in the chromatogram, and expressed in percentage. RT: room temperature.

When a stronger base, such as NaOH (5M aqueous solution) was used, the reaction results primarily in the formation of a single radioactive peak with retention time = 1.5 min (Fig. 3.6d). According to our previous experience, the formation of $[^{11}C]CH_3OH$ often occurs when strong bases are used in methylation reactions, and hence we hypothesize, similarly to the previous case, that the peak corresponds to $[^{11}C]CH_3OH$ which is formed due to hydrolysis of $[^{11}C]CH_3I$.

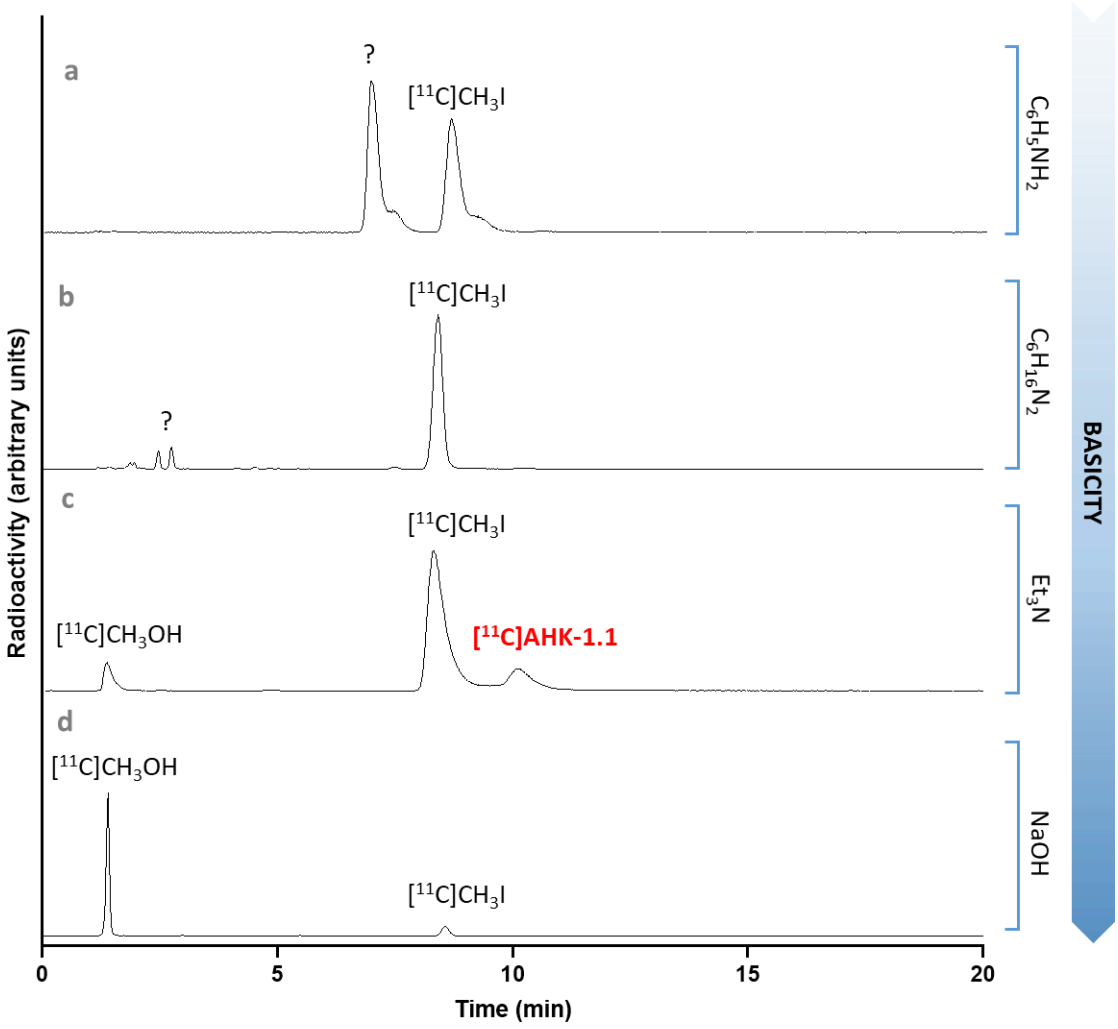

Fig. 3.6: Chromatograms (radioactivity detector) corresponding to the analysis of the crude after reaction of precursor **1** with $[^{11}C]CH_3I$ in the presence of aniline ($C_6H_5NH_2$, a), tetramethylethylenediamine ($C_6H_{16}N_2$, b), trimethylamine (Et_3N, c) and sodium hydroxide (NaOH, d) as the base.

The use of weaker bases also did not yield the desired product. When tetramethylethylenediamine ($C_6H_{16}N_2$) was used, only one peak with retention time = 8.5 min was observed in the chromatogram, confirming the presence of unreacted $[^{11}C]CH_3I$ (Fig. 3.6b).

On the contrary, the use of aniline ($C_6H_5NH_2$) as the base resulted in the formation of two major peaks, one of them corresponding to unreacted [^{11}C]CH_3I, and the second one whose identity could not be confirmed. However, it is worth mentioning that nucleophilic substitution reactions require the addition of non-nucleophilic bases. The nitrogen atom in aniline has certain nucleophilic character, and hence it may compete with the carboxylate group in precursor **1** to react with [^{11}C]CH_3I. Hence, although not proven, it seems plausible to assume that the peak with retention time = 7 min (Fig. 3.6a) corresponds to [^{11}C]*N*-methylaniline.

With the aim of improving chromatographic yields and considering that the only base that led to the formation of the desired labelled compound was Et_3N, we decided to modify the other experimental parameters of the reaction. First, we increased both the amount of the base (Table 3.2, entries 1-2) and the reaction time (Table 3.2, entry 3), although similar chromatographic yields to those previously achieved were obtained. Noteworthy, increasing the temperature to 50°C and 100°C resulted in progressive increase of the chromatographic yields to *ca.* 25% and 75%, respectively (Table 3.2, entry 5; Fig. 3.7). In the latter, the peak corresponding to [^{11}C]CH_3I is very minor, confirming quantitative consumption of the radiolabelling agent to yield the desired labelled compound [^{11}C]AHK-1.1 and [^{11}C]CH_3OH as the major by-product.

Table 3.2: Optimization of the [^{11}C] AHK-1.1 labelling process.

Entry	N°	Base	Volume (µl)	Time (min)	Temperature (°C)	Chromatographic yields (%)
1	2	Et_3N	8	5	RT	14.8±2.4
2	2	Et_3N	15	5	RT	10.7±3.1
3	2	Et_3N	5	7	RT	8.8±1.8
4	3	Et_3N	5	5	50	23.5±5.7
5	3	Et_3N	5	5	100	77±1.7

* Calculated as the ratio between the area under the peak corresponding to [^{11}C]AHK-1.1, and the sum of the areas under all peaks in the chromatogram, and expressed in percentage. RT: room temperature.

The full automatic synthesis of [^{11}C]AHK-1.1, including purification via HPLC, was then tackled under optimised experimental conditions. Purification by HPLC using a C-18 column and 0.1 M ammonium formate solution (pH = 3.9)/ACN (50/50) as the mobile phase resulted in good separation of the desired labelled compound (retention time = 8.4 min; Fig. 3.8a), which was collected and reformulated with ethanol and physiologic saline solution (1/9, v/v) to yield the

radiotracer ready for injection. Quality control by radio-HPLC confirmed radiochemical purity > 95% (Fig. 3.8b) and co-elution with reference standard which confirmed the identity of the compound (Fig. 3.8b). Radiochemical yield (non-decay corrected) was 8.6±1.2% in overall production time of *ca.* 30 min from EOB.

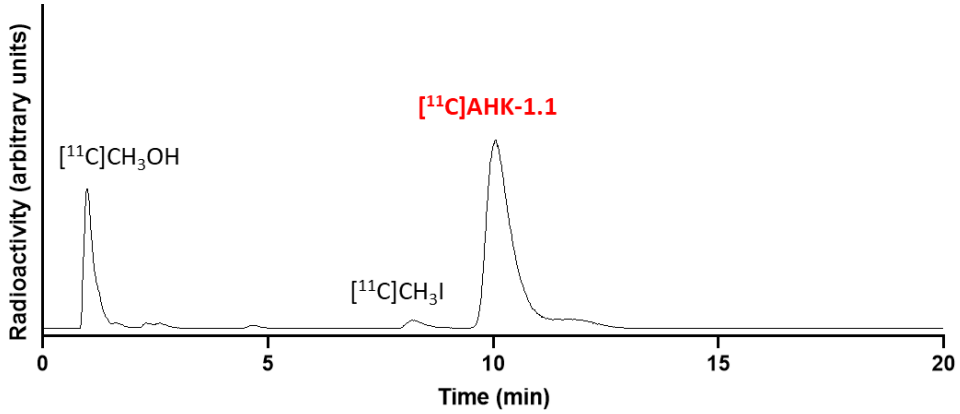

Fig. 3.7: Chromatograms (radioactivity detector) corresponding to the analysis of crude reaction when trimethylamine (Et_3N) was used as base and the temperature was increase up to 100 °C. The position of the peak corresponding to the identified compounds are shown.

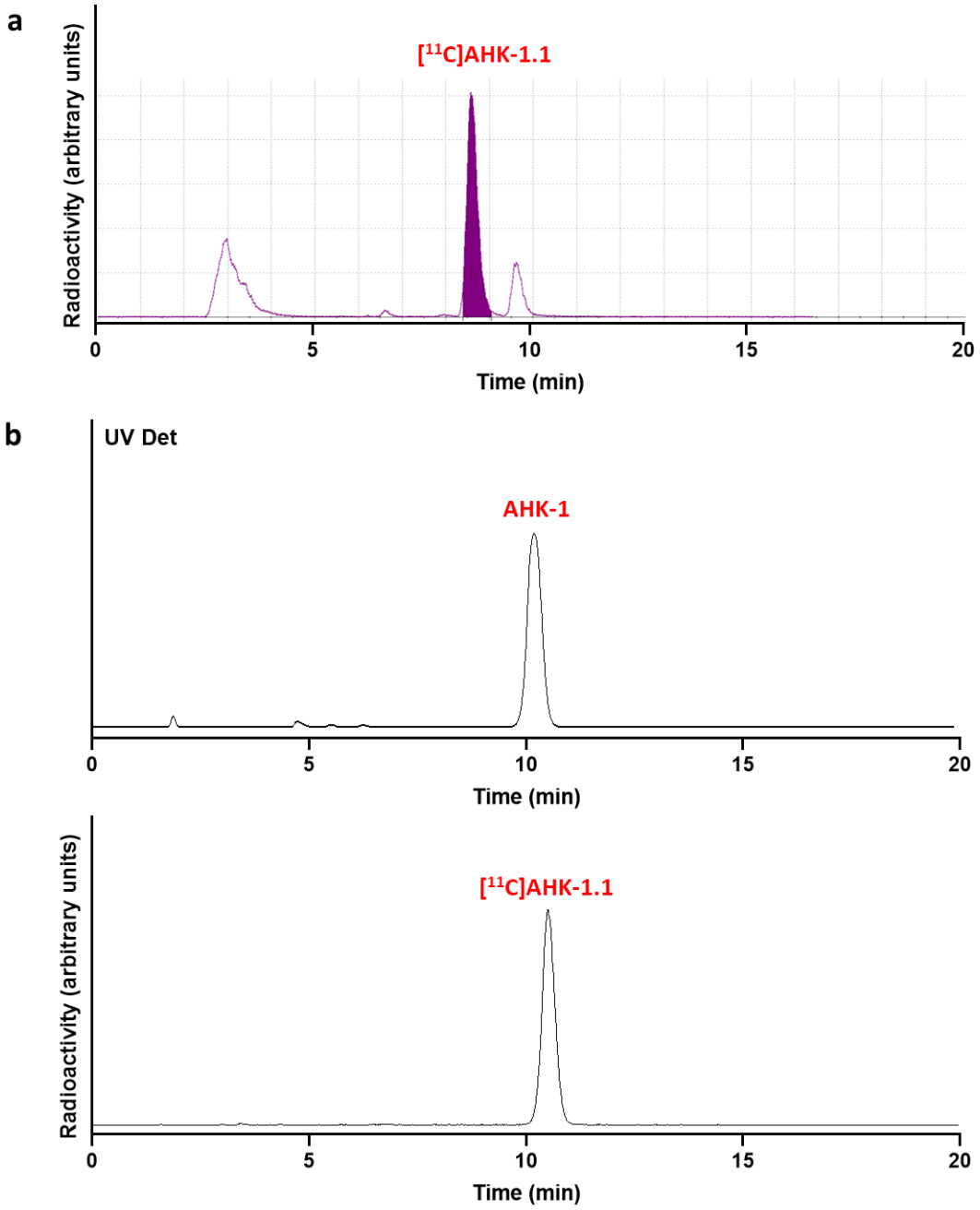

Fig. 3.8: a) Chromatogram (radioactivity detector) obtained during the purification of [^{11}C]AHK-1.1. b) Chromatograms (UV detector, top; radioactivity detector, bottom) of quality control co-injected whit the no radioactive compound (AHK-1) as reference.

Synthesis of [^{11}C] AHK-1.2

The radiolabelling of compound AHK-1.2, which has the same chemical structure than compound AHK-1.1 but with the ^{11}C attached to the phenol group, was tackled by methylation of precursor **2** (Fig. 3.9).

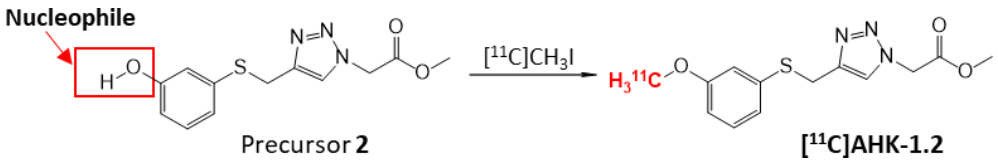

Fig. 3.9: ^{11}C-methylation reaction of precursor **2**.

Considering that the proton on the phenol group is less acidic than the proton on the carboxylic acid group, we decided to use a stronger base to generate the nucleophile. For this reason, the reaction was initially investigated using different amounts of an aqueous 5M NaOH solution (Table 3.3, entries 1-4, Fig. 3.10), a base widely used in radiochemistry to deprotonate the phenol group[13,14]. When 5 and 3 µL of 5M NaOH solution were used, only two major peaks were detected in the chromatogram, corresponding to unreacted [^{11}C]CH_3I (minor peak) and [^{11}C]CH_3OH (major peak), probably due to the hydrolysis of the labelling agent due to the high concentration of base (Table 3.3, entries 1-2). The presence of the desired compound was detected when 1 µL of 5M NaOH solution was added (Table 3.3, entry 3). In this case, no presence of unreacted [^{11}C]CH_3I could be detected, although the peak corresponding to [^{11}C]CH_3OH still accounted for a significant fraction of the total radioactivity. Considering this, and that the addition of just 1 µL of the solution is experimentally challenging and may compromise reproducibility of the method, we decided to use a more diluted NaOH solution (1M) and increase the added volume to 3 µL (Table 3.3, entry 4). As it can be seen in the table, under these conditions the major peak in the chromatogram corresponds to the desired compound [^{11}C]AHK-1.2. Minor peaks corresponding to [^{11}C]CH_3OH and unreacted [^{11}C]CH_3I were also identified. The chromatographic yield was

[13] de Vries, E. F. J., Kortekaas, R., van Waarde, A., Dijkstra, D., Elsinga, P. H., Vaalburg, W. Synthesis and Evaluation of Dopamine D_3 Receptor Antagonist ^{11}C-GR218231 as PET Tracer for P-Glycoprotein. *J Nucl Med* (2005).

[14] Janssen, B., Vugts, D. J., Wilkinson, S. M., Ory, D., Chalon, S., Hoozemans, J. J. M. Windhorst, A. D. Identification of the allosteric P2X7 receptor antagonist [^{11}C]SMW139 as a PET tracer of microglial activation. *Scientific Reports* (2018) doi:10.1038/s41598-018-24814-0.

anticipated to be sufficient to tackle the purification step, and hence these experimental conditions were not further optimised.

The optimised experimental conditions were applied to the fully-automated production of [^{11}C] AHK-1.2. After purification using HPLC (Fig. 3.11a) and reformulation with ethanol and physiologic saline solution (1/9, v/v) the radiotracer was obtained ready for injection. Quality control by radio-HPLC confirmed radiochemical purity > 95% (Fig. 3.11b) and co-elution with reference standard confirmed the identity of the compound (Fig. 3.11b). Radiochemical yield (non-decay corrected) was 5.3±0.5% in overall production time of *ca.* 30 min from EOB.

Table 3.3: Optimization of the [^{11}C] AHK-1.2 labelling process.

Entry	N°	Base	Volume (µl)	Time (min)	Temperature (°C)	Chromatographic yields (%)*
1	2	NaOH 5M	5	5	RT	0
2	2	NaOH 5M	3	5	RT	0
3	2	NaOH 5M	1	5	RT	38.2±9.3
4	3	NaOH 1M	3	5	RT	55.3±14.4

* Calculated as the ratio between the area under the peak corresponding to [^{11}C]AHK-1.2, and the sum of the areas under all peaks in the chromatogram, and expressed in percentage. RT: room temperature.

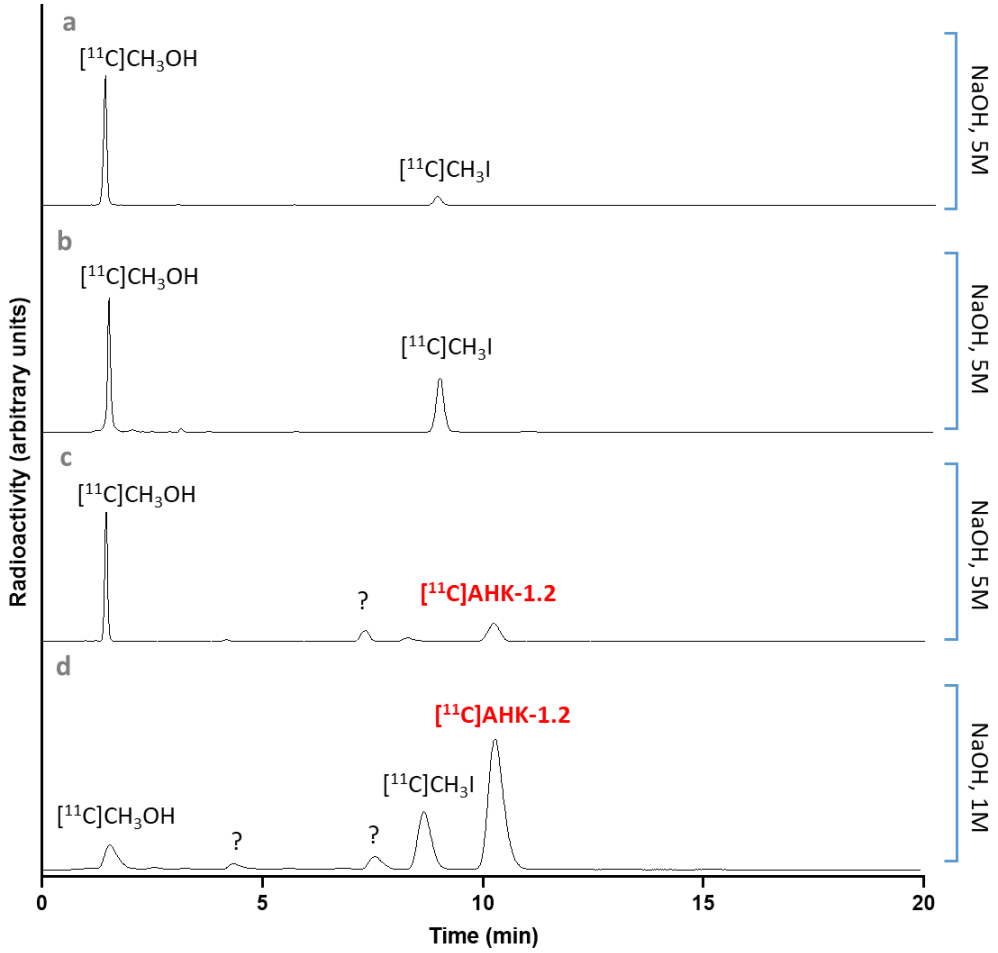

Fig. 3.10: Chromatograms (radioactivity detector) corresponding to the analysis of the crude after reaction of precursor **2** with [^{11}C]CH_3I in the presence of 5 µl of NaOH 5M (a), 3 µl of NaOH 5M (b), 1 µl of NaOH 5M (c) and 3 µl of NaOH 1M (d) as the base.

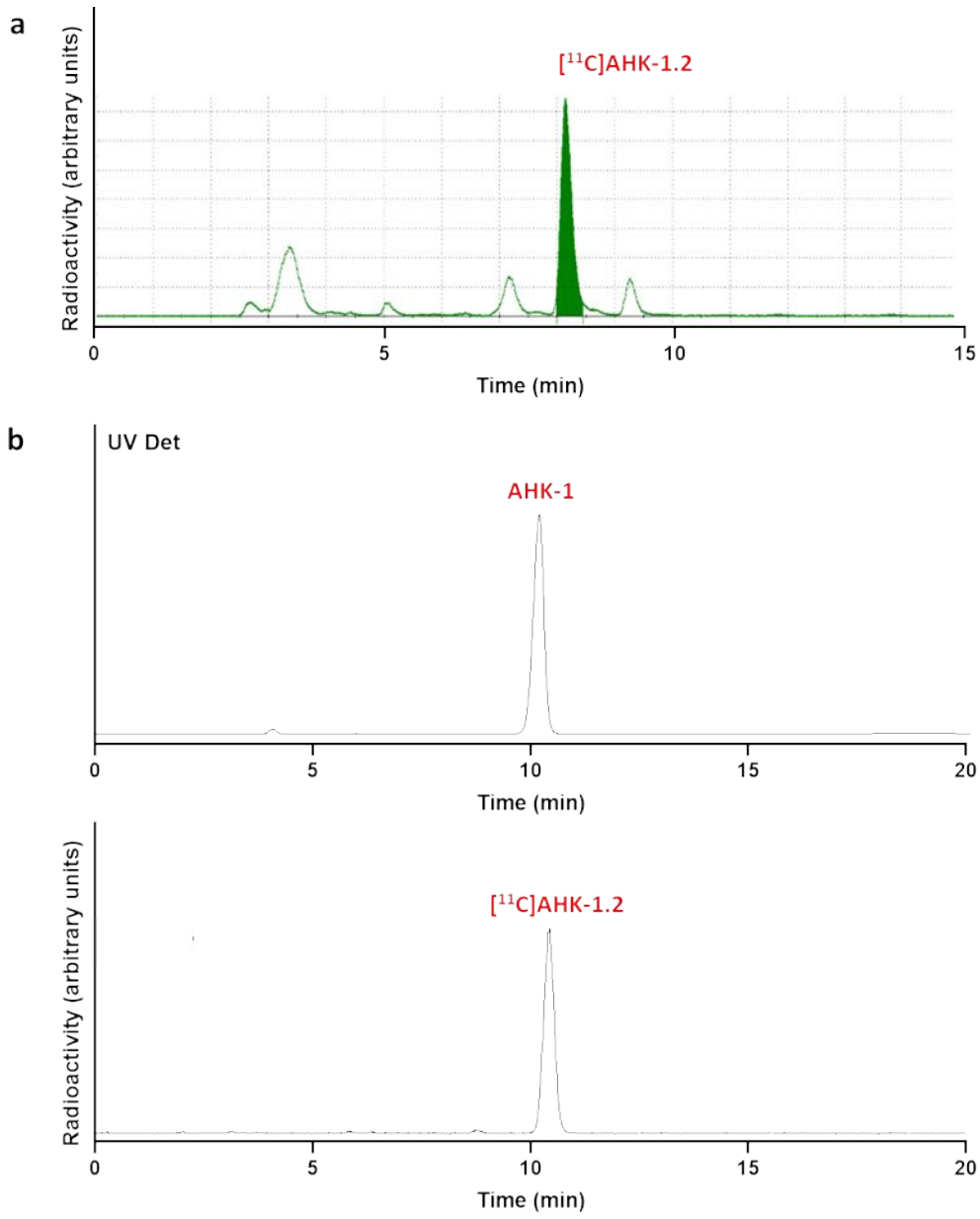

Fig. 3.11: a) Chromatogram (radioactivity detector) obtained during the purification of [^{11}C] AHK-1.2. b) Chromatograms (UV detector, top; radioactivity detector, bottom) of quality control co-injected whit the no radioactive compound (AHK-1) as reference.

Synthesis of [^{11}C] AHK-2.1

The compound AHK-2 has two positions susceptible to be ^{11}C-methylated (see Figure 3.3). First, we tackled the incorporation of [^{11}C]CH_3- on the amine group using precursor **3** to yield [^{11}C]AHK-2.1 (Fig. 3.12a). Thanks to the nucleophilic properties of the ammine group and its basic

properties, it was no necessary to add an additional base to the reaction mixture[15,16]. Because our previous experience with radiolabelling secondary aliphatic amines suggested fast reaction, we initially assayed the reaction at room temperature. As expected, analysis of the crude by radio-HPLC (Fig. 3.12b) confirmed the presence of the desired labelled compound [^{11}C]AHK-2.2 with a minor peak corresponding to unreacted [^{11}C]CH_3I. Longer reaction times may lead to higher chromatographic yields. Noteworthy, the longer the reaction time the higher the radioactive decay. Hence, we decided to use these experimental conditions for the fully automated synthesis of [^{11}C]AHK-2.1.

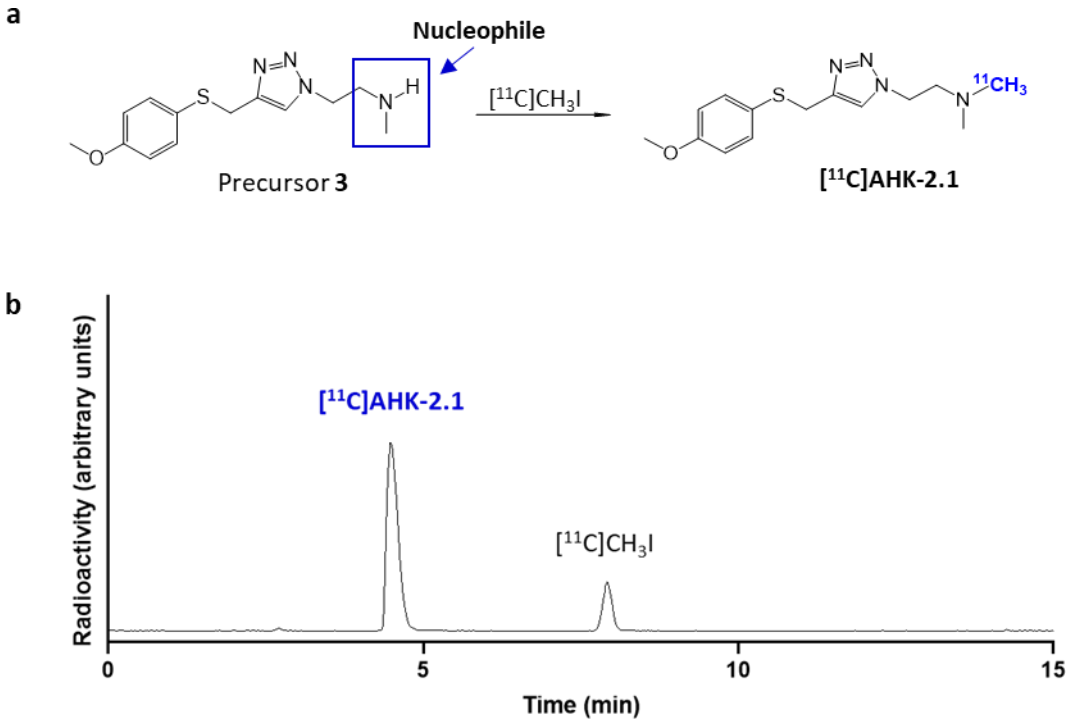

Fig. 3.12: a) ^{11}C-methylation reaction of precursor **3**. b) Chromatogram (radioactivity detector) corresponding to the analysis of crude reaction.

After purification by HPLC (Fig. 3.13a) and reformulation with ethanol and physiologic saline solution (1/9, v/v) the radiotracer was obtained ready for injection. Quality control by radio-HPLC

[15] Tarkiainen, J., Vercouillie, J., Emond, P., Sandell, J., Hiltunen, J., Frangin, Y., Guilloteau, D., Halldin, C. Carbon-11 labelling of MADAM in two different positions: a highly selective PET radioligand for the serotonin transporter. *J Labelled Cpd Radiopharm* (2001) doi:10.1002/jlcr.523.

[16] Verouillie, J., Tarkiainen, J., Halldin, C., Emond, P., Chalon, S., Sandell, J., Langer, O., Guilloteau, D. Precursor synthesis and radiolabelling of [^{11}C]ADAM: a potential radioligand for the serotonin transporter exploration by PET. *J Labelled Cpd Radiopharm* (2001) doi:10.1002/jlcr.436.

confirmed radiochemical purity > 95% (Fig. 3.13b) and co-elution with reference standard confirmed the identity of the compound (Fig. 3.13b). Radiochemical yield (non-decay corrected) was 14.4±2.3% in overall production time of *ca.* 30 min from EOB.

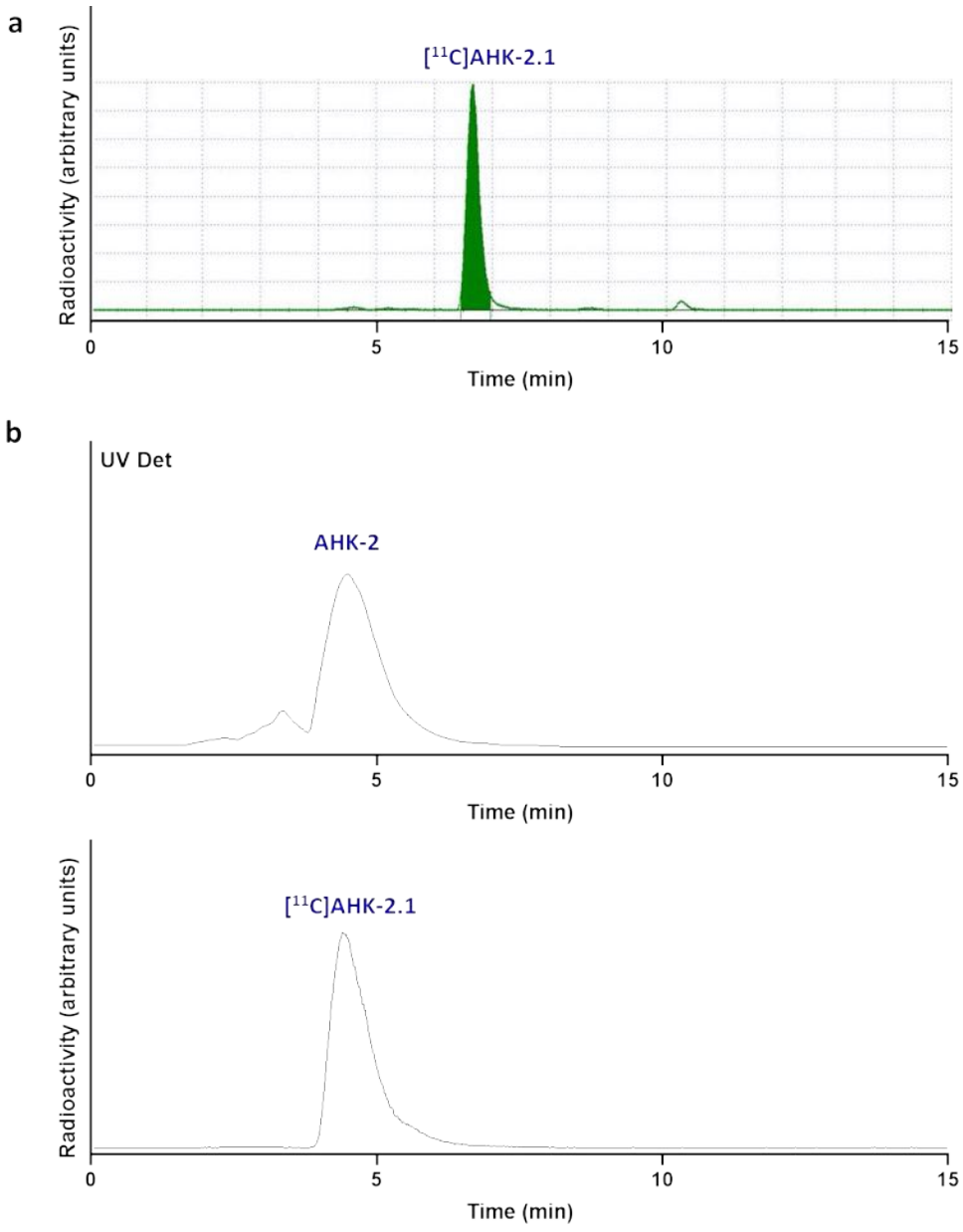

Fig. 3.13: a) Chromatogram (radioactivity detector) obtained during the purification of [^{11}C] AHK-2.1. b) Chromatograms (UV detector, top; radioactivity detector, bottom) corresponding to quality control of [^{11}C]AHK-2.1, co-injected whit the reference compound AHK-2.

Synthesis of [^{11}C] AHK-2.2

The synthesis of [^{11}C]AHK-2.2 was similar to [^{11}C]AHK-1.2, as the [^{11}C]CH_3- was to be inserted on a phenol group (Fig. 3.14). Hence, we started our optimization process using the same conditions as those used for the preparation of [^{11}C]AHK-1.2 (3 µl of aqueous 1M NaOH solution as the base, 5 min reaction time, room temperature).

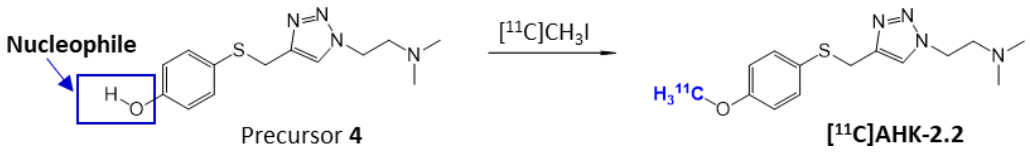

Fig. 3.14: ^{11}C-methylation reaction of precursor **4**.

The chromatographic yield using 3 µl of aqueous 1M NaOH solution was 40.1±8.7% (Table 3.4, entry 1). This percentage in general would be considered to tackle subsequent steps, including *in vivo* experiments. However, the high amount of [^{11}C]CH_3OH as side-product together with the presence of unreacted [^{11}C]CH_3I (Fig. 3.15a) suggested that other bases may lead to better results. Hence, we decided to investigate sodium hydride (NaH; dispersion in mineral oil). Analysis of crude reaction (Fig. 3.15b) showed almost quantitative chromatographic yield under these experimental conditions. No unreacted [^{11}C]CH_3I was detected, and only the presence of two very minor unidentified peaks could be observed in the chromatogram. Considering the high chromatographic yield and the good reproducibility of the method, we decided to use these experimental conditions for the fully automated production.

After purification by HPLC (Fig. 3.16a) and reformulation with ethanol and physiologic saline solution (1/9, v/v) the radiotracer was obtained ready for injection. Quality control by radio-HPLC confirmed radiochemical purity > 95% (Fig. 3.16b) and co-elution with reference standard confirmed the identity of the compound (Fig. 3.16b). Radiochemical yield (non-decay corrected) was 14.8±1.1% in overall production time of *ca.* 30 min from EOB.

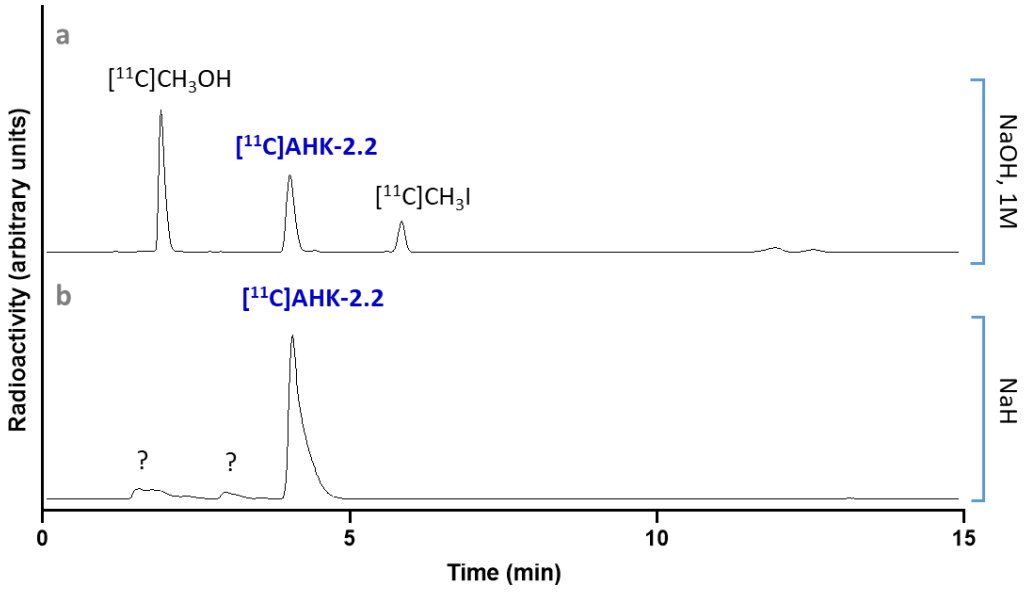

Fig. 3.15: Chromatograms (radioactivity detector) corresponding to the analysis of the crude after reaction of precursor **4** with $[^{11}C]CH_3I$ in the presence 3 µl of NaOH 1M (a) and NaH (dispersion in mineral oil) (b) were used as base. The position of the peak corresponding to the identified compounds are shown.

Table 3.4: Optimization of the $[^{11}C]$ AHK-2.2 labelling process.

Entry	N°	Base	Amount	Time (min)	Temperature (°C)	Chromatographic yields (%)*
1	3	NaOH 1M	3 µl	5	RT	40.1±8.7
2	3	NaH (dispersion in mineral oil)	1.7 mg	5	RT	89.3±4.4

* Calculated as the ratio between the area under the peak corresponding to $[^{11}C]$AHK-2.2, and the sum of the areas under all peaks in the chromatogram, and expressed in percentage. RT: room temperature.

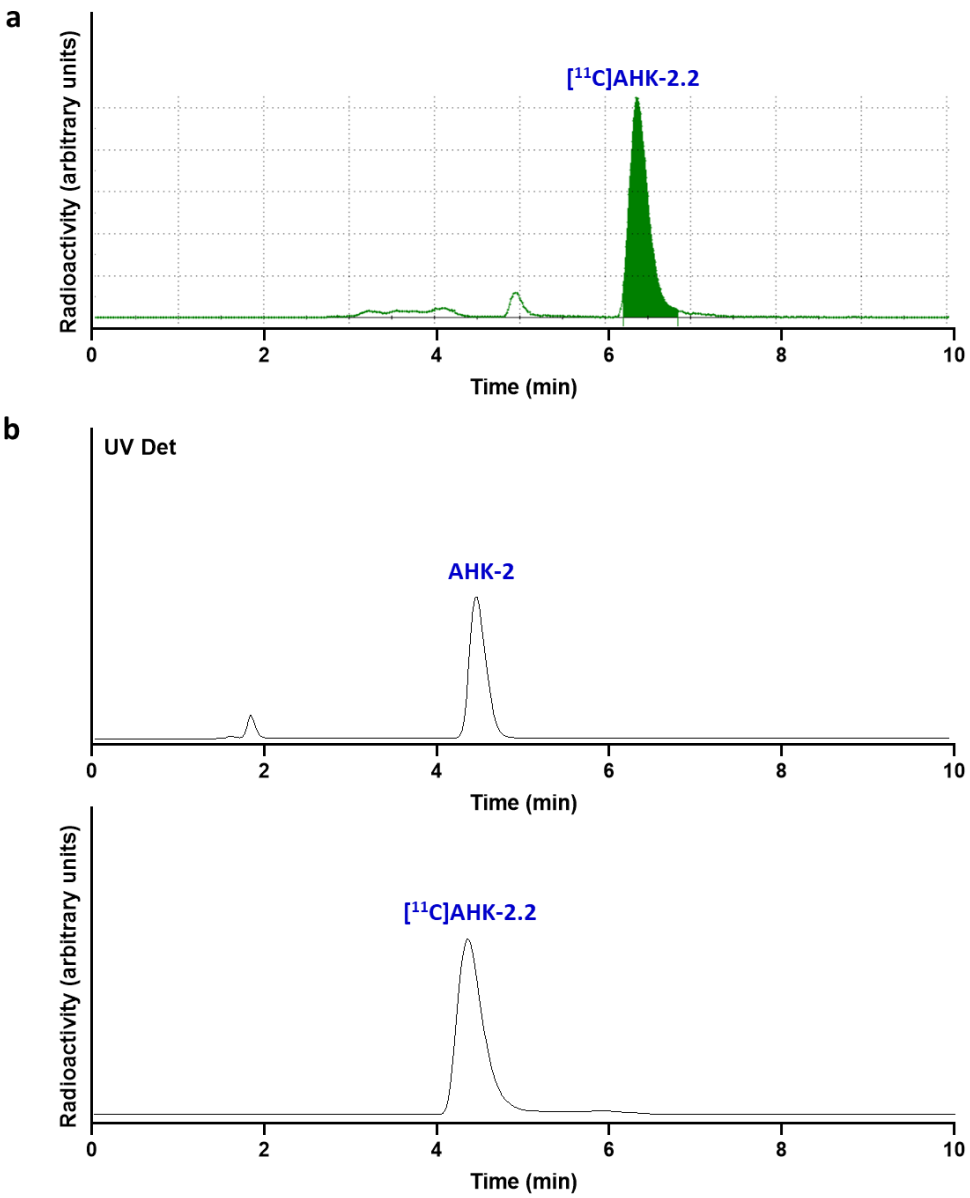

Fig. 3.16: a) Chromatogram (radioactivity detector) obtained during the purification of [^{11}C]AHK-2.2. b) Chromatograms (UV detector, top; radioactivity detector, bottom) corresponding to quality control of [^{11}C]AHK-2.2, co-injected whit the reference compound AHK-2.

As described in the paragraphs above, after optimization of the radiolabelling conditions, the radiosynthesis of [^{11}C]AHK-1.1, [^{11}C]AHK-1.2, [^{11}C]AHK-2.1, and [^{11}C]AHK-2.2 could be achieved by ^{11}C-methylation of precursors **1**-**4**, respectively, with non-decay corrected radiochemical yields in the range 5-15% and in overall production times of *ca.* 30 min from the end of bombardment (Scheme 1, Table 3.5, entries 1-4). Radiochemical purity was above 95% in all cases and specific activity values at the end of the synthesis were between 40-140 GBq/µmol.

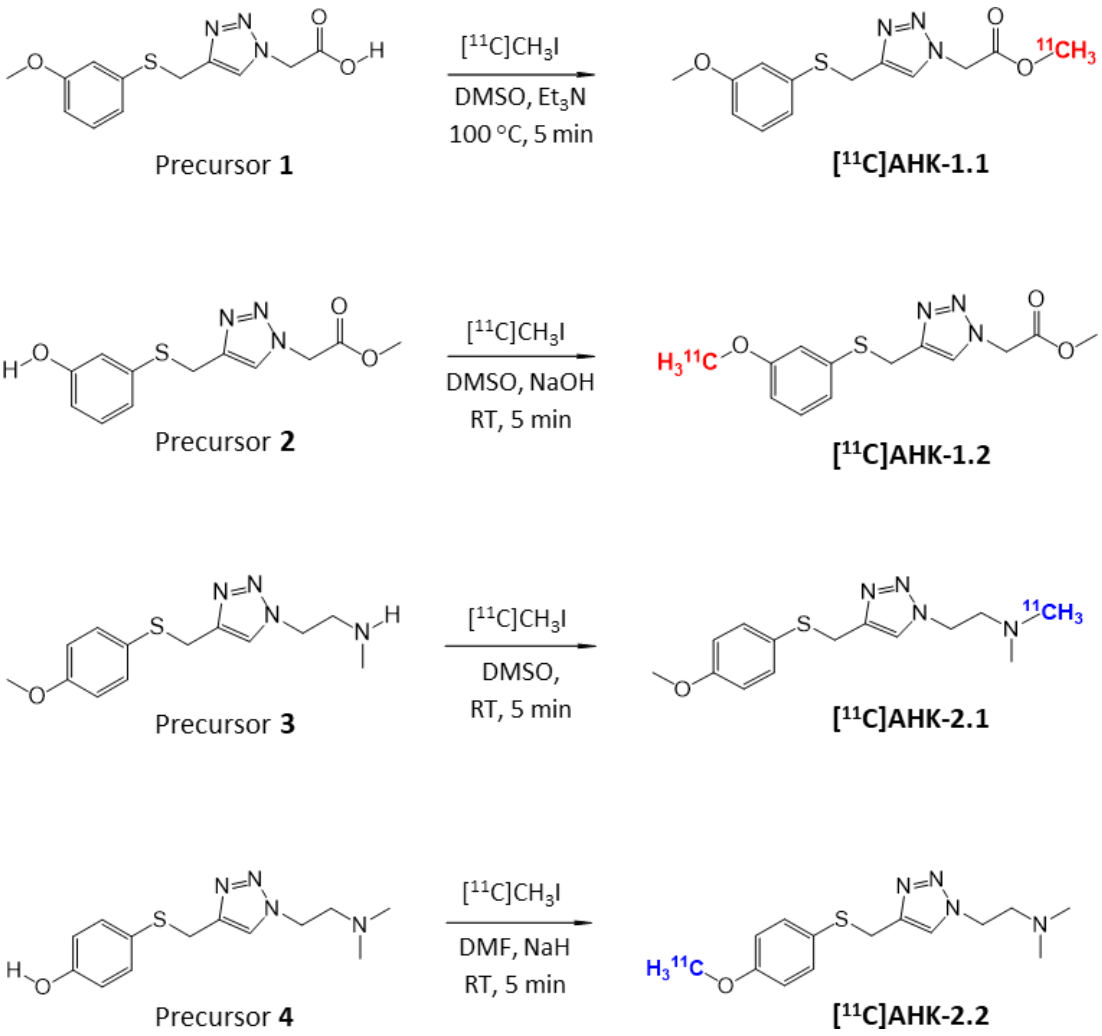

Scheme 1: Summary of radiochemical reactions for the production of compounds [^{11}C]AHK-1.1, [^{11}C]AHK-1.2, [^{11}C]AHK-2.1, and [^{11}C]AHK-2.2 via ^{11}C-methylation of precursors **1**-**4**.

Table 3.5: Production yields, overall production times, molar activity and radiochemical purity values obtained for [^{11}C]AHK-1.1, [^{11}C]AHK-1.2, [^{11}C]AHK-2.1, and [^{11}C]AHK-2.2.

Entry	Compound	t[1]	RCY[2]	MA[3]	RCP[4]
1	**[^{11}C] AHK-1.1**	30	8.6±1.2%	64±39 GBq/µmol	>95%
2	**[^{11}C] AHK-1.2**	30	5.3±0.5%	129±141 GBq/µmol	>95%
3	**[^{11}C] AHK-2.1**	30	14.4±2.3%	134±90 GBq/µmol	>95%
4	**[^{11}C] AHK-2.2**	30	14.8±1.1%	38±5 GBq/µmol	>95%

[1]overall production time, in min; [2]radiochemical yield, non-decay corrected; [3]Molar activity at the end of synthesis; [4]radiochemical purity, as determined by radio-HPLC.

3.3.2 *IN VITRO* PRECLINICAL EVALUATION OF METABOLISM

Once the radiolabelling process for the preparation of [^{11}C]AHK-1.1, [^{11}C]AHK-1.2, [^{11}C]AHK-2.1 and [^{11}C]AHK-2.2 had been established, we tackled the *in vitro* investigation of metabolic stability using rat (Sprague Dawley) microsomes, which are a sub- cellular fraction of hepatocytes containing enzymes responsible for the metabolism of over 90% of commercial drugs. Both compounds, AHK-1 and AHK-2, labelled with ^{11}C were used. Experimentally, rat liver microsomes were incubated with the different radioactive derivatives of AHK-1 and AHK-2 in the presence of NADPH as the cofactor, and the mixtures were analysed by radio-HPLC at 5, 10, 15, 30 and 60 min of incubation. In order to have a proper separaVon of the different labelled species in the HPLC system, a gradient method was implemented (see experimental section).

In vitro metabolism of compound AHK-1

Analysis of HPLC chromatograms when [^{11}C]AHK-1.1 was used (Fig. 3.23a) showed a fast and quantitative formation of one radioactive metabolite, with retention time = 2 min, suggesting that the –COO[^{11}C]CH $_3$residue is immediately hydrolyzed resulting in the formation of the corresponding carboxylic acid (–COOH) and [^{11}C]CH_3OH. We hypothesised that the compound AHK-1 could be a kind of prodrug, which after administration may become the free acid, which further metabolizes. Thanks to our multi-radionuclide/multi-position labelling approach we were able to track the further metabolism of the free acid by using the radiolabelled derivatives [^{11}C]AHK-1.2. Results obtained when [^{11}C]AHK-1.2 was used (Fig. 3.23a) in fact shown that the parent compound (retention time = 28 min) was mostly converted into the radioactive metabolites with retention time of 18 and 20 min. With the aim to confirm our hypothesis regarding the formation of the free acid, we moved to mass spectrometry analysis. Experimentally we perform the same experiment incubating the reference compound AHK-1, instead of the radioactive derivatives, with the rat liver microsomes and the resulting mixtures were analysed by LC-MS. The results obtained confirmed the presence of the free acid H_3COAr-R-COOH (Fig. 3.23b).

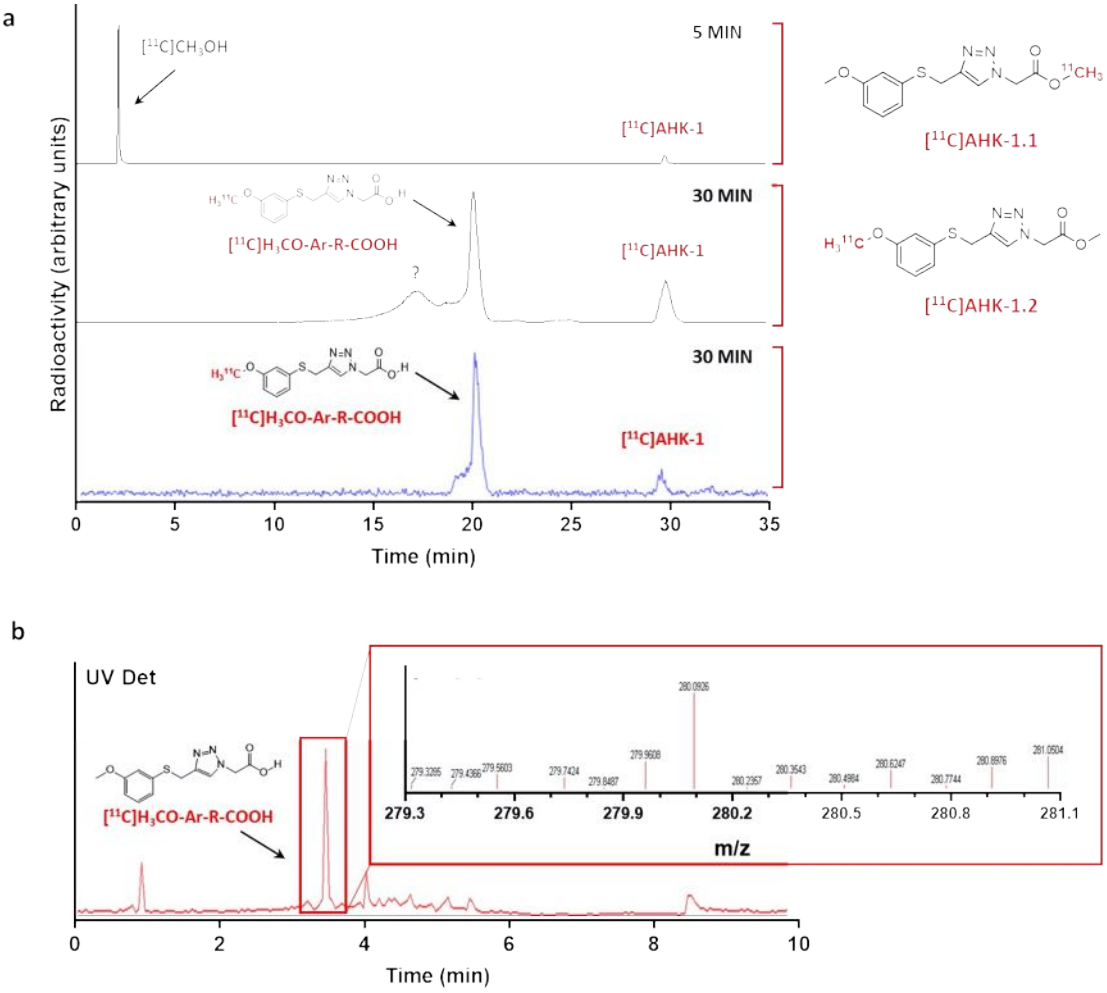

Fig. 3.23: a) Chromatograms corresponding to the *in vitro* metabolism (radioactivity detector) of AHK-1, labelled in two different positions. The position of the peaks corresponding to the parent compound and the identified metabolites are shown with black arrows. b) Chromatograms (MS detector, top) and mass spectra of the compound (bottom) corresponding to the analysis of AHK-1. The peaks corresponding to the identified metabolites are shown.

In vitro metabolism of compound AHK-2

Moving to the compound AHK-2, HPLC analysis of [$_{11}$C] AHK-2.1 (Fig. 3.24a), showed the formation of two polar metabolites with retention times of *ca.* 2 and 3 min, probably reflecting the presence of the [$_{11}$C]N(CH$_3$) $_2$and [$_{11}$C]NHCH $_3$groups. Additionally, two non-polar radioactive metabolites were found with retention time = 21 and 22 min. Moving to the compound [$_{11}$C]AHK-2.2, the radio-HPLC analysis showed the presence of one single peak with strong polarity and short retention time (t = 2 min) suggesting, similarly to the compound AHK.1, the formation of [$_{11}$C]CH$_3$OH and another metabolite with retention time = 22 min (Fig. 3.24a). One of them (retention time = 22 min) was already observed when the C-11 labelled compounds were used. Hence, we started thinking about what metabolite might be in common for the three radioactive derivatives, and we concluded that it might probably be the sulfoxide derivative. This in fact keeps both alkyl chains besides the triazole ring. As previously described for the compound AHK-1, we moved to mass spectrometry analysis to confirm our hypothesis. For this, we incubate the reference compound AHK-2 with the rat liver microsomes and we analysed the resulted mixture by LC-MS. The results obtained confirmed the presence of the sulfoxide derivative (Fig. 3.24b)

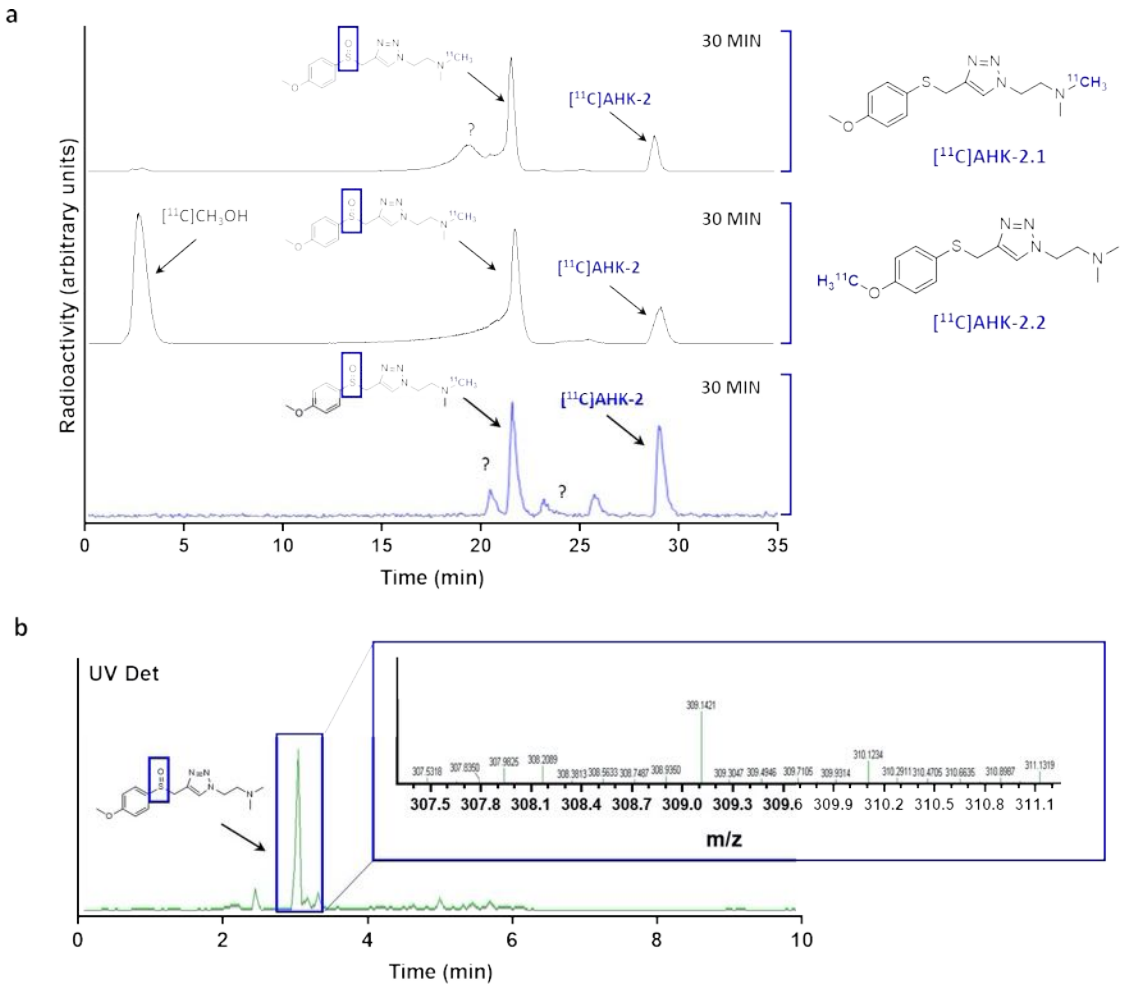

Fig. 3.24: a) Chromatograms corresponding to the *in vitro* metabolism (radioactivity detector) of AHK-2, labelled in two different positions. The position of the peaks corresponding to the parent compound and the identified metabolites are shown with black arrows. b) Chromatograms (MS detector, top) and mass spectra of the compound (bottom) corresponding to the analysis of AHK-2. The peaks corresponding to the identified metabolites are shown.

3.4 CONCLUSION

This chapter described the process towards the incorporation, in different positions, either positron or beta emitters into the new triazole-based FKBP12-RyR stabilizers AHK-1 and AHK-2, with the aim to carried out the *in vitro* metabolism evaluation by using Positron Emission Tomography (PET) and complementary techniques. The labelling with the positron emitters was achieved by C-11 methylation using [^{11}C]CH_3I as labelling agent. Compounds [^{11}C]AHK-1.1, [^{11}C]AHK-1.2, [^{11}C]AHK-2.1 and [^{11}C]AHK-2.2 were obtained with non-decay corrected

radiochemical yields in the range of 5-15% and overall production times of about 30 minutes from the end of the bombardment. Radiochemical purity was above 95% in all cases and specific activity values at the end of synthesis were between 40-140 GBq/µmol. The multi-radionuclide/multi-position labelling approach resulted to be useful to get a good overview of metabolism and the identification of some of the metabolites. The results of the *in vitro* metabolism evaluation, by using rat microsomes, showed that, for compound AHK-1, the –COO[$_{11}$C]CH $_3$residue is immediately hydrolyzed resulting in the formation of the corresponding carboxylic acid (–COOH) and [$_{11}$C]CH$_3$OH, suggesting that if any therapeutic efficacy will be observed for the compound the active part would be probably the acid or some metabolites derived from it. In this case, the compound AHK-1 will be a kind of prodrug that, after administration, is immediately converted into the free acid, which further metabolizes. For the compound AHK-2 the main metabolic pathway was the demethylation of the CH$_3$O-Ar residue followed by oxidation of the thioether group into sulfoxide and demethylation of –N(CH$_3$)$_2$.

3.5 EXPERIMENTAL PART

3.5.1 GENERAL REMARKS

The precursors and all compounds used to identify metabolites were synthetized by the group of Professor Jesús María Aizpurua, from the Organic Chemistry-I department at UPV/EHU-University of the Basque Country.

3.5.2 ^{11}C-METHYLATION

The synthesis of [^{11}C]CH$_3$I was carried out, in all cases, using a TRACERlab FXC Pro synthesis module (GE Healthcare). [^{11}C]CH$_4$ was generated in an IBA Cyclone 18/9 cyclotron by proton irradiation (target current=22 µA, integrated current = 2 µAh) of a gas N$_2$/H$_2$ mixture (99/1, starting pressure=16 bar) with high energy (18 MeV) protons. The radioactive gas was trapped in Carbosphere 60/80 (Alltech Associates, Inc.) at T = -140°C, desorbed by heating (80°C) and allowed to react with iodine at 720°C to form [^{11}C]CH$_3$I in a gas circulating process. [^{11}C]CH$_3$I was selectively retained in a trap containing PorapakTM Q (50-80 mesh, Waters Corporation) at room temperature, while unreacted [^{11}C]CH$_4$ was recirculated. At the end of the process (8-9 cycles),

the Porapak™ Q trap was heated at 190°C and [^{11}C]CH_3I was distilled under continuous helium flow (20 mL/min, 2.5 min). The gas stream was passed through a trap containing phosphorous pentoxide and Ascarite II® (20-30 mesh) before being introduced in the reaction loop to carry out the ^{11}C-methylation reaction (see below for conditions).

Synthesis of [^{11}C]AHK-1.1

The reaction loop was prefilled with a solution of precursor **1** (1 mg) in 80 µL dimethylsulfoxide containing 3 µL of Et_3N. After trapping of the [^{11}C]CH_3I, the reaction was allowed to occur for 5 min at 100°C. The reaction mixture was purified by HPLC, using a Phenomenex Luna C18 column (250 x 10mm, 5 µm) as the stationary phase and 0.1 M ammonium formate solution (pH = 3.9)/ACN (50/50) as the mobile phase (flow rate=5 mL/min, retention time = 8.4 min).

Synthesis of [^{11}C] AHK-1.2

The reaction loop was prefilled with a solution of precursor **2** (1 mg) in 80 µL dimethylsulfoxide containing 3 µL of NaOH 1M. After trapping of the [^{11}C]CH_3I, the reaction was allowed to occur for 5 min at room temperature. The reaction mixture was purified by HPLC, under the same conditions as above.

Synthesis of [^{11}C] AHK-2.1

The reaction loop was prefilled with a solution of precursor **3** (1 mg) in 80 µL dimethylsulfoxide. After trapping of the [^{11}C]CH_3I, the reaction was allowed to occur for 5 min at room temperature. The reaction mixture was purified by HPLC, using a Phenomenex Luna C18 column (250 x 10mm, 5 µm) as the stationary phase and 10 mM ammonium formate solution (pH = 8.3)/ACN (50/50) as the mobile phase (flow rate=5 mL/min, retention time = 6.5 min).

Synthesis of [^{11}C] AHK-2.2

The reaction loop was prefilled with a solution of precursor **4** (2 mg) in 100 µL dimethylformamide containing 1.7 mg of NaH (60% dispersion in mineral oil). After trapping of the [^{11}C]CH_3I, the reaction was allowed to occur for 5 min at room temperature. The reaction mixture was purified by HPLC, under the same conditions as above.

In all cases, the desired fraction (monitored by using a radioactivity detector) was collected, diluted with ultrapure water (20 mL, obtained from a Milli-Q® Purification System, Millipore®,

Merck KGaA, Darmstadt, Germany) and flushed through a C-18 cartridge (Sep-Pak® Light, Waters) to selectivity retain the labelled compound. The cartridge was washed with ultrapure water and the labelled compound was finally eluted with ethanol (1 mL) and reconstituted with physiologic solution (9 mL).

The amount of radioactivity of the final radiotracer was measured in a dose calibrator (PETDOSE HC, Comecer) and a sample was submitted to quality control. The radiochemical purity and the specific activity were determined by HPLC, using an Agilent 1200 Series HPLC system with a multiple wavelength UV detector (λ = 254 nm) and a radiometric detector (Raytest). A RP-C18 column (Mediterranean Sea18, 4.6x150 mm, 5 µm particle size) was used as stationary phase. For compounds AHK-1.1 and AHK-1.2, the mobile phase was 10 mM ammonium formate solution (pH = 3.9)/ACN (60/40, flow rate 1mL/min, retention time = 10.2 min). For compounds AHK-2.1 and AHK-2.2, the mobile phase was 10 mM ammonium formate solution (pH = 8.3)/ACN (50/50, flow rate 1mL/min, retention time = 4.2 min).

3.5.4 *IN VITRO* PRECLINICAL EVALUATION OF METABOLISM

Test compounds (labelled with ^{11}C) and microsomal protein (20 mg/ml) were pre- incubated for 5 min with gentle agitation (300 rpm) in 100 mM phosphate buffer (pH 7.4). Reaction was initiated by the addition of 10 µl freshly prepared 20 mM NADPH in 100 mM phosphate buffer, pH 7.4. At different time points (5, 10, 15, 30, 60 min) the reaction was

terminated by the addition of 200 µl of acetonitrile (ACN). Samples were centrifuged at 5800 rpm for 5 min to pellet the precipitated protein. The resulting supernatants were analysed by HPLC, using an Agilent 1200 Series chromatograph equipped with a multiple wavelength UV detector (λ = 254 nm) and two radioactivity detectors, one of them equipped with a solid scintillation cell, especially designed to detect low energy β -(Raytest), and one of them equipped with a NaI crystal, for the detection of γ-rays. A RP-C18 column (Mediterranean Sea18, 4.6x150 mm, 5 µm particle size) was used as stationary phase, with an Eclipse XDB-C18 (4.6×12.5 mm, 5 µm particle size) guard column. As the mobile phase, 10 mM ammonium formate solution (pH = 3.9)/ACN was used for [$_{11}$C]AHK-1.1, [$_{11}$C]AHK-1.2, and 10 mM ammonium formate solution (pH = 8.3)/ACN was used for [$_{11}$C]AHK-2.1 and [$_{11}$C]AHK-2.2. In all cases, chromatographic runs were performed under gradient conditions at a flow rate of 1 mL/ min, with a total chromatographic time of 35 min (0-5 minutes 5% ACN; 5-25 minutes 60% ACN for compound AHK-1 / 50% ACN for compound AHK-2; 25-30 minutes 60% ACN for compound AHK-1 / 50% ACN for compound AHK-2; 30-35 minutes 5% ACN).

CHAPTER 4: DETERMINATION OF ARTERIAL INPUT FUNCTION (AIF): A KEY POINT FOR QUANTITATIVE PET DATA ANALYSIS. ^{18}F-FDG PET STUDIES.

4.1 INTRODUCTION

The determination of the input concentration of the tracer delivered to the tissues represents a key point in a PET study especially when the development of new radiotracers is tackled. The concentration of the non-metabolized compound in arterial plasma (or blood, depending on the tracer) is the gold standard input function (IF) in quantitative PET data analysis. In the recent years, several possibilities have been developed to determine the IF such as image derived input function (IDIF), online measurement by vessel catheterization, venous-based input function and population-based input function.

The IDIF, which aims to extract the blood information directly from PET images[1], is probably the most commonly used method for the determination of the blood concentration of a radiotracer. It offers different advantages for PET quantitative data analysis especially if compared to the online measurement of input function by vessel catheterization. On the one hand, it is a relatively simple and non-invasive procedure that reduces the animal stress and thus the alteration of physiological parameters. On the other hand, it allows longitudinal tracking since it is non-invasive and the animal can be reused. However, it has certain limitations that cannot be neglected. First, it requires a correct visualization of the vascular space for appropriate delineation of a volume of interest (VOI) to obtain the correspondent blood time activity curve. Especially in preclinical research, this is challenging since the spatial resolution of PET scanners, in most of the cases, results to be insufficient for the correct visualization of blood vessels in small animals. The limited spatial resolution also results in the presence of several artefacts such as spillover effect (if the delineated VOI is surrounded by a region with higher concentration of radioactivity) and spill out effect (if the VOI is surrounded by a region with lower concentration of radioactivity). These, ultimately, lead to over- or underestimation of the radioactivity

[1] Zanotti-Fregonara, P., Liow, J.-S., Fujita, M., Dusch, E., Zoghbi, S. S., Luong, E., Boellaard, R., Pike, V. W., Comtat, C., Innis, R. B. Image-Derived Input Function for Human Brain Using High Resolution PET Imaging with [^{11}C](R)-rolipram and [^{11}C]PBR28. *PLoS ONE* (2011) doi:10.1371/journal.pone.0017056.

concentration in the VOI, respectively[2,3,4]. Generally speaking, delineation of VOIs is performed in: (I) the vena cava, which is clearly visible in the first frames of dynamic images when the tracer is administered via one of the lateral tail veins; (II) the left ventricle, which is clearly visible in early frames or late frames when the tracer is uptaken by the myocardium; or (III) the aortic arch, also visible in early frames after administration. Obviously, the determination of the IDIF from the vena cava results in venous input function, while delineation of the VOI in the left ventricle or the aortic arch better represent arterial IF.

Second, it has to be noted that image derived input functions provide information about the total amount of radioactivity in the blood pool. However, with some notable exceptions such as 2-deoxy-2-(^{18}F)fluoro-D-glucose ([^{18}F]FDG), almost all tracers produce variable (and sometimes significant) amounts of radiometabolites, which cannot be identified on the PET images, but contribute to the overall signal. As a consequence, if the metabolism is not negligible, there is always an overestimation of the real concentration of parent (non-metabolised) compound in blood[5], and such overestimation varies with time as the presence of metabolites in blood is not constant. In this scenario, data from PET images must be carefully corrected for resolution effects and metabolism, which ultimately means that blood samples have to be withdrawn to determine the real concentration of radioactivity using a gamma counter, and analysed by *e.g.* high performance liquid chromatography (HPLC) to determine the percentage of unmodified parent compound in the plasmatic fraction. With this additional information, the IDIF can be appropriately corrected and used in subsequent kinetic analysis.

The second option to determine IF is the online (real time) measurement of arterial input function, which consists of catheterising one of the animal's main arteries to create an extracorporeal circulation by-pass[6]. The blood is circulated through a radioactivity detector and

[2] Hoffman, E. J., Huang, S.-C., & Phelps, M. E. Quantitation in Positron Emission Computed Tomography. *Journal of Computer Assisted Tomography* (1979) doi:10.1097/00004728-197906000-00001.

[3] Kessler, R. M., Ellis, J. R., & Eden, M. Analysis of Emission Tomographic Scan Data: Limitations Imposed by Resolution and Background. *Journal of Computer Assisted Tomography* (1984) doi:10.1097/00004728-198406000-00028.

[4] Lehnert, W., Gregoire, M.-C., Reilhac, A., & Meikle, S. R. Characterisation of partial volume effect and region-based correction in small animal positron emission tomography (PET) of the rat brain. NeuroImage (2012) doi:10.1016/j.neuroimage.2012.02.032.

[5] Ghosh, K. K., Padmanabhan, P., Yang, C.-T., Mishra, S., Halldin, C., Gulyás, B. Dealing with PET radiometabolites. *EJNMMI Research* (2020) doi:10.1186/s13550-020-00692-4.

[6] Mann, T., Kurth, J., Möller, A., Förster, J., Vollmar, B., Krause, B. J.,bWree, A., Stenzel, J., Lindner, T. Continuous Blood Sampling in Small Animal Positron Emission Tomography/Computed Tomography Enables the Measurement of the Arterial Input Function. *Journal of Visualized* Experiments (2019) doi:10.3791/59701.

the concentration of radioactivity is measured in a continuous and real time mode. If the detector is appropriately calibrated, this determination of the arterial input function is not affected by problems linked to spatial resolution and artefacts, and blood samples can be obtained to perform subsequent HPLC analysis and determine the fraction of parent compound that remains unchanged. Still, the major disadvantage is the costly and time-consuming preparation of the animal, which requires a proper preparation of the operator in charge of the surgery. In addition, all the extracorporeal circulation system (including tubing and detector cell) has a dead volume that result in a time delay between real and determined input functions, and alteration of the curve profile due to diffusion[7]. Finally, this method is very invasive and requires surgery, and hence it is considered as a terminal procedure which limits the longitudinal evaluation of the animals.

Venous-based input function can be an alternative method when, beside avoiding problems linked to spatial resolution and artefacts, the catheterization is not possible. It consists of replacing continuous arterial blood sampling with discrete venous blood sampling. Venous samples can be readily obtained from one of the lateral tail veins (particularly in rats) and the procedure is minimally invasive, which enables longitudinal studies. However, this alternative has also limitations: first, the input function corresponds to venous blood, which is less appropriate than arterial blood to apply subsequent kinetic analysis models. The relation between arterial and venous input functions changes with time, differs from one radiotracer to another and shows high inter-subject variability[8,9]. Additionally, in this approach the operator needs to be close to the investigated animal, with the consequent radiation exposure. Finally, only a limited number of discrete samples can be obtained, thus impacting the temporal resolution of the time activity curve.

Population-based input function (PBIF) determination is an alternative to the above-mentioned methods. This is applied when the shape of the arterial input function shows low inter-subject

[7] Meyer, E. Simultaneous correction for tracer arrival delay and dispersion in CBF deasurements by the $H_2{}^{15}O$ autoradiographic method and dynamic PET. *J Nucl Med* (1989).

[8] Nishizawa, S., Leyton, M., Okazawa, H., Benkelfat, C., Mzengeza, S., & Diksic, M. Validation of a Less-Invasive Method for Measurement of Serotonin Synthesis Rate with α-[^{11}C]Methyl-Tryptophan. *Journal of Cerebral Blood Flow & Metabolism* (1998) doi:10.1097/00004647-199810000-00009.

[9] Zanotti-Fregonara, P., Leroy, C., Roumenov, D., Trichard, C., Martinot, J.-L., & Bottlaender, M. Kinetic analysis of [^{11}C]befloxatone in the human brain, a selective radioligand to image monoamine oxidase A. *EJNMMI Research* (2013) doi:10.1186/2191-219x-3-78.

variability. If this is the case, an average input function is determined invasively (*e.g.* by cannulating one artery) in a group of animals. Then, it is assumed that the shape of the input function will be similar in all animals of the same species and strain. In subsequent animals, only one blood sample is obtained at a pre-defined time point and its concentration of radioactivity is measured in a gamma counter. The input function is assumed to be equal to the average IF corrected by the concentration value obtained from the blood sample that has been withdrawn. Although is not affected by problems linked to image quality and resolution, and radiometabolite correction can be inherently considered, the variability between subjects may affect the suitability of the PBIF[10].

The narrative above clearly shows that the determination of the arterial input function for the evaluation of PET tracers is challenging and remains unresolved. All the approaches have pros and cons, and the selection of one or another will depend on the availability of animals, the need for longitudinal studies, the presence of metabolism, etc.

During the execution of this PhD thesis, we decided to compare two different methods for the determination of the input function in our hands, in order to select the most appropriate methodology for the determination of pharmacokinetics properties of the triazole-based FKBP12-Ryr stabilizers AHK-1 and AHK-2, which will be discussed extensively in the next chapter. The two approaches assayed were (I) image-derived input function (IDIF) and (II) online measurement of arterial input function by vessel catheterization. In both cases [^{18}F]FDG, a radiotracer widely used in the clinical field for the early diagnose and evaluation of the response to treatment of different cancer types, was used in healthy Sprague Dawley rats.

[10] Zanotti-Fregonara, P., Hirvonen, J., Lyoo, C. H., Zoghbi, S. S., Rallis-Frutos, D., Huestis, M. A., Morse, C., Pike, V. W., Innis, R. B. Population-Based Input Function Modeling for [^{18}F]FMPEP-d2, an Inverse Agonist Radioligand for Cannabinoid CB1 Receptors: Validation in Clinical Studies. *PLoS ONE* (2013) doi: 10.1371/journal.pone.0060231.

4.2 OBJECTIVES

The specific objectives of this chapter are:

1. To compare two different methods to determine the input function, in terms of: (I) simplicity; and (II) accuracy.

4.3 RESULTS AND DISCUSSION

4.3.1 GENERAL CONSIDERATIONS

[^{18}F]FDG is the most commonly used PET radiotracer both in clinical diagnostics and basic and applied research. In this radiotracer, an ^{18}F atom is incorporated in substitution of the hydroxyl group on the 2-carbon position of a glucose molecule. After administration to a living organism, [^{18}F]FDG is distributed all over the organism and taken up by cells through the same pathways as glucose (GluT, glucose transporters). Because the physiological metabolic steps after phosphorylation cannot occur due to the presence of the fluorine atom, [^{18}F]FDG accumulates within cells in proportion to the rate of utilization of glucose in a process known as metabolic trapping (Fig. 4.1).

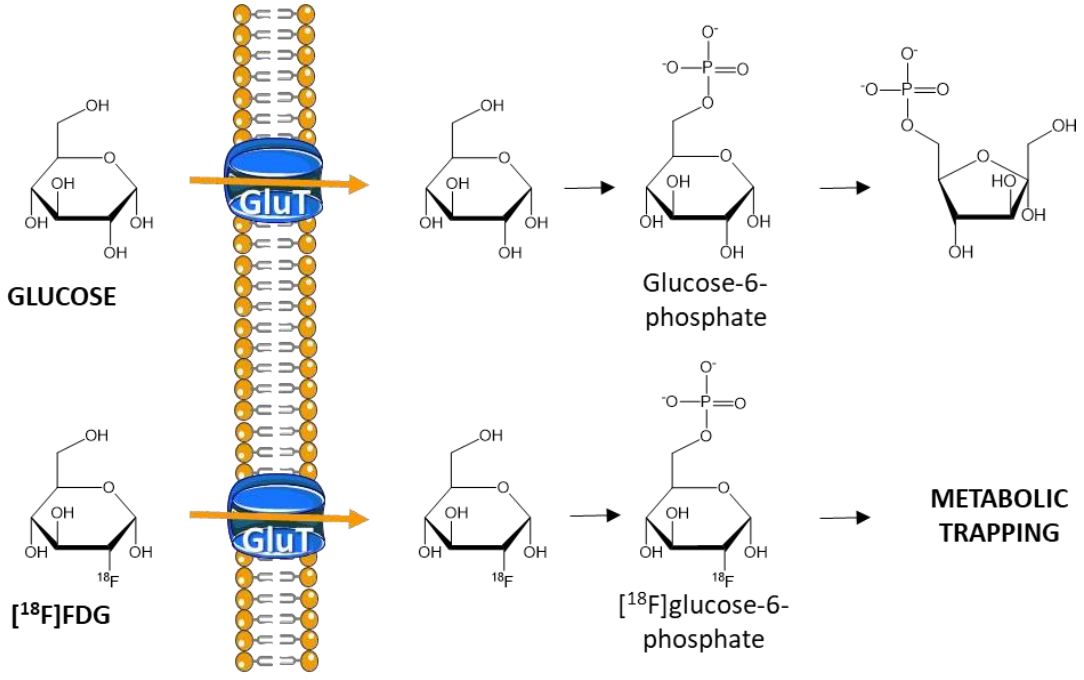

Fig. 4.1: Intracellular metabolism of glucose and [^{18}F]FDG. Both are taken up by cells by means of glucose transporters (GluT). Once into the cell, they are phosphorylated to glucose-6-phosphate and [^{18}F]glucose-6-phosphate, respectively. Unlike glucose-6-phosphate, [^{18}F]glucose-6-phosphate does not undergo further metabolism and is trapped in the cell.

After intravenous administration, [^{18}F]FDG remains as the only radioactive species in blood. In other words, no metabolites are found in blood. Because of this, it was used within the aim of this chapter. The [^{18}F]FDG solution was kindly provided by CURIUM Spain and hence a description of its production has not been included in this thesis.

Once the objectives were settled and [^{18}F]FDG was selected as standard radiotracer for this kind of study, we first investigated the experimental setting necessary for the measurement of input function especially in the case of the online measurement by vessel catheterization. To that aim, after a careful literature search, we selected a procedure previously reported[11] and which was implemented in our group [12]. Briefly, to create an extracorporeal circulation by-pass, the femoral artery and the femoral vein of the rat were catheterized using a fine bore polythene tubing. The catheters were then connected to an in-house developed system composed by a peristaltic pump and gamma-radiation coincidence detector to enable the extracorporeal circulation of blood and continuous measurement of radioactivity in the blood following the scheme in Fig. 4.2.

[11] Mann, T., Kurth, J., Möller, A., Förster, J., Vollmar, B., Krause, B. J., Were, A., Stenzel, J., Lindner, T. Continuous Blood Sampling in Small Animal Positron Emission Tomography/Computed Tomography Enables the Measurement of the Arterial Input Function. *Journal of Visualized Experiments* (2019) doi:10.3791/59701.

[12] Guarra, F., Terenzi, A., Pirker, C., Passannante, R., Baier, D.; Zangrando, E., Gómez-Vallejo, V., Biver, T., Gabbiani, C., Berger, W.; Llop, J., Salassa, L. 124 I Radiolabeling of a Au III -NHC Complex for In Vivo Biodistribution Studies. *Angew. Chem.* (2020) doi:10.1002/ange.202008046.

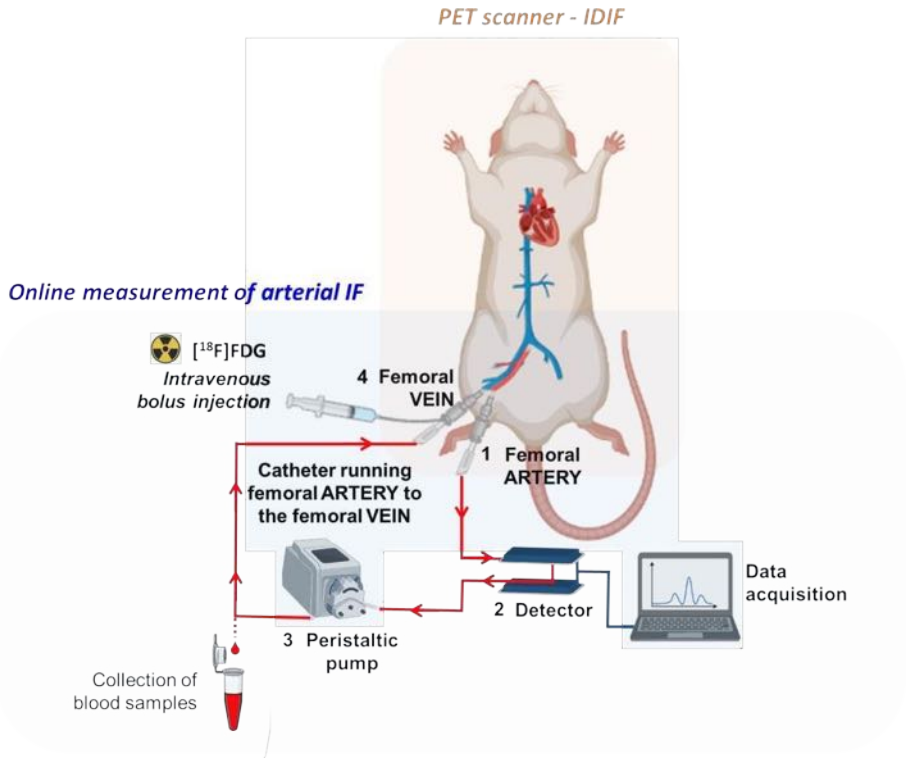

Fig. 4.2: Schematic representation of experimental setting used for the determination of both Image-Derived Input Function (IDIF) and arterial input function by continuous measurement of radioactivity in the blood. Two catheters were first inserted into the femoral artery and vein, respectively. The blood was pumped through a radioactive detector using a peristaltic pump and an extracorporeal circulation system was created. The animal was remained in the PET scanner where dynamic images were acquired, and both IFs were determined.

4.3.2 IMAGE-DERIVED INPUT FUNCTION

Image-derived input functions (IDIFs) are the time activity curves obtained from regions over the major vascular structures, such as the ventricular cavity, aorta, or large arteries or veins[13]. Depending on the scanner and on the subject used during the study, the aorta or in general large arteries could be difficult to visualize. For this reason, in the current work our approach was to determine the IDIFs from: (I) the left ventricular cavity after intravenous administration of [^{18}F]FDG; this is clearly visible at late time frames due to radiotracer uptake in the myocardium; and (II) from the inferior vena cava, which was visible during the first-time frames due to the fact that the radiotracer was administrated through the femoral vein.

[13] Lanz, B., Poitry-Yamate, C., Gruetter, R. Image-Derived Input Function from the Vena Cava for ^{18}F-FDG PET Studies in Rats and Mice. *Journal of Nuclear Medicine* (2014) doi:10.2967/jnumed.113.127381.

For each animal, the image-derived input functions were determined simultaneously to the online (real time) measurement of arterial input function by the external gamma-radiation coincidence detector. In this way, the three input functions could be directly compared to each other. Experimentally, before the PET acquisition, the femoral artery and the femoral vein were cannulated (see section 4.3.2 for a detailed explanation of the cannulation process). The animal was then placed in the PET scanner with the hearth and the inferior vena cava within the field of view (FOV), and the extracorporeal circulation was started. Concomitantly with the start of dynamic PET acquisition and the online measurement of IF, a solution of [^{18}F]FDG was administrated through the femoral vein (Fig. 4.3a).

In small animal the major vascular structures, although they might be visualized in the images, are small compared to the spatial resolution of the scanner. Consequently, vascular radioactivity can be blurred into adjacent tissues and vice versa. For example, when the image-derived input function is calculated from the left ventricle, two effects have to be considered and corrections applied (Fig. 4.3b). During the first frames, the radioactivity is mainly concentrated in the blood. Because the concentration of radioactivity in the blood is higher than that in the surrounding tissue, the determination of the concentration of radioactivity in blood is biased due to the blurring into surrounding tissue (partial volume effect). At late time points, on the other hand, the radioactivity starts to be distributed to different organs and the opposite effect may occur. It is well know that, in the case of [^{18}F]FDG, for example, at late time points after injection, the radiotracer accumulates in myocardial tissue. When this occurs, the radioactivity in the myocardium is higher than that in the blood. This fact helps in delineating the VOI within the left ventricle. However, the radioactivity of the myocardium spills into the left ventricle. Hence, the concentration of radioactivity measured in the myocardium is overestimated (spillover effect). Depending on which effect dominates, the real radioactivity concentration can be higher or lower compared to the one directly measured from the image without any correction.

On the other hand, when the image-derived input function is calculated from the inferior vena cava, other factors need to be taken into account. First, the IF obtained is a venous-based IF, and not arterial. Second, since in general the inferior vena cava is surrounded by areas without uptake of radioactivity, it can be assumed that, in general terms, one can expect an underestimation of radioactivity concentration unless the partial volume effect is considered (Fig. 4.3c).

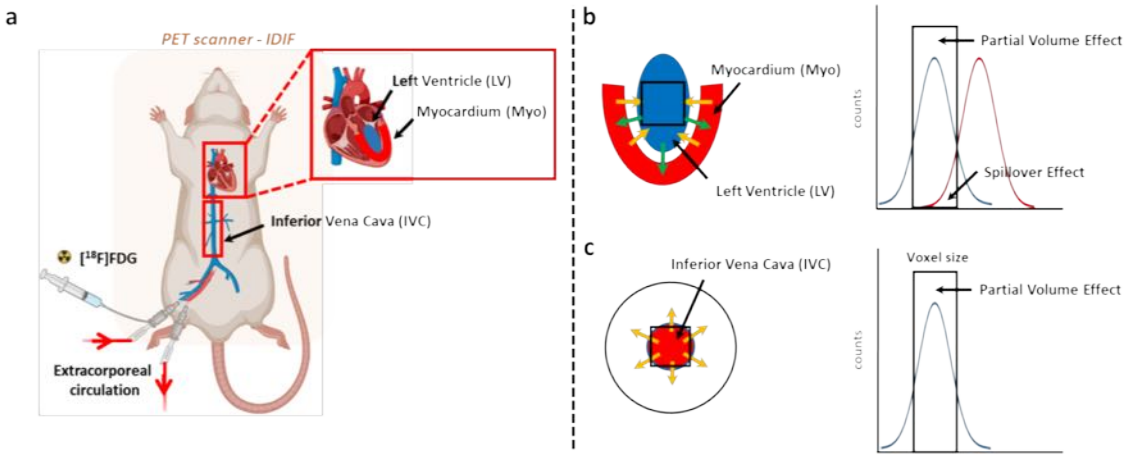

Fig. 4.3: a) Image-derived input function. After the cannulation of femoral artery and vein, the animal was moved into the PET scanner and the extracorporeal circulation was started. Concomitantly with the start of PET acquisition and measurement of online arterial input function, a solution of [^{18}F]FDG was administrated through the femoral vein. The left ventricle and the inferior vena cava, where the image-derived input functions were obtained, are indicated. b) Effects to consider when the image-derived input function is obtained from the left ventricle. Due to a partial volume effect, the radioactivity from the LV is blurred into adjacent tissue (green arrows in the figure) contributing to an underestimation of radioactivity concentration (blue curve in the left part of the image). Due to a spillover effect, the radioactivity from the myocardium is blurred into the left ventricle (yellow arrows in the figure) contributing to an overestimation of radioactivity concentration (red curve in the left part of the image). c) Effect to consider when the image-derived input function is obtained from the inferior vena cava. Due to a partial volume effect, the radioactivity from the vein is blurred into adjacent tissue (yellow arrows in the figure) contributing to an underestimation of radioactivity concentration (blue curve in the left part of the image).

Evaluation of dynamic images, after intravenous administration of [^{18}F]FDG, showed the typical biodistribution pattern for the tracer (Fig. 4.4). High radioactivity at early time points was present in the inferior vena cava; high accumulation of radioactivity was detected in the kidneys and the bladder due to elimination mainly via urine, while uptake was observed in the myocardium (organ that is known to consume glucose) at late time points after administration. As a result, the curve obtained by drawing a VOI in the inferior vena cava was expected to be underestimated due to partial volume effect and, the curve obtained by drawing a VOI in the ventricular cavity was expected to account for the contribution of the presence of radioactivity in the left ventricle, plus the contribution of the concentration of radioactivity in the myocardium. Noteworthy, in this last case, the cardiac and respiratory motion creates additional signal cross-contamination between vascular structures and surrounding tissues making more difficult the proper

quantification[14]. Considering this and all the limitation of an IDIF mentioned above, we proposed to correct data from PET images using two different methods: (I) by using correction factors obtained with a phantom study as previously reported [15] ; and (II) by using the software COmpartment Model Kinetic Analysis Tool (COMKAT).

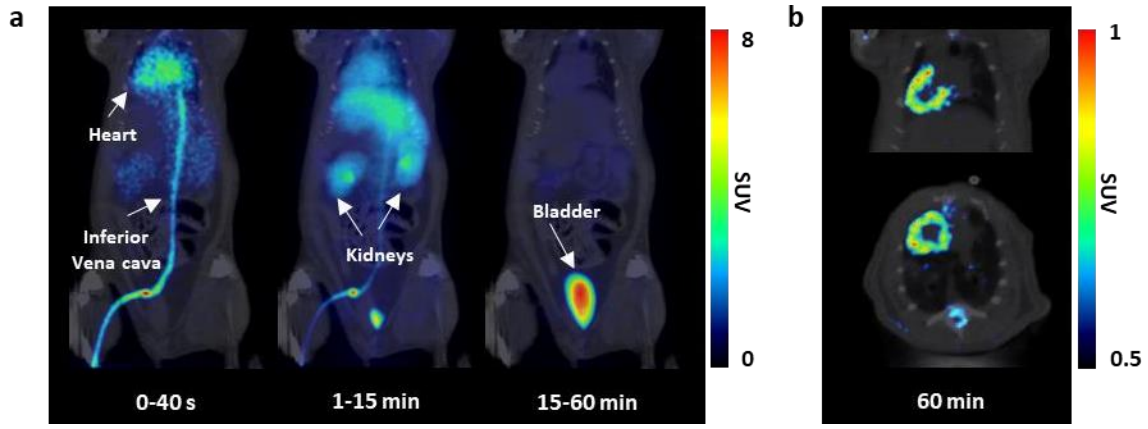

Fig. 4.4: Biodistribution of [^{18}F]FDG after intravenous administration through the femoral vein. a) Representative whole body coronal PET images (projections) obtained at different time points after administration. PET images have been co-registered with a representative CT slice for the localization of the radioactive signal. Positions of the inferior vena cava, heart, kidneys and bladder are indicated. b) Representative coronal (top) and axial (bottom) PET slices obtained at 60 minutes after administration, when the myocardium uptake is visible. PET images have been co-registered with CT image for the localization of the radioactive signal.

Our first approach to obtain corrected image derived input functions by drawing a volume of interest in the inferior vena cava and the left ventricle, was carried out by using two correction factors calculated from studies with phantoms. The first one was the partial volume effect factor obtained using the hot rod phantom (Fig. 4.5a) and the recovery coefficient (RC) curve generated from it showed in Fig. 4.5b. The hot rod phantom is a tool usually used to evaluate spatial resolution of PET and SPECT systems. It consists of fillable rods of different size. In this work, at least one rod per dimension was filled with a known amount of radioactivity and a static PET image was acquired. Using PMOD image analysis software, volumes of interest were drawn in

[14] Daouk, J., Fin, L., Bailly, P., & Meyer, M.-E. Respiratory-gated positron emission tomography and breath-hold computed tomography coupling to reduce the influence of respiratory motion: Methodology and feasibility. *Acta Radiologica* (2009) doi:10.1080/02841850802627437.

[15] Pérez-Campaña, C., Gómez-Vallejo, V., Puigivila, M., Martin, A., Calvo-Fernández, T., Moya, S. E.,Larsen, S. T., Gispert, J., D., Llop, J. Assessing Lung Inflammation After Nanoparticle Inhalation Using 2-deoxy-2-[^{18}F]fluoro-d-glucose Positron Emission Tomography Imaging. *Molecular Imaging and Biology* (2013) doi:10.1007/s11307-013-0682-3.

the different filled rods to determine the concentration of radioactivity detected by the scanner. The VOI-derived radioactivity concentration values measured for the different rods were divided by the true activity concentration to obtain an RC curve covering the whole rod size range (Fig. 4.5 b). Among the different rods, the ones with 1.2 mm and 2.4 mm diameter, were the ones with closest sizes to those of the inferior vena cava and left ventricle, respectively.

The second correction factor calculated was the spillover effect factor. This was determined using the cold rod phantom (Fig. 4.5c) which consists of a filled cylinder with cold spots inserted. Also in this case, the phantom was filled with a known amount of radioactivity and a static PET image was acquired. To calculate the spillover coefficient factor, a VOI equivalent with the one drawn in the ventricle cavity (2.4 mm) was drawn in the middle of the cold spot with 6 mm dimeter dimension, which simulates the heart segment delineated by the myocardium. The VOI-derived radioactivity concentration was divided by the real activity concentration to obtain the spillover coefficient (SC) used for correction (Fig. 4.5d).

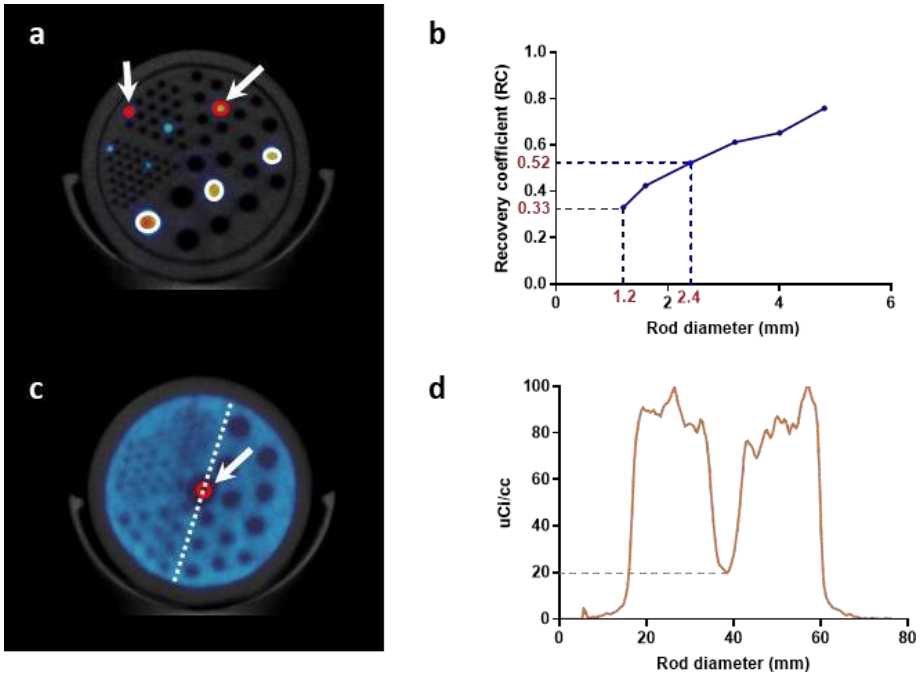

Fig. 4.5: a) PET-CT image (axial view) of hot rod phantom. VOIs used for quantification are indicated. b) Recovery coefficient (RC) curve generated from hot rod phantom. c) PET-CT image (axial view) of cold rod phantom. VOI used to obtained image derived input function (IDIF) from ventricle cavity is shown in red. d) Radioactivity profile along the white dotted line in c to calculate the contribution of surrounding high activity region into VOI.

Once the corrections factors had been calculated from phantom studies, we focused our attention firstly on the image-derived input function obtained from the left ventricle. This vascular structure in fact was the only one visible in the PET image that could reflect the arterial blood distribution of the radiotracer. As mentioned above, at early time points after radiotracer administration the region is surrounded by regions with low uptake, while at late time points a significant accumulation is visible in the myocardium (see Fig. 4.4b). Because of this, corrections for both partial volume effect and spillover effect were necessary. Since the VOI that was drawn in the myocardium had a diameter of 2.4 mm, the recovery coefficient used for the partial volume effect correction was 0.52 (Fig. 4.5c). On the other hand, the spillover contribution by myocardium into a VOI with the same dimension of the one drawn in left ventricle was calculated to be 19% (Fig. 4.5d). Considering this, the IDIF obtained from the left ventricle was corrected by partial volume effect and by spillover using Eq. 4.1:

$$IDIF = \frac{C_{lv}}{RC} - (C_M \times SC) \qquad \text{Eq. 4.1}$$

where C_{lv} is the concentration of radioactivity in the left ventricle, RC is the recovery coefficient, C_M is the concentration of radioactivity in the myocardium and SC is the spillover coefficient.

As shown in Fig 4.6, the corrected IDIF obtained confirms that, when corrections are not applied, the concentration of radioactivity in blood is underestimated. Between the two effects considered, the partial volume effect is the most relevant, and therefore the corrected IDIF curve resulted to be practically isomorphic but with higher values with respect to the non-corrected curve.

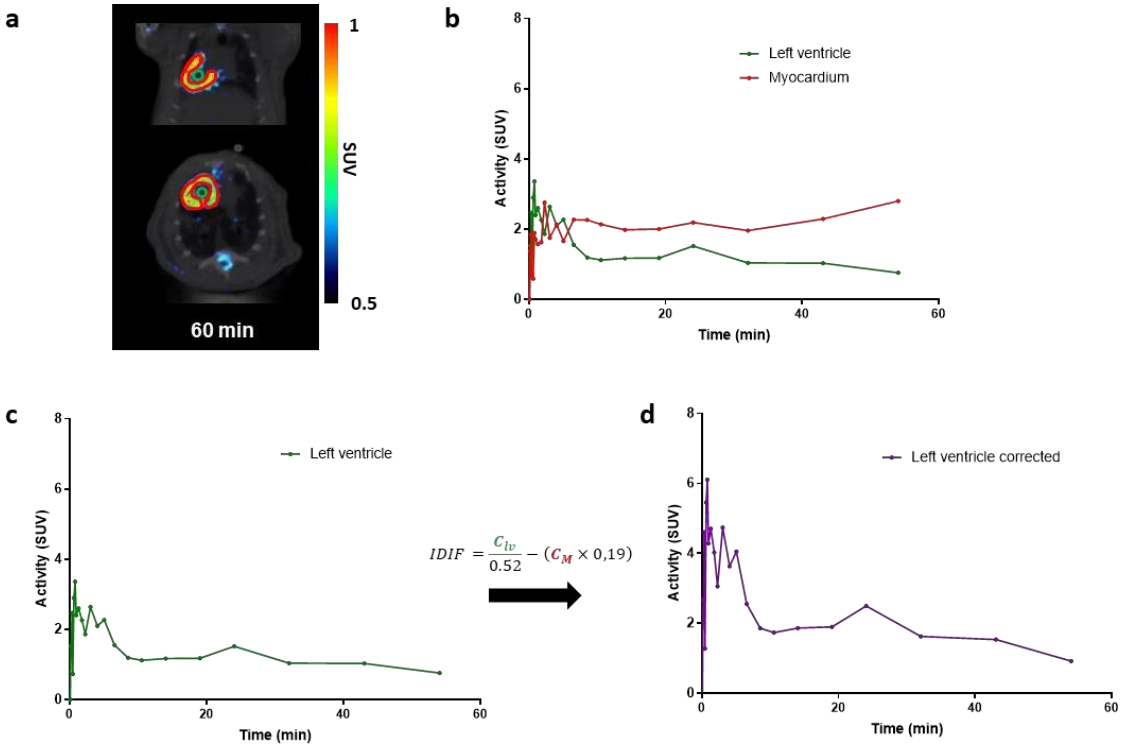

Fig 4.6: a) Representative coronal (top) and axial (bottom) PET slices obtained at 60 minutes after administration where the myocardium uptake is visible. PET images have been co-registered with a representative CT slice for the localization of the radioactive signal. The VOIs used for the quantifications are shown. b) Representative time-activity curves obtained from VOIs drawn in the myocardium (red line) and in the left ventricle (green line). c) Representative image-derived input function (IDIF) obtained from ventricular activity before spillover and partial volume effect correction. d) Image-derived input function (IDIF) obtained from ventricular activity after spillover and partial volume effect correction.

The second approach to obtain a corrected IDIF from ventricular cavity was by using the software COmpartment Model Kinetic Analysis Tool (COMKAT) that consists of functions for defining compartment models to obtain model output and estimating parameter values[16]. The method validated to correct the IDIF for spillover and partial volume effect assumes that the IDIF from the ventricle cavity is a mixture of the true input function and the myocardium uptake. Experimentally, by introducing the original values of the time activity curves of activity distribution in myocardium and left ventricle (red and green curve in Fig. 4.6) the software is able to estimate the curve corrected by spillover and partial volume effect, also called model-

[16] Muzic, R. F., Cornelius, S. COMKAT: Compartment Model Kinetic Analysis Tool. *Journal of Nuclear Medicine* (2001).

corrected input function (MCIF). The kinetic model implemented by Feng in 1993[17] and used by COMKAT consist of fitting the input functions obtained from the left ventricle and myocardium to Model 2 in reference 17.

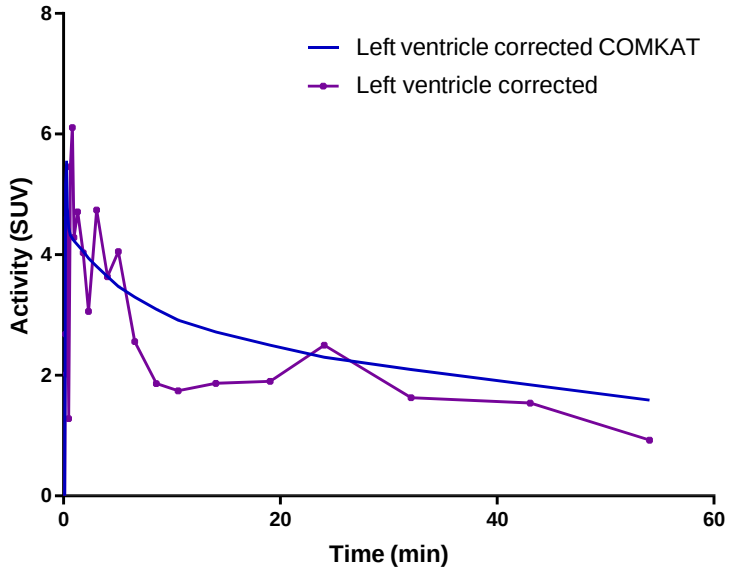

Fig 4.7: Representative image-derived input functions (IDIF) obtained from ventricular activity corrected by using the software COmpartment Model Kinetic Analysis Tool (blue curve) and by using correction factors obtained with the phantom study (purple curve).

Although the corrected IDIF obtained by using this method does not match perfectly, in terms of absolute values, with the corrected IDIF obtained by applying Eq. 4.1 to the original image values, the trend of the two curves is closely correlated (Fig. 4.7), confirming that the two correction methods are similar, and both can be applied to the determination of the corrected IDIf for our subsequent studies.

We subsequently explored the possibility to determine the IDIF from the vena cava. Although the vena cava is a small structure in comparison to the resolution of the PET scanner, it was possible to draw a VOI at short time frames due to the fact that the radiotracer administration through the femoral vein made this vessel clearly visible. The diameter of the VOIs drawn in the vena cava had a diameter of 1.2 mm. As shown in the Fig. 4.5 the recovery coefficient for a VOI

[17] Feng, D., Huang, S.-C., Wang, X. Models for computer simulation studies of input functions for tracer kinetic modeling with positron emission tomography. *International Journal of Bio-Medical Computing* (1993) doi:10.1016/0020-7101(93)90049-c.

of 1.2 mm is 0.33, which was applied to prevent underestimation of the concentration of radioactivity. Although, compared with other anatomical structures, the vena cava should be much less affected by spillover contamination from neighbouring tissues, we did not discard the possibility that depending on where the VOI was drawn, it might be necessary to consider the contribution from adjacent organs (spillover). To evaluate spillover from surrounding tissues, we defined three different VOIs, composed of 1.2 mm diameter discs on 20 consecutive slices, in three different positions along the vena cava (Fig. 4.8a). In all cases, the IDIFs obtained present 2 sharp peaks (Fig. 4.8b), corresponding to the passage of [^{18}F]FDG followed by the saline solution, which is administrated to rinse the catheter. At early time points, progressively higher values were observed from VOI 1 to VOI 3 and, since by visual inspection of the image no accumulation of [^{18}F]FDG was observed in adjacent tissues, we concluded that the spillover effect was not affecting the quantification of [^{18}F]FDG at early time points. The reason why the values of radioactivity concentration were different, depending on where the VOI was drawn, was because the radiotracer was progressively diluting in the blood circulation along the passage through the inferior vena cava (Fig. 4.8c).

The IDIFs obtained from the inferior vena cava were corrected only by partial volume effect (Fig. 4.8 d) using Eq. 4.2.

$$IDIF = \frac{C_{vc}}{RC} \qquad \text{Eq. 4.2}$$

where C_{vc} is the concentration of radioactivity in the vena cava and RC is the recovery coefficient.

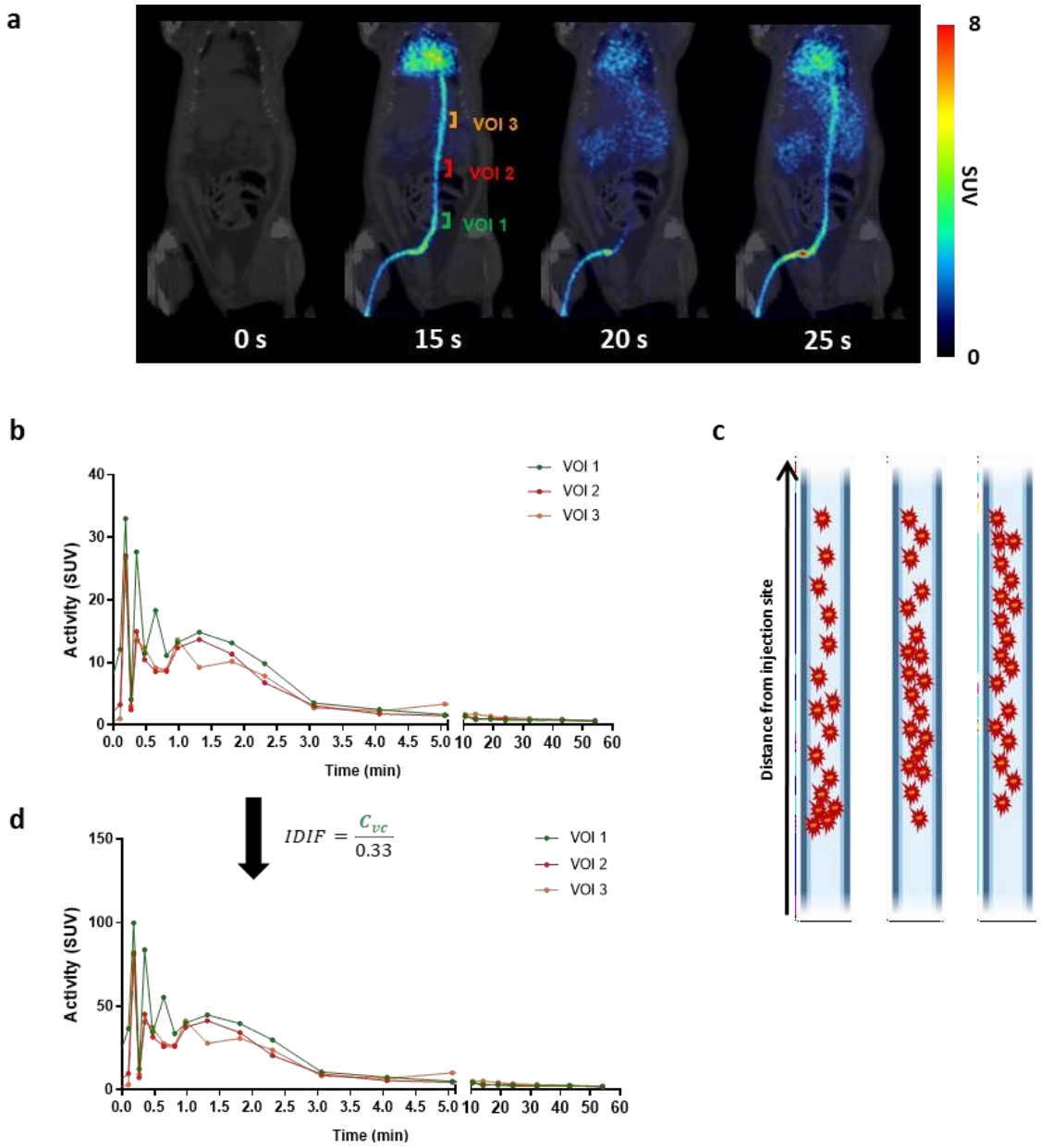

Fig. 4.8: a) Representative coronal PET images where [^{18}F]FDG first passage in vena cava is visible. PET images have been co-registered with representative CT slices for localization of the radioactive signal. The different VOIs used to determine the IDIF are indicated. b) Representative image-derived input functions obtained from VOIs drawn in different position on the vena cava. c) Image-derived input function obtained from VOIs drawn in different positions on the vena cava corrected by partial volume effect. d) Schematic illustration of the [^{18}F]FDG dilution effect through the inferior vena cava over time.

Among the three corrected image derived input functions obtained from the inferior vena cava, we arbitrarily chose the one obtained from VOI 2, which we considered to be the less affected

by the surroundings at later time points after injection. Comparing this curve, with the corrected IDIF obtained from the ventricular cavity, the radioactivity in the first one reached a higher value at shorter time frames while the values at longer time points are similar for both curves (Fig. 4.9). The differences between the two curves can be explained by the dilution effect of radiotracer introduced above. In fact, before arriving to the left ventricle, the radiotracer covers a significant distance from the inferior vena cava. Initially, it enters the right atrium. Then it flows from the right atrium into the right ventricle and then into the lungs via the pulmonary artery. From the lungs, blood flows into the left atrium and finally into the left ventricle. Thus, a significant dilution of the radioactivity takes place.

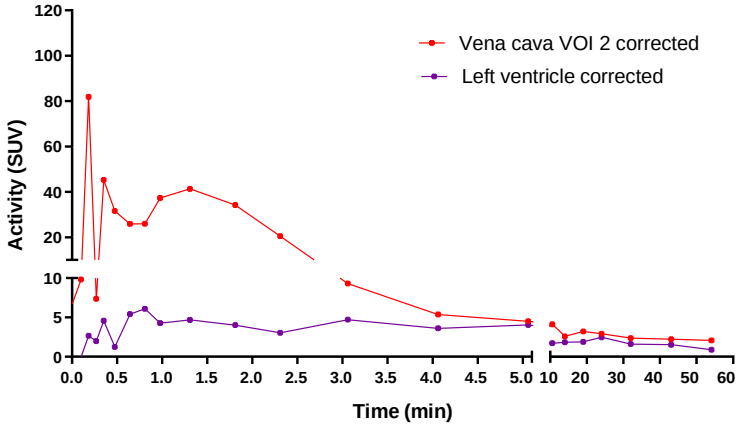

Fig. 4.9: Representative corrected image-derived input function obtained from VOI 2 drawn in the inferior vena cava (red curve) compared with a representative corrected image-derived input function obtained from the left ventricle (purple curve).

IDIFs from the ascending aorta, left ventricle or in general from large vessels are largely used for practical reason[18] although AIF is considered the gold standard for the determination of time-activity curve. There are several factors that can affect the accuracy of IDIFs such as partial volume effect, spillover from surrounding areas, as already discussed, but also patient movement and finally the noise introduced by the limited number of counts acquired in each time frame, particularly for short frames. All these factors have a greater effect for small VOI size due to the limited spatial resolution of preclinical PET scanners.

[18] Iida, H., Rhodes, C. G., de Silva, R., Araujo, L. I., Bloomfield, P. M., Lammertsma, A. A., Jones, T. Use of the left ventricular time-activity curve as a noninvasive input function in dynamic oxygen-15-water positron emission tomography. *J Nucl Med.* (1992).

The ventricle cavity was the only major vascular region identified in the image that better could represent and/or replace the gold standard AIF. The corrected IDIFs obtained from this region showed similar trends and absolute values, irrespective of the correction method chosen. The fact that the IDIFs manually corrected compared well with the ones corrected using the COMKAT software (Fig. 4.7) suggest that the partial volume effect and spillover correction factors obtained from the phantom studies provide reliable data. The partial volume effect factor allowed us to correct the error introduced by the fact the ROI drawn in the ventricle cavity is small when compared with the spatial resolution of the scanner, which results in an underestimation of radioactivity concentration. On the other hand, the spillover effect factor allowed for correcting the error introduced by the spill-in of radioactivity from surrounding high activity regions, which result in an overestimation of radiotracer uptake, if not considered. The error introduced due to subject movement, despite particularly relevant when the organs of interest are the heart or lungs, were not considered in our study. In any case, this can be easily corrected intrinsically through special acquisition protocols.

Considering the positive results obtained by manual correction of the IDIF, when we investigated the possibility to estimate the IDIF from the vena cava we only applied the manual method. Noteworthy, the volume of interest was expected to be located in a region with low uptake in the surrounding tissue, and hence we just applied partial volume effect correction. Still, in order to validate our method and confirm that spillover effect was negligible, particularly at long acquisition times when accumulation in the kidneys and elimination through the bladder could be significant, we decided to draw three different VOIs along the vena cava (Figure 4.8a). Although the three curves resulted to be almost equivalent, higher values were obtained when transitioning from VOI 1 to VOI 3 (Figure 4.8b and d). This trend was observed in all animals used for the study (n=3) and was associated with the dilution effect as the radiotracer is distributed in the blood stream (Figure 4.8c). Having to make a decision on the position in which to draw the VOI in order to reduce the error when different animals were analysed, we decided to draw the VOI in the middle part of the vena cava. Even though no influence of the spillover effect was observed in this anatomical region, visual inspection of the images at late acquisition times confirmed that this region had less surrounding radioactivity.

The radiotracer is progressively diluted in the blood stream after bolus injection. As a consequence, the corrected IDIFs from vena cava (which is closer to the injection site) presented

higher maximum values when compared with the corrected IDIF from left ventricle. Considering this and that the IDIFs from vena cava represents a venous-based IF we selected the corrected IDIF from left ventricle for further comparison with the online arterial blood input function.

4.3.2 Online arterial blood input function

As mentioned above, the determination of the temporal blood time-activity concentration also known as arterial input function (AIF) is a key point, especially in the development process of a new radiotracer. Considering all the limitation in terms of spatial resolution of preclinical PET camera, which results in the presence of several artefacts, and the impossibility of distinguish the signal of the parent compound from the signal of its radioactive metabolites unless blood samples are withdrawn and processed, we decided to investigate the suitability of the vessel catheterization method for the determination of the AIF.

This method consists of creating an extracorporeal circulation by introducing surgically a catheter into main blood vessels, a vein, and an artery. To that aim, the extracorporeal circulation of the arterial blood was achieved by externally by-passing the femoral artery and the femoral vein of the rat using a fine bore polythene tubing (ID 0.58 mm, OD 0.98 mm). The catheters were then connected to the in-house developed system composed by a peristaltic pump and gamma-radiation coincidence detector (Bioscan, B-FC-4100). The femoral artery catheter, the gamma detector, the peristaltic pump, and the femoral vein catheter were thus connected in series, to enable the extracorporeal circulation of blood (flow 150 µl/s from femoral artery to femoral vein) and continuous measurement of radioactivity in the blood. The animal was placed into the PET scanner for the simultaneous acquisition of images. Concomitantly with the start of dynamic PET acquisition and the online measurement of IF, a solution of [^{18}F]FDG was administrated through the femoral vein. In the case of online measurement of IF, data was imported in real time to an excel sheet using PLX-DAX add-on for Microsoft Excel (measured in volts). During the acquisition one blood sample was withdrawn to determine the amount of radioactivity of a fixed volume (10 µL) of whole blood in an automatic gamma counter (2470 Wizard, PerkinElmer). This was used to convert data imported with PLX-DAX (Volts) into Bq/ml.

The AIF (Fig. 4.10a) presented several differences compared with the corrected IDIFs previously calculated. First, the measured radioactivity peak appears with a time delay probably due to the distance between the different vascular structures, where the IDIFs were previously calculated,

and the extracorporeal detector. However, as the characteristics of the catheter and the flow rate were known, it was possible to correct for such delay (orange curve, Fig. 4.10b). Second, differences are also present in the shape of the radioactivity concentration after the peak. In the case of IDIFs, the concentration of radioactivity decreases rapidly after the maximum, to reach a plateau at longer times, whereas in the case of AIFs the decrease is less dramatic but constant over time. Due to the dead volume of the catheter that was introduced in the radioactivity detector, a slight broadening of the peak could be expected. However, the progressive decay, which lasts much longer than that observed for IDIFs, must have a different explanation. We hypothesize that the higher sensitivity of the methodology, when compared with PET imaging, and the lack of partial volume and spillover effects, result in a more reliable time-activity curve. It is worth mentioning that the reduction in the catheter diameter or length, which would result in a lower dead volume, may contribute to achieve more accurate AIFs. However, there is a compromise with sensitivity, and hence the dispersion is a phenomenon that, intrinsically, will be always present when a measurement of the concentration of radioactivity is carried out through an extracorporeal circulation. Therefore, different mathematical functions have been developed to correct curves for tracer dispersion[19] but none of them were applied in this context since this was beyond our area of knowledge and the scope of this work.

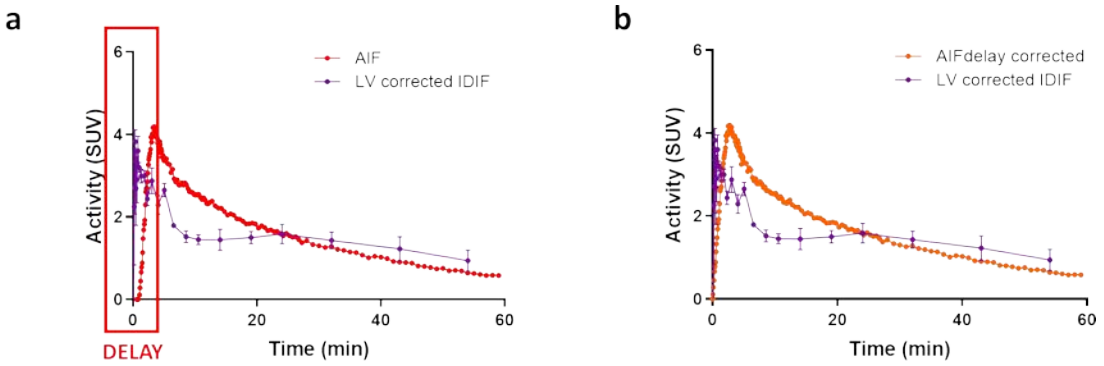

Fig 4.10: Arterial Input Function (AIF) obtained by continuous measurement of radioactivity in the blood before (red curve) (a) and after (orange curve) delay correction (b) compared with the Image Derived Input Function (IDIF) manually corrected by spillover and partial volume effect (purple curves) (a, b).

[19] Munk, O. L., Keiding, S., & Bass, L. A method to estimate dispersion in sampling catheters and to calculate dispersion-free blood time-activity curves. *Medical Physics* (2008) doi:10.1118/1.2948391.

This method although require a time-consuming preparation to catheterize the animal vessels, offers several valuable advantages. On one hand it allows the determination of a real arterial input function. On the other hand, it enables arterial blood sample collection and processing (eventually enabling metabolite analysis) and subsequent correction. Still, it requires quite an invasive surgery, and hence its application in longitudinal imaging studies is severely limited.

4.4 Summary and Conclusions

The work presented in this chapter shows different alternatives for the determination of the input function (IF). We established an experimental setting which enables the simultaneous determination of the IF from dynamic PET images (image derived input function; IDIF) and from and external gamma coincidence detector (online arterial blood measurement IF). For the latter, an extracorporeal circulation of the arterial blood was achieved by externally by-passing the femoral artery and the femoral vein of the rat using a fine bore polythene tubing. As radiotracer, we selected [^{18}F]FDG since after intravenous administration, it remains as the only radioactive species in blood, thus simplifying data processing. As major vascular structures visible in the PET images, we selected the left ventricle and the inferior vena cava. Compared with the online arterial blood measurement, IDIFs resulted to be easier to determine and less invasive, although there was variability in the results depending on the vascular structure selected (vena cava, left ventricle) and even in the position where the VOI was drawn. Our results show that the IDIF obtained from the inferior vena cava shows a high peak at early time points. On the other hand, the IDIF obtained from the left ventricle does not show such a sharp peak, probably due to dilution of the radioactivity in the blood. The determination of the IDIF required for corrections related to spillover and partial volume effects. In addition, IDIFs do not allow the determination of the presence of metabolites in plasma or the blood/plasma drug distribution, unless combined with discrete blood sample extraction. This piece of information might not be relevant for stable radiotracers such as [^{18}F]FDG, but becomes critical when new compounds are evaluated.

Our approach to determine AIF directly enables extraction of arterial blood samples for subsequent analysis. Despite the method is quite invasive and technically challenging, and the data obtained requires for certain corrections including delay and dispersion (the latter not applied in this work), we decided to apply this alternative for subsequent studies (see Chapter 5).

4.5 EXPERIMENTAL PART

4.5.1 GENERAL CONSIDERATIONS

Female Sprague-Dawley rats (8-9 weeks old, Janvier Labs) were used to determine the input function. The animals were maintained and handled in accordance with the Guidelines for Accommodation and Care of Animals (European Convention for the Protection of Vertebrate Animals Used for Experimental and Other Scientific Purposes) and internal guidelines. All experimental procedures were approved by ethical committee of CIC biomaGUNE and local authorities before conducting experimental work. All animals were housed in ventilate cages and fed on standard diet *ad libitum*.

4.5.2 IMAGING SESSION. IMAGE-DERIVED INPUT FUNCTION

Animal preparation – extracorporeal circulation

During experiment, rats (n=3) were kept normothermic using a heating blanket (Homeothermic Blanket Control Unit; Bruker). Anesthesia was induced with 5% isoflurane (IsoFlo®, Abbott Laboratories) and maintained by 2% of isoflurane in 100% O_2. The rat was positioned in supine position on an operating table and the two distal hind limbs were fixed forming an approximately 30° angle with the horizontal plane. The surgical region was scrubbed using Betadine, starting in the centre and making a circular sweep outward. A skin incision was made in the femoral region. Soft tissue was dissected to expose the femoral neurovascular bundle, consisting of femoral vein, artery, and nerve. Fine tip forceps were placed between the artery, vein and nerve and were slowly opened to separate the vessels, exposing an approximately 1 cm length section of artery/vein. The vena profunda femoris was sutured to avoid retrograde bleeding via this vessel, and the sapheno-femoral junction was cauterized. A few millimetres from venatomy, a vascular clip was inserted in the direction of the catheter (to control the flow) and a suture was applied in the opposite direction (to avoid retrograde bleeding). The same operation was carried out both on the femoral vein and femoral artery. An appropriate syringe filled with 50 U/ml Heparin/physiologic saline solution was fixed at the terminus of the catheters and these were filled with heparinized saline solution. On the upper half of the vessel circumference, at a 45° angle, an incision was done and the catheter (fine bore polythene tubing: ID 0.58 mm, OD 0.98 mm) was inserted through the venotomy and advanced to the vascular clip. The vascular clip was then removed, and the catheter advanced distally towards the level of the inguinal ligament. The

catheter was finally secured to the femoral vein/artery proximally and distally with 2 single knots using 4-0 braided silk suture. The catheters were connected to an in-house developed system composed by a peristaltic pump and gamma-radiation coincidence detector (Bioascan, B-FC-4100). The femoral artery catheter, the gamma detector, the peristaltic pump and the femoral vein catheter were thus connected in series, to enable the extracorporeal circulation of blood (flow 150 µl/s from femoral artery to femoral vein) and continuous measurement of radioactivity in the blood.

Image Acquisition and Reconstruction

After surgery, the animal was introduced into a MOLECUBES β-CUBE scanner to perform the imaging session. A solution of [^{18}F]FDG was injected concomitantly with the start of PET acquisition via the femoral vein (*ca.* 5 MBq in 300 µL of saline solution). Dynamic whole body PET images were acquired using MOLECUBES β-CUBE scanner (23 frames: 4 x 5 s, 4 x 10 s, 4 x 30 s, 3 x 60 s, 3 x 120 s, 3 x 300 s, 3 x 660 s, total acquisition time of 60 min). After each PET scan, CT acquisitions were performed on the MOLECUBES X-CUBE scanner to provide anatomical information of each animal as well as the attenuation map for the later reconstruction of the PET images. The PET images were reconstructed using 3D OSEM reconstruction algorithm and applying random, scatter and attenuation corrections.

Image Analysis

After reconstruction, PET-CT images of the same animal were co-registered and analysed using PMOD image processing tool (PMOD Technologies Ltd, Zürich, Switzerland). Volumes of interest (VOIs) were manually placed on ventricle cavity, myocardium and inferior vena cava in order to get an estimation of the image derived input function (IDIF). Time-activity curves (decay corrected) were obtained as cps/cm^3. Curves were transformed into real activity (Bq/cm^3) curves by using a calibration factor, obtained from previous scans performed on a phantom (micro-deluxe, Data spectrum Corp.) under the same experimental conditions (isotope, reconstruction algorithm and energetic window). Finally, the corrected IDIF was determined by applying the spillover and/or partial volume effect correction coefficient obtained from previous scans performed on rod hot and cold rod Micro Deluxe phantom respectively.

Phantoms imaging session

For the calculation of the recovery coefficient (RC), a Micro Deluxe phantom (ECT/DLX/MMP, Data Spectrum Corporation, Hillsborough, NC, USA) with a Hot Spot Insert possessing six different rod sizes (1.2, 1.6, 2.4, 3.2, 4.0, and 4.8 mm) was filled with a known concentration of [^{18}F]FDG. Only some of the rods were filled to prevent spillover from surrounding rods. Static PET imaging was acquired using MOLECUBES β-CUBE scanner for 10 minutes. After each PET scan, CT acquisition was also performed on the MOLECUBES X-CUBE scanner to provide to correct visualization of the rods as well as the attenuation map for the later reconstruction of the PET images. The image was reconstructed using the same protocol as described above. The average VOI-derived radioactivity concentration measured in the different rods were divided by the true activity concentration to obtain and RC curve covering the whole rod size range. The appropriate partial volume effect correction factor was determined from the RC curve.

For the calculation of the spillover correction factor, a Micro Deluxe phantom (ECT/DLX/MMP, Data Spectrum Corporation, Hillsborough, NC, USA) with a Cold Spot Insert possessing seven different rod sizes (1.2, 1.6, 2.4, 3.2, 4.0, 4.8 and 6.0 mm) was filled with a known concentration of [^{18}F]FDG. Static PET imaging was acquired using MOLECUBES β-CUBE scanner for 10 minutes. After each PET scan, CT acquisition was also performed on the MOLECUBES X-CUBE scanner to provide to correct visualization of the rods as well as the attenuation map for the later reconstruction of the PET images. The image was reconstructed using the same protocol as described above. A VOI with Ø=2.4 mm was drawn at the center of the 6.0 mm rod. The VOI-derived radioactivity concentration was divided by the real activity concentration to obtain a spillover coefficient.

4.5.3 Arterial Input Function. Measurement by continuous blood sampling

Animal preparation

Animal were prepared following the methodology previously described.

Determination of the Arterial Input Function

A solution of [^{18}F]FDG (*ca.* 5 MBq in 300 µL of saline solution) was injected concomitantly with the start of the acquisition via the femoral vein. Data were imported in real time to an excel sheet using PLX-DAX add-on for Microsoft Excel (measured in volts per second). A blood sample was withdrawn and the amount of activity, of a fixed volume (10 µL), was measured in an automatic

gamma counter (2470 Wizard, PerkinElmer) to convert data imported with PLX-DAX (Volts per seconds) into Bq/s using a calibration curve obtained from previous measurement of a known activity of ^{18}F in the automatic gamma counter. Values were than expressed as Bq/cm^3. The obtained curves were finally corrected by time delay

CHAPTER 5: *IN VIVO* PRECLINICAL EVALUATION IN EXPERIMENTAL RODENTS

5.1 INTRODUCTION

When new drugs are evaluated, gathering pharmacokinetics information including absorption, distribution, metabolism, and elimination (ADME) is paramount. At early stages, this information can aid in the identification of poor candidates and select those with more favourable properties for further evaluation. At later stages, relevant information to decide dosage and administration route can be obtained. The investigation of pharmacokinetics is based on the existence of specific and sensitive analytical techniques that allow the measurement of the drug concentration in different tissues and body fluids over time. The more sensitive the analytical method employed, the more complete concentration-time profiles can be obtained, thus providing more accurate information. Experimental data are then simulated with compartment models which allow the calculation of relevant pharmacokinetic parameters such as volume of distribution (V_d), plasma clearance (Cl), elimination half-life ($t_{1/2}$), area under the curve (AUC), mean residence time (MRT) and bioavailability (F).

Compartment models are mathematical tools, based on a schematic representation of the organism that do not have any connection with the anatomy and that allow simulating drug concentration levels in the blood and tissues over time. Pharmacokinetic models usually have three or fewer compartments. Compartment 1 is typically the plasma and tissues where the distribution of the drug is practically instantaneous; compartments 2 and 3 represent tissues where the distribution of the drug is slower compared to compartment 1 (Fig. 5.1). However, pharmacokinetic parameters can be also calculated considering the time course of measured drug concentration without any need of a compartmental model.

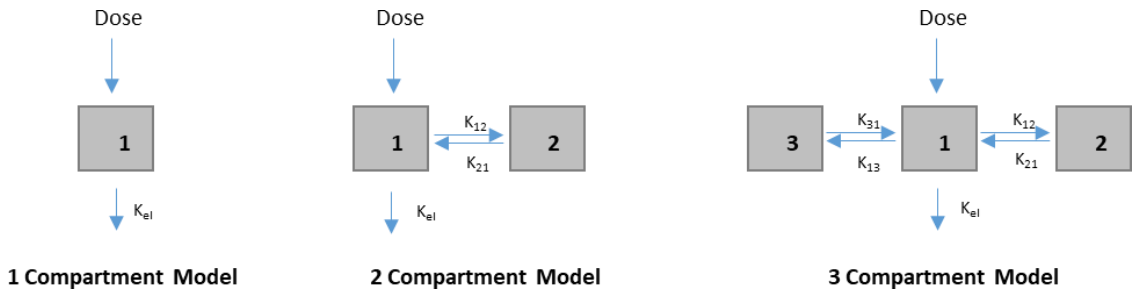

Fig. 5.1: Different pharmacokinetics compartmental models

Another important aspect to take into account for the elaboration of the pharmacokinetics models is if that model is linear or not. In a linear pharmacokinetic model, the kinetic processes respond to first order kinetics and, therefore, the values of the pharmacokinetic parameters do not change with the dose. If the value of one or more pharmacokinetic parameters changes with the administered dose, the drug has a non-linear or dose-dependent pharmacokinetics.

The most important pharmacokinetic parameters are described below:

Volume of distribution, which is used to quantify the distribution of a drug in the body. It is defined as the volume in which the administered amount of drug would need to be uniformly distributed to achieve in all organs or compartments an equal concentration to that in the plasma. It is calculated as follows:

$$V_d = \frac{D}{C_0} \tag{1}$$

where D represent the administered dose and C_0 is the initial concentration of drug in the plasma.

Plasma clearance, which indicates the rate of drug elimination. It represents the volume of blood cleared of drug per unit of time. It correlates the rate of drug elimination with a plasma concentration at the same time according to the following equation:

$$Cl_p = \frac{V_d}{K_{el}} \tag{2}$$

where V_d represents the volume of distribution and K_{el} the elimination rate constant.

Elimination half-life is the time required to eliminate 50% of the drug in the body and, depends on both clearance and volume of distribution. The elimination process is dependent on how

much drug is available in the plasma volume. If most of the drug is in the tissue compartment, only a small fraction will be present in the plasma and therefore the clearance rate will be slower. The relationship between elimination half-life, volume of distribution and plasma clearance is expressed as follows:

$$t_{1/2} = \frac{0.693 \times V_d}{Cl_p} \quad (3)$$

Area under the curve, represents the amount of drug into the body, in its unchanged form, after administration of a determinate dose.

Mean residence time: after administration, not all the drug is excreted at the same time. Some of the molecules will stay longer in the organism than others before being excreted. The mean residence time can be easily defined as the average time that drug molecules spend in the body or in a specific organ and is based on statistical moments theory. The mean residence time is expressed according to equation 4:

$$MRT = \frac{\int_0^\infty t\, c\, dt}{\int_0^\infty c\, dt} = \frac{AUMC_0^\infty}{AUC_0^\infty} \quad (4)$$

where AUC represents the area under the curve and AUMC (Area Under Moment Curve) the area under the curve concentration (c) per time (t) versus time.

Bioavailability: is a term used to describe the percentage (or the fraction F) of an administered dose of a drug that reaches the systemic circulation. Bioavailability is 100% (F=1) following an intravenous administration and less than 100% (F⩽1) following a different administration route.

In this chapter, we tackled the *in vivo* preclinical evaluation of new triazole-based FKBP12-RyR stabilizers (AHK-1 and AHK-2) in experimental animals using positron emission tomography and complementary techniques.

5.2 OBJECTIVES

The specific objectives of this chapter are:

1. To determine the metabolite-corrected arterial plasma Time Activity Curves (TACs) of the ^{11}C-labelled triazole-based FKBP12-Ryr stabilizers AHK-1 and AHK-2 after intravenous administration.
2. To determine the metabolite-corrected arterial plasma Time Activity Curves (TACs) of the ^{11}C-labelled triazole-based FKBP12-Ryr stabilizers AHK-1 and AHK-2 after oral administration.
3. To evaluate biodistribution and pharmacokinetics parameters of the triazole-based FKBP12-Ryr stabilizers AHK-1 and AHK-2 after intravenous administration using Positron Emission Tomography (PET).
4. To evaluate biodistribution and pharmacokinetics parameters of the triazole-based FKBP12-Ryr stabilizers AHK-1 and AHK-2 after oral administration using Positron Emission Tomography (PET).
5. To evaluate the Plasma Protein Binding (PPB).

5.3 RESULTS AND DISCUSSION

5.3.1 DETERMINATION OF METABOLITE-CORRECTED ARTERIAL PLASMA TIME ACTIVITY CURVES (TACS) AFTER INTRAVENOUS ADMINISTRATION

A key factor when tackling quantitative PET studies is the measurement of the Input Function (IF), that represents the concentration of the non-metabolized labelled compound in plasma as a function of time. The blood that irrigates the tissues is supplied by arteries, and hence the application of pharmacokinetic modelling requires the determination of the arterial time activity curve, which can significantly differ from the venous time activity curve[1]. Additionally, it must be considered that a fraction of the labelled drug can be attached to blood cells, and hence it will not be available for tissue extraction during the blood passage through the capillaries (Fig. 5.2).

[1] Chiou, W. L. The Phenomenon and Rationale of Marked Dependence of Drug Concentration on Blood Sampling Site. *Clin. Pharmacokinet.* (1989) doi:10.2165/00003088-198917040-00005.

Because of this, it is important to differentiate between total blood arterial TAC and plasma TAC. Finally, a fraction of the radiolabelled drug can be metabolised over time. The formation of radiolabelled metabolites complicates image interpretation and quantification, as PET only detects the radionuclide, and hence it cannot distinguish between parent compound and radiolabelled metabolites[2]. Because of this, accurate determination of the *in vivo* metabolism of labelled compounds is paramount to investigate pharmacokinetics.

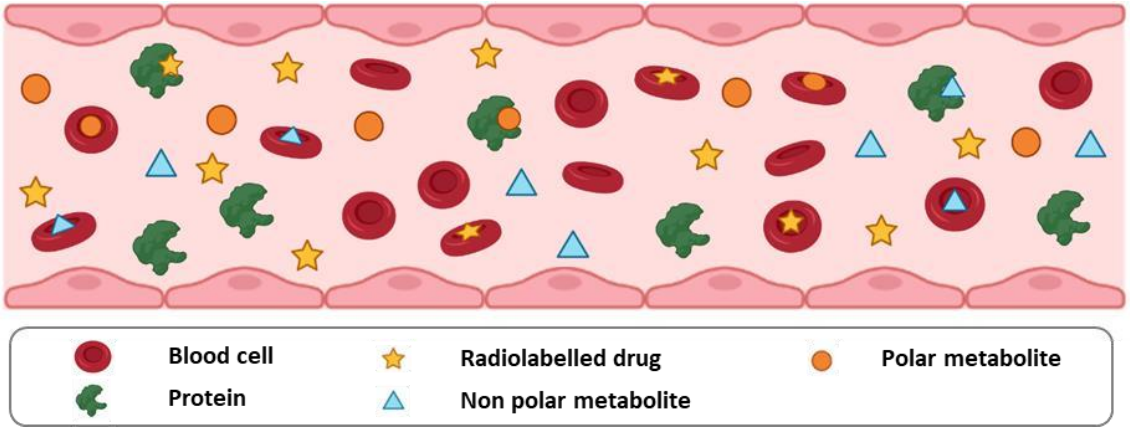

Fig. 5.2: Schematic representation of the blood composition after administration of a radiolabelled compound. Part of the radiolabelled drug remains unchanged, and a fraction metabolises into polar and non-polar metabolites. All labelled entities can be present either as free species in plasma, bound to blood cells or bound to plasma proteins.

The first objective of this part of the PhD thesis was the determination of the metabolite-corrected arterial plasma TAC for compounds AHK-1 and AHK-2. This was achieved by catheterization and online blood sampling, using an in-house developed monitoring system, previously reported by our group[3], which enables extracorporeal blood circulation, continuous measurement of radioactivity in the blood and analysis of plasma samples by HPLC, the latter to quantify radioactive metabolites. Because the bioavailability and biodistribution of the drug

[2] Tonietto, M., Rizzo, G., Veronese, M., Fujita, M., Zoghbi, S. S., Zanotti-Fregonara, P., Bertoldo, A. Plasma radiometabolite correction in dynamic PET studies: Insights on the available modeling approaches. *J. Cereb. Blood Flow Metab.* (2015) doi:10.1177/0271678x15610585.

[3] Guarra, F., Terenzi, A., Pirker, C., Passannante, R., Baier, D., Zangrando, E., Gómez-Vallejo, V., Biver, T., Gabbiani, C., Berger, W., Llop, J., Salassa, L. 124 I Radiolabeling of a Au III -NHC Complex for In Vivo Biodistribution Studies. *Angew. Chem.* (2020) doi:10.1002/ange.202008046.

strongly depend on the administration route and dosage[4,5], we decided to investigate two different administration routes: intravenous bolus injection (sections 5.3.1 and 5.3.3) and oral bolus administration (sections 5.3.2 and 5.3.4), and two different doses: 1 µg/Kg and 5 mg/Kg. The lower dose (micro-dose) corresponds to the one that would be used in imaging studies; the higher dose was achieved by adding non-radioactive compound to the labelled drug and was used to investigate pharmacokinetics at pharmacologically relevant doses. In this section, we will discuss the determination of metabolite-corrected arterial TACs after intravenous administration.

As mentioned in Chapter 4, extracorporeal circulation of the arterial blood was achieved by externally by-passing the femoral artery and the femoral vein of the rat using a fine bore polythene tubing (ID 0.58 mm, OD 0.98 mm). The catheters were then connected to the in-house developed system composed by a peristaltic pump and a gamma-radiation coincidence detector (Bioscan, B-FC-4100). The femoral artery catheter, the gamma detector, the peristaltic pump, and the femoral vein catheter were thus connected in series, to enable the extracorporeal circulation of blood (flow 150 µl/s from femoral artery to femoral vein) and continuous measurement of radioactivity in the blood. Data was imported in real time to an excel sheet using PLX-DAX add-on for Microsoft Excel (measured in volts). At different time points, arterial blood samples (150 µL) were withdrawn to determine the presence of radioactive metabolites by radio HPLC. In addition of these arterial blood samples, one extra sample was withdrawn to determine the proportion of blood volume that is occupied by red blood cells, also called hematocrit; and a second sample was withdrawn to determine the amount of radioactivity of a fixed volume (10 µL) of whole blood in an automatic gamma counter (2470 Wizard, PerkinElmer). The amount of radioactivity present in the whole blood was used to convert data imported with PLX-DAX (Volts) firstly into Bq/s and finally as percentage of injected dose per gram of fluid (% ID/g). The percentage of radioactivity present in the plasma fraction was used to calculate the real plasma-to-blood ratio. This, together with the value of the hematocrit (HCT), allowed us to calculate the arterial plasma TAC (Fig. 5.3).

[4] Hernández, R. M., Gascón, A. R., Calvo, M. B., Caramella, C., Conte, U., Domínguez-Gil, A., Pedraz, J. L. Influence of route of administration and dosage form in the pharmacokinetics and bioavailability of salbutamol. *Eur. J. Drug Metab. Pharmacokinet.* (1997) doi:10.1007/bf03189798.

[5] Sun, S., Fan, Z., Hu, L., Ma, Y., Si, L., Qiu, J., Li, G. Influence of Dose and Route of Administration on the Enantioselective Pharmacokinetics of TJ0711 Hydrochloride in Rats. *Chirality* (2014) doi:10.1002/chir.22387.

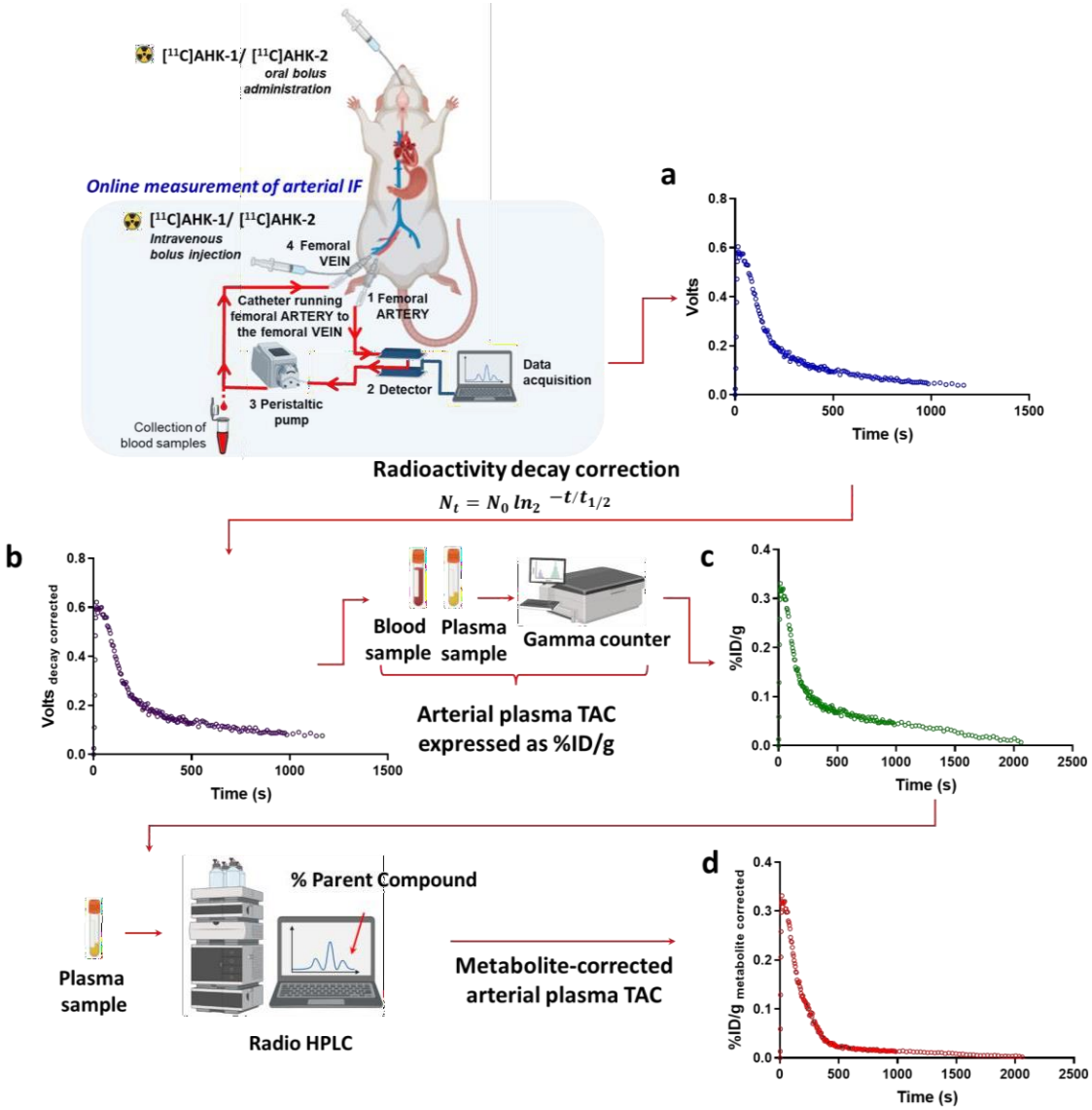

Fig. 5.3: Schematic representation of the process to obtain metabolite-corrected arterial plasma TACs. Firstly, data was imported in real time to an excel sheet using PLX-DAX add-on for Microsoft Excel (measured in volts) (a). Data was corrected by decay (b). A blood sample was withdrawn to determine the amount of radioactivity in a fixed volume of whole blood and in plasma, using an automatic gamma counter. The radioactivity measured in the whole blood was used to convert data firstly into Bq/s and finally as percentage of injected dose per gram of fluid (% ID/g), while the radioactivity measured in the plasma fraction was used to calculate the arterial plasma TAC (c). At different time points, arterial blood samples were withdrawn and processed to determine the presence of radioactive metabolites in plasma by radio HPLC. The percentage of parent compound in plasma over time was used to calculate the metabolite-corrected arterial plasma TAC (d).

Distribution between plasma and blood cells

When a new radiotracer is used, hematocrit and radioactivity concentrations in both plasma and blood must be measured during the length of the PET imaging. Hematocrit (HCT) is the proportion of blood volume that is occupied by red blood cells (RBCs) and is normally between 0.37-0.43 in male rats and 0.35-0.42 in female rats[6]. The radioactivity concentration in whole blood can be expressed as the sum of concentrations in plasma and red blood cells, weighed by their volume fractions, represented by hematocrit (Eq.5).

$$C_B = (1 - HCT) \times C_P + HCT \times C_{RBC} \quad (5)$$

where C_B represents the blood concentration, C_P the plasma concentration and C_{RBC} the red blood cells concentration.

While concentration in the blood, plasma and HCT can be easily measured, radioactivity concentration in red blood cells (RBC) cannot be measured directly from centrifuged blood samples, because RBC preparations always contain some plasma and if plasma is washed away, then part of the radioactivity inside the cells or bound to the surface could be removed. For that reason, concentration in RBC is generally calculated by using the Eq. 6[7].

$$C_{RBC} = \frac{C_B - (1 - HCT) \times C_P}{HCT} \quad (6)$$

where C_{RBC} represents the red blood cells concentration, C_B the blood concentration, C_P the plasma concentration and HTC the hematocrit.

Experimentally, we first calculated the HCT of wild-type rats by centrifuging a small amount of blood in a hematocrit capillary, to verify that the obtained values fell within the broad range found in the literature. Then, per each animal, after the intravenous administration of the corresponding labelled compound ([^{11}C]AHK-1.1, [^{11}C]AHK-1.2, [^{11}C]AHK-2.1 or [^{11}C]AHK-2.2) an arterial blood sample was withdrawn from the femoral artery catheter and the amount of radioactivity in a fixed volume was measured in an automated gamma counter to calculate C_B.

[6] Probst, R. J., Lim, J. M., Bird, D. N., Pole, G. L., Sato, A. K.;, Claybaugh, J. R. Gender Differences in the Blood Volume of Conscious Sprague-Dawley Rats. *J Am Assoc Lab Anim Sci* (2006).

[7] Hagenfeldt, L. & Arvidsson, A. The distribution of amino acids between plasma and erythrocytes. *Clinica Chimica Acta* (1980) doi:10.1016/0009-8981(80)90074-1.

By centrifuging the sample and sampling a known volume of plasma, C_P was also calculated. Whit these values, the ratio between the amount of radioactivity in a known volume of plasma and the amount of radioactivity in a known volume of blood (C_P/C_B) was calculated and used to transform the arterial TAC of the corresponding animal into arterial plasma TAC (Fig. 5.3c) assuming that the distribution between plasma and blood remains constant over time. Knowing the values of HCT, C_P and C_B, per each animal, the C_{RBC} was calculated following Eq. 6.

In order to increase the statistical power of our results, for the determination of PK parameters the results obtained after the administration of either [^{11}C]AHK-1.1 and [^{11}C]AHK-1.2 or [^{11}C]AHK-2.1 and [^{11}C]AHK-2.2 were pooled. The HCT, C_{RBC}, plasma-to-blood ratio (C_P/C_B) the percentage of compound present in plasma or bound to the red blood cells are summarized in the **table 5.1**.

Compound	HCT[1]	C_{RBC}[2]	C_P/C_B experimental[3]	% Plasma	% RBC
AHK-1*	0.43±0.02	7.4±4.1 KBq/ml	1.46±0.20	83.19	16.80
AHK-2*	0.44±0.03	9.2±5.2 KBq/ml	1.37±0.19	79.39	20.60

[1]Hematocrit, [2]red blood cells concentration, [3]plasma-to-blood ratio, [4]percentage of compound in plasma, [5]percentage of compound penetrate or bound the surface of red blood cells.
* Considering results obtained after the IV administration of [^{11}C]AHK-1.1 and [^{11}C]AHK-1.2.
** Considering results obtained after the IV administration of [^{11}C]AHK-2.1 and [^{11}C]AHK-2.2.

From the results obtained is evident that the radioactivity signal, independently of whether it comes from the parent compound or any of its metabolites, persists in the plasma and no substantial trapping from red blood cells was observed for both compounds.

In vivo metabolism of AHK-1 after intravenous administration

In a PET study, blood measures are necessary to obtain the IF of the tracer delivered to the tissues, *e. g.* the free tracer concentration in arterial plasma. Because of this, we next explored the *in vivo* metabolism, to ultimately obtain metabolite-corrected arterial plasma TACs.

Experimentally, compound AHK-1 labelled with carbon-11 in two different positions (Fig. 5.4) was administrated by intravenous bolus injection through the femoral vein at two different concentrations, 1 μg/Kg and 5 mg/Kg, to experimental rats. As already mentioned, if a molecule decomposes or undergoes metabolism, only the fragment containing the radionuclide will be detected. Because of this, the approach of introduce the radionuclide in different positions was

used with the aim to get quantitative data regarding the formation of different metabolites over time.

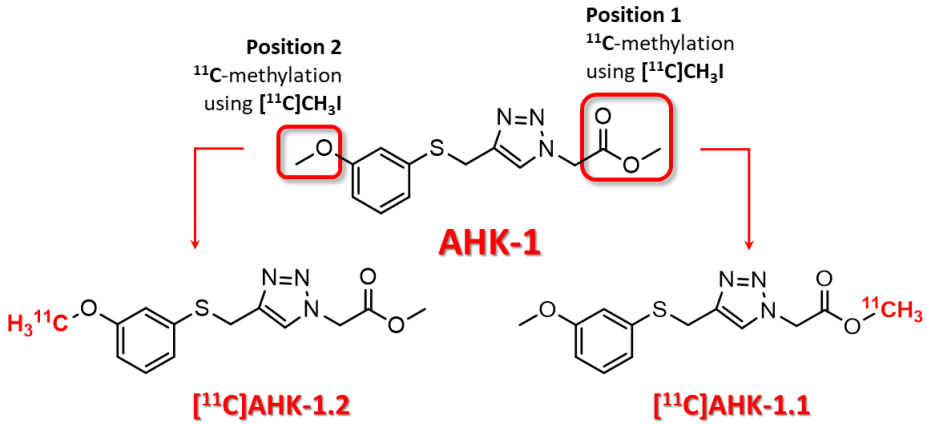

Fig. 5.4: Chemical structure of the drug candidate AHK-1. The positions where the ^{11}C-methylation was performed are highlighted and the chemical structures of the resulting compounds ([^{11}C]AHK-1.1 and [^{11}C]AHK-1.2) are shown.

At different time points, arterial blood samples were withdrawn through the arterial femoral catheter and processed to determine the percentage of unmodified parent compound and the presence of radioactive metabolites by radio-HPLC analysis of the plasmatic fraction (Fig. 5.5).

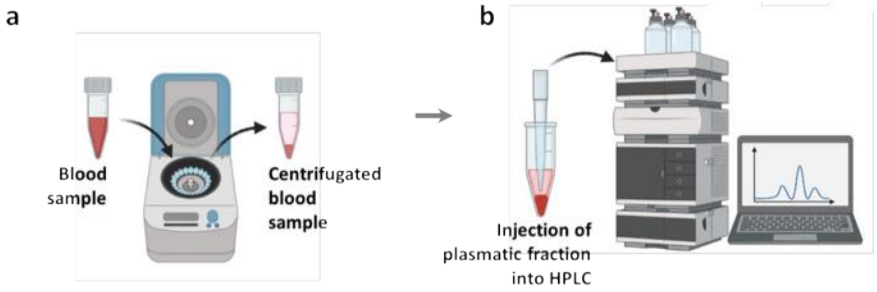

Fig. 5.5: Schematic representation of the procedure for the analysis of the plasmatic fraction. Firstly, the plasma was separated from the whole blood by mechanical centrifugation of the arterial blood sample and processed to be injectable in the HPLC (a). Secondly, the processed plasmatic fraction was injected into the HPLC system, equipped with a radioactive detector to determine the percentage of unmodified parent compound and the presence of radioactive metabolites.

HPLC chromatograms obtained for compound [^{11}C]AHK-1.1 confirmed the results obtained *in vitro*. The –COO[^{11}C]CH_3 residue is immediately hydrolyzed resulting in the formation of the corresponding carboxylic acid (–COOH) and [^{11}C]CH_3OH (Fig. 5.6a) suggesting that if any therapeutic efficacy will be observed for the compound AHK-1, the active part would be probably

the free acid form or any other metabolite turning compound AHK-1 into a prodrug. The use of prodrugs, molecules with little or no pharmacological activity, that are converted to the active parent drug *in vivo* by enzymatic or chemical reactions, are widely used in the clinical practice since they can overcome several problems linked with formulation or unacceptable pharmacokinetics[8]. The formation of the carboxylic acid could be confirmed by co-injection with the no-radioactive carboxylic acid derivative as reference compound, which was provided by the Organic Chemistry-I department at UPV/EHU-University of the Basque Country. Analysis of the plasmatic fraction by mass spectrometry (Fig. 5.7b, c) further confirmed this result.

Thanks to our multi-position labelling approach and hence the administration of the radiolabelled compound [^{11}C]AHK-1.2 we were able to track how the carboxylic acid derivative further metabolizes. Results obtained after the administration of [^{11}C]AHK-1.2 showed that the percentage of non-metabolized carboxylic acid derivative ([^{11}C]H_3CO-Ar-COOH, retention time = 20 min) progressively decreased with time, to reach a value of *ca.* 12% at 20 minutes after administration (Fig. 5.6c). This decrease is paralleled by the formation of three polar metabolites (Fig. 5.6b). The first one, with retention time = 2 min, accounted for *ca.* 50% of the total radioactivity at t=20 minutes after administration. The strong polarity and short retention time (equivalent to that obtained for [^{11}C]CH_3OH when [^{11}C]AHK-1.1 was administered) strongly suggest that the [^{11}C]H_3COAr-R moiety suffers hydrolysis with the consequent formation of [^{11}C]CH_3OH. However, in this case the reaction was slower probably due to the steric effect of the aromatic ring. The second radioactive metabolite, with retention time = 4.7 min, accounted for *ca.* 20% of the total radioactivity at t=20 minutes after administration; the last metabolite, with retention time = 18 min, accounted for *ca.* 19% of the total radioactivity at the same time point. These two radioactive metabolites could not be identified despite several metabolic routes have been hypothesized and the possible metabolites synthetized at the Organic Chemistry-I department at UPV/EHU-University of the Basque Country as reference for the identification (Fig. 5.8).

[8] Rautio, J., Meanwell, N. A., Di, L., Hageman, M. J. The expanding role of prodrugs in contemporary drug design and development. *Nature Reviews Drug Discovery* (2018) doi:10.1038/nrd.2018.46.

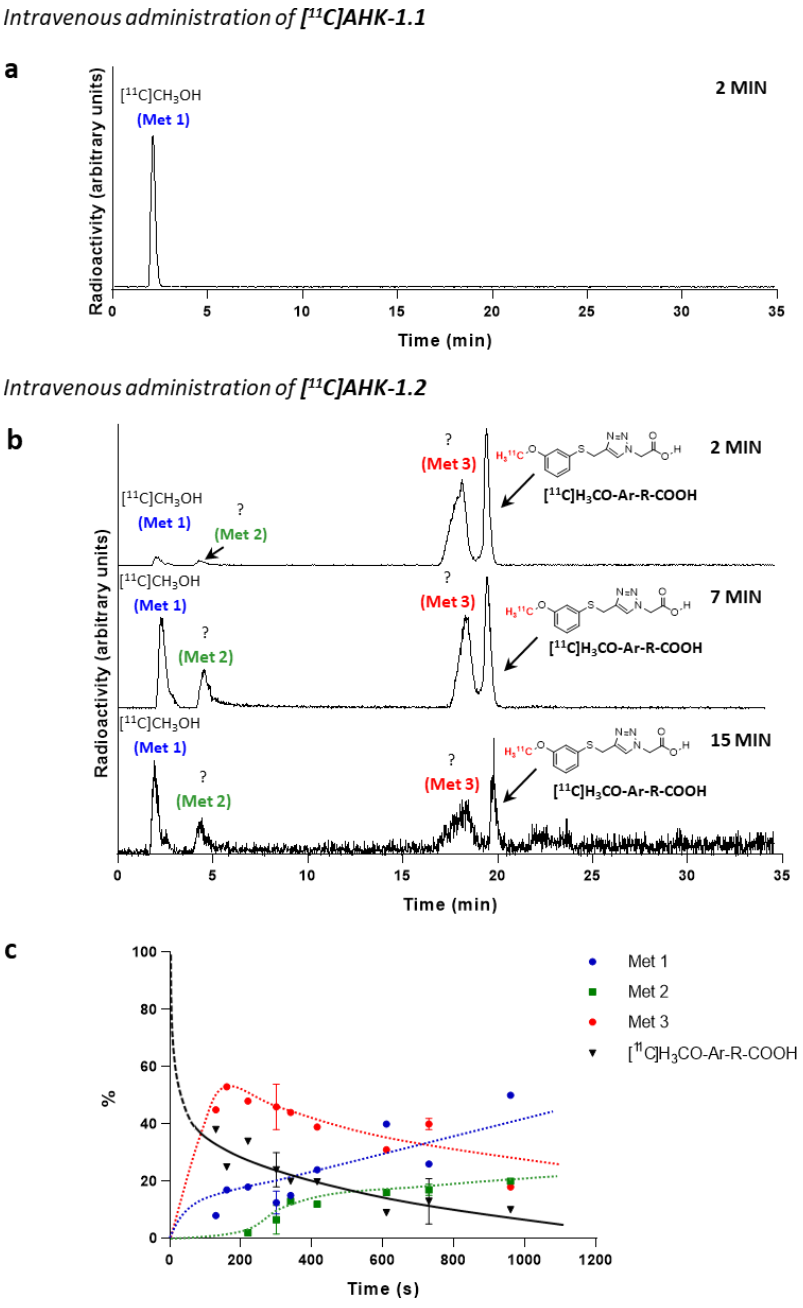

Fig. 5.6: a) Representative chromatogram corresponding to the *in vivo* metabolism (radioactivity detector) after intravenous administration of [^{11}C]AHK-1.1 (1 µg/Kg). b) Representative chromatograms corresponding to the *in vivo* metabolism (radioactivity detector) after intravenous administration of [^{11}C]AHK-1.2. The position of the peaks corresponding to the identified metabolites are shown. c) Metabolite kinetic profile over time after intravenous administration of [^{11}C]AHK-1.2 (1 µg/Kg). Data are expressed as the area under the corresponding peak, divided by the sum of the areas under all peaks, and expressed in percentage.

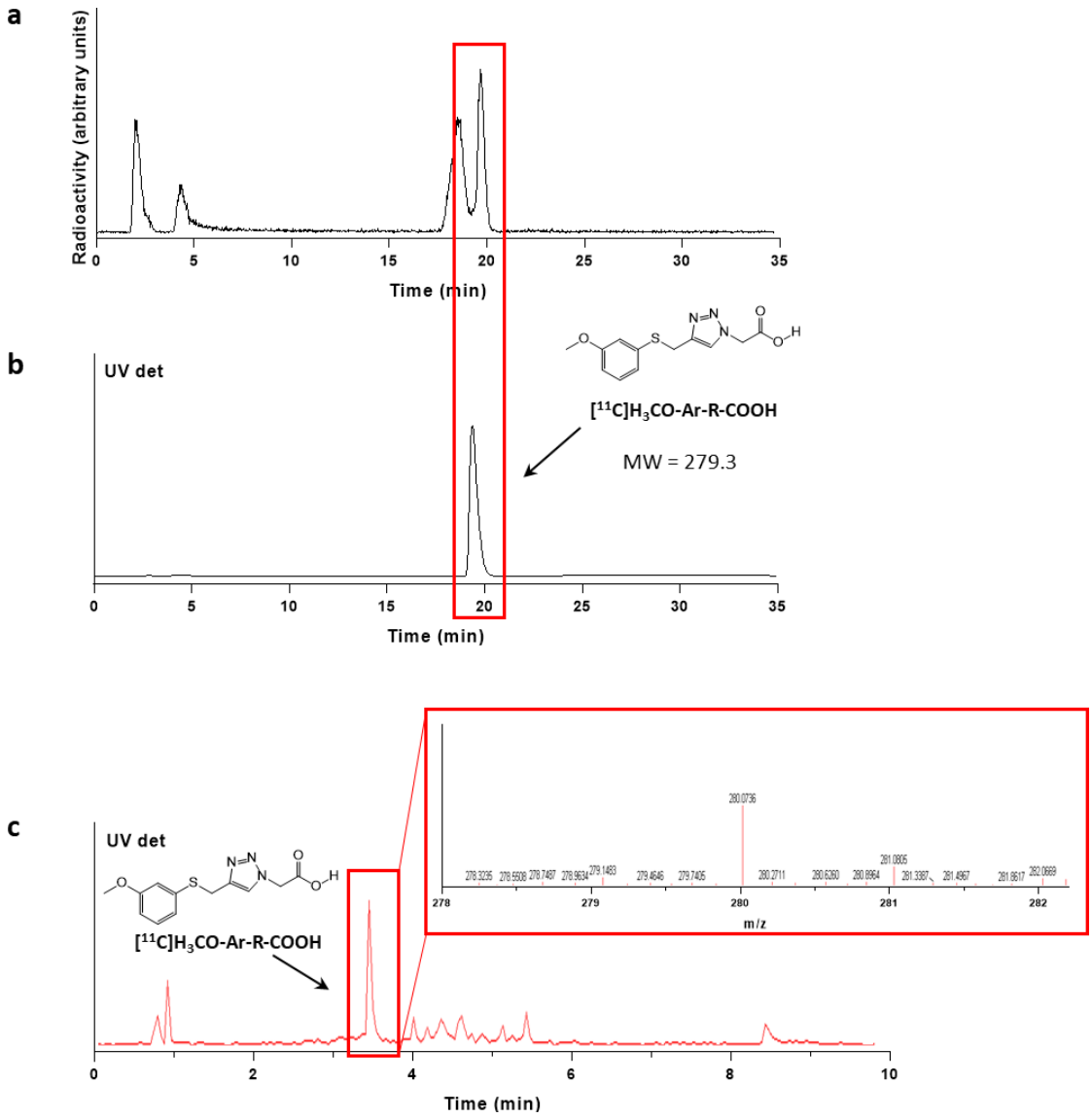

Fig. 5.7: a) Representative chromatogram corresponding to the *in vivo* metabolism (radioactivity detector) after intravenous administration of [^{11}C]AHK-1.2 (1 µg/Kg). The position of the peak corresponding to the carboxylic acid is shown. b) Chromatogram (UV detector) corresponding to the reference of carboxylic acid. The retention time coincides with the chromatogram in (a). c) Chromatogram (UV detector) corresponding to the analysis of the plasmatic fraction after intravenous administration of AHK-1 (5 mg/Kg). The mass spectrum corresponding to carboxylic acid (highlighted in red in the chromatogram) confirms formation of the carboxylic acid *in vivo*.

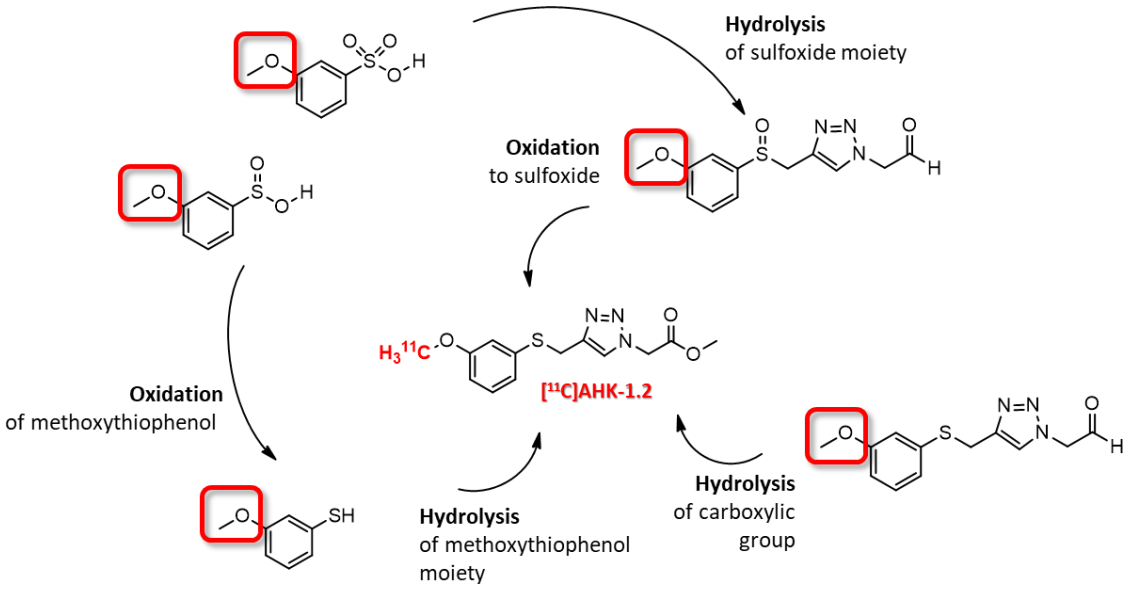

Fig. 5.8: Metabolic route hypothesized to try to identify the radioactive metabolites observed after the intravenous administration of [^{11}C]AHK-1.2.

Due to the relative long HPLC method (35 min; necessary for a proper separation of the different labelled species) and the rapid decay of carbon-11 (half-life = 20.4 min) only few blood samples per animal were withdrawn and analysed. In order to obtain a continuous time course of the concentration of parent compound in plasma, we decided to fit the discrete data to a Hill-type function (Eq. 8), which is generally used to this purpose[9].

$$fp = d - \frac{(d-a)t^b}{c + t^b} \tag{8}$$

where *d* represents the initial level of parent fraction, *a* the plateau, *b* and *c* the shape modulation factors.

In this way, the arterial plasma TACs, that consider the total amount of radioactivity in the arterial plasma (Fig. 5.9a), were transformed into metabolite-corrected arterial plasma TACs (Fig. 5.9c), which were subsequently used for the determination of the pharmacokinetics parameters. Two

[9] Jødal, L., Roivainen, A., Oikonen, V., Jalkanen, S., Hansen, S. B., Afzelius, P., Alstrup, A. K. O., Nielsen, O., L., Jensen, S. B. Kinetic Modelling of [^{68}Ga]Ga-DOTA-Siglec-9 in Porcine Osteomyelitis and Soft Tissue Infections. *Molecules* (2019) doi:10.3390/molecules24224094.

different fittings were carried out, one for each administered dose (1 µg/Kg and 5 mg/Kg; Fig. 5.9b).

Due to the fast degradation of [^{11}C]AHK1.1 to the free acid form, this compound was eliminated from the study. For compound [^{11}C]AHK-1.2, *d* values of the Hill function (which represent the initial level of compound) of *ca.* 0.40 were obtained, suggesting that more than the half of the compound is metabolized before the blood collecting site is reached. The best-fit values for the parameter *a*, which represents the plateau of the curve, were 0.013 and 0.064 for 1 µg/Kg and 5 mg/Kg, respectively, suggesting a slight dose-dependent effect on pharmacokinetics at long times after administration.

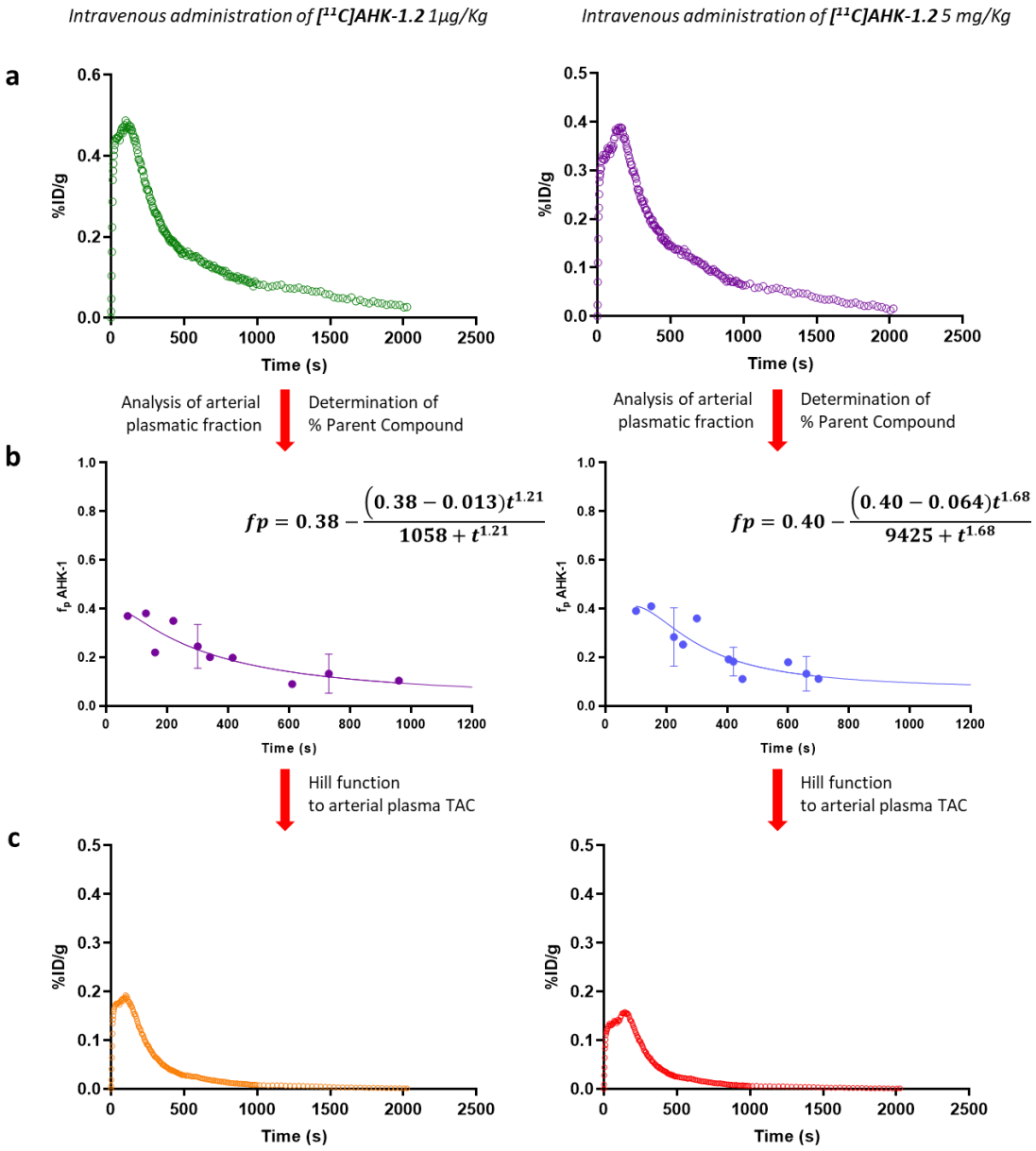

Fig. 5.9: a) Representative arterial plasma Time Activity Curves (TACs) after intravenous administration of [^{11}C]AHK-1.2 at [1 µg/Kg] (left) and [5 mg/Kg] (right). b) Graphic representation of plasma concentration over time of the carboxylic acid of AHK-1 after intravenous administration of [^{11}C]AHK-1.2 at [1 µg/Kg] (left) and [5 mg/Kg] (right). The experimental values of unmetabolized compound (dots in the figure) were fitted using Hill type function (line) to obtain a continuous time course of plasma concentration. c) Metabolite-corrected arterial plasma Time Activity Curves (TACs) after intravenous administration of [^{11}C]AHK-1.2 at [1 µg/Kg] (left) and [5 mg/Kg] (right). The curves were obtained by applying the Hill type function in (b) to the curve in (a).

In vivo metabolism of AHK-2 after intravenous administration

A parallel experimental design was followed for compound AHK-2, this is, compound AHK-2 labelled with carbon-11 in two different positions (Fig. 5.10) was administered by intravenous bolus injection through the femoral vein at two different concentrations, 1 µg/Kg and 5 mg/Kg.

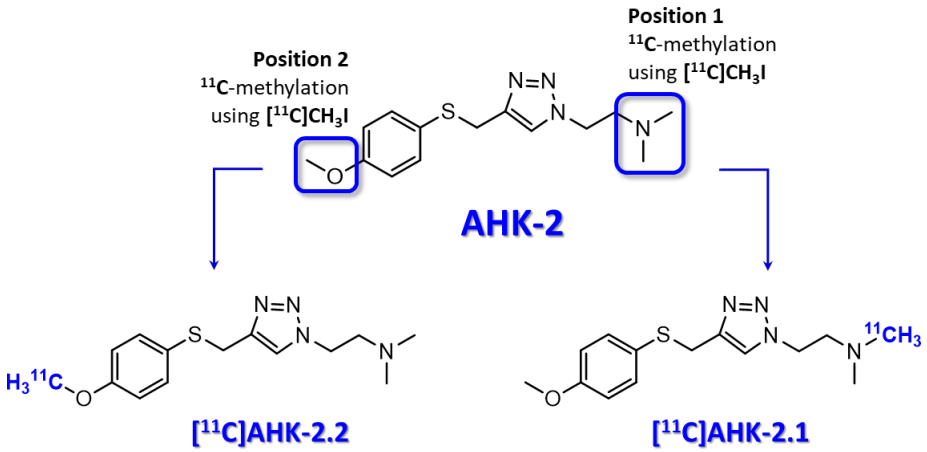

Fig. 5.10: Chemical structure of the drug candidate AHK-2. The positions where the ^{11}C-methylation was performed are highlighted and the chemical structures of the resulting compounds ([^{11}C]AHK-2.1 and [^{11}C]AHK-2.2) are shown.

The analysis of the plasmatic fraction, after the intravenous administration of the labelled compound [^{11}C]AHK-2.1, showed the presence of two metabolites with short retention times (t = 2 and 3 min, respectively; red dots and blue square in Fig. 5.11) that progressively increase over time until reach approximately 25% and 30% at later time points. The short retention time confirms the high polarity of the metabolites and suggests that the metabolic pathways go *via* demethylation of the amine group and/or hydrolysis of the alkyl chain of the triazole ring. Two further metabolites, with retention times = 21 and 22 min, respectively (Fig. 5.11, green and purple triangles in Fig. 5.11) were also observed. These represent the major metabolites at early time points. Their concentration then decreases over time probably due to further metabolism ractions and/or elimination.

Analysis of the plasmatic fraction after the intravenous administration of the labelled compound [^{11}C]AHK-2.2, showed the presence of one single peak with strong polarity and short retention time (t = 2 min, red dots in Fig. 5.12) suggesting the formation of [^{11}C]CH_3OH as major metabolite.

Two further other metabolites with retention times = 21 and 22 min, respectively, were also observed (Fig.5.12).

Since the radioactive peaks observed were the same of the ones observed with the *in vitro* microsomes assay, we further confirmed the formation of the sulfoxide derivative (H_3COAr-S=O-R) by co-injection with the no-radioactive sulfoxide derivative as reference compound (Fig. 5.13b), which was provided by the Organic Chemistry-I department at UPV/EHU-University of the Basque Country. Analysis of the plasmatic fraction by mass spectrometry (Fig. 5.13c) further confirmed this result.

As for AHK-1, a metabolic route has been hypothesized, and the possible metabolites have been synthetized by the Organic Chemistry-I department at UPV/EHU-University of the Basque Country, to be used as reference compounds (Fig. 5.14). Unfortunately, the metabolite with retention time of 21 min could not be identified.

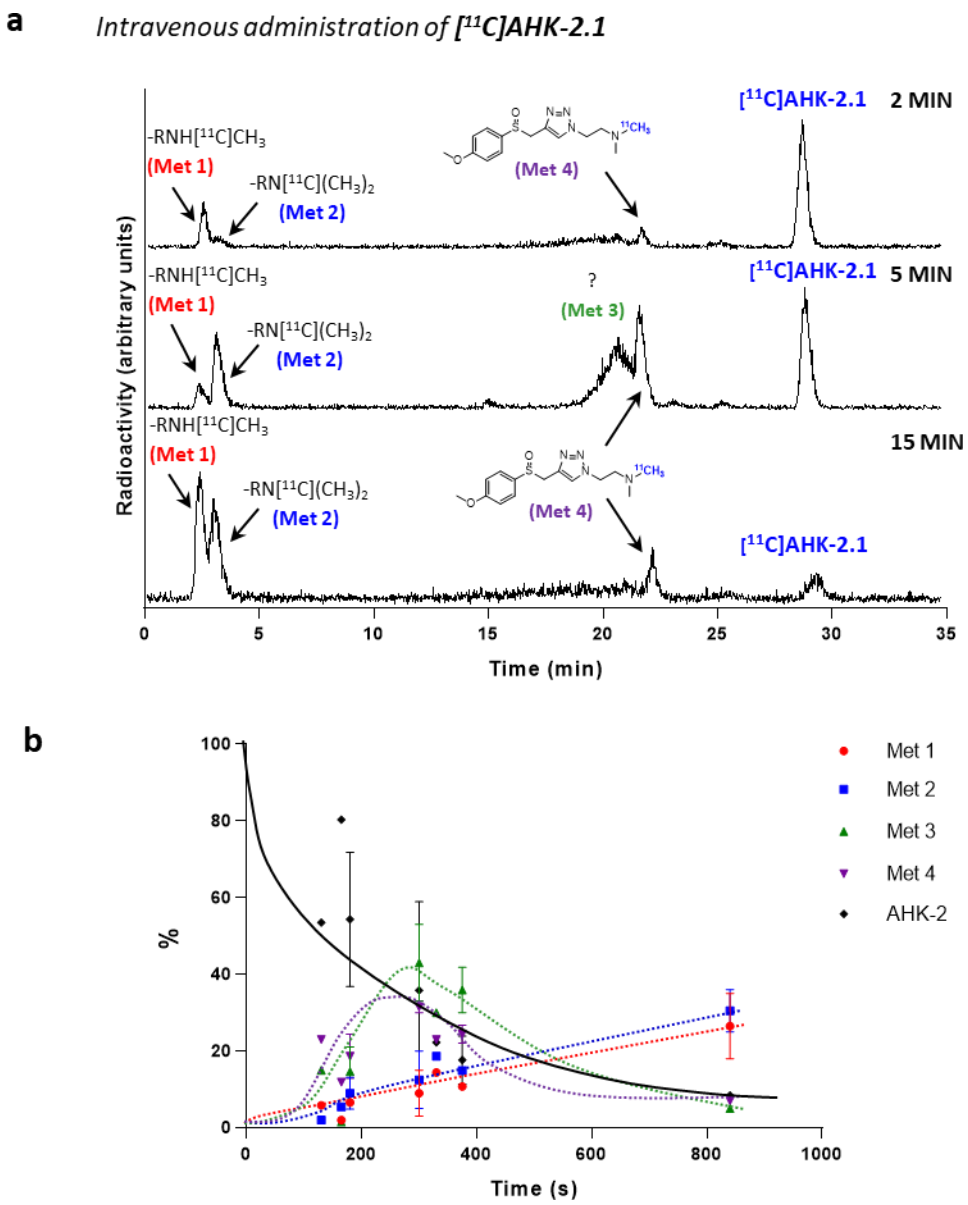

Fig. 5.11: a) Representative chromatograms corresponding to the *in vivo* (radioactivity detector) after intravenous administration of [^{11}C]AHK-2.1 (1 µg/Kg). The position of the peaks corresponding to the identified metabolites are shown. b) Metabolite kinetics profile after intravenous administration of [^{11}C]AHK-2.1 (1 µg/Kg). Data are expressed as percentage obtained from HPLC chromatograms.

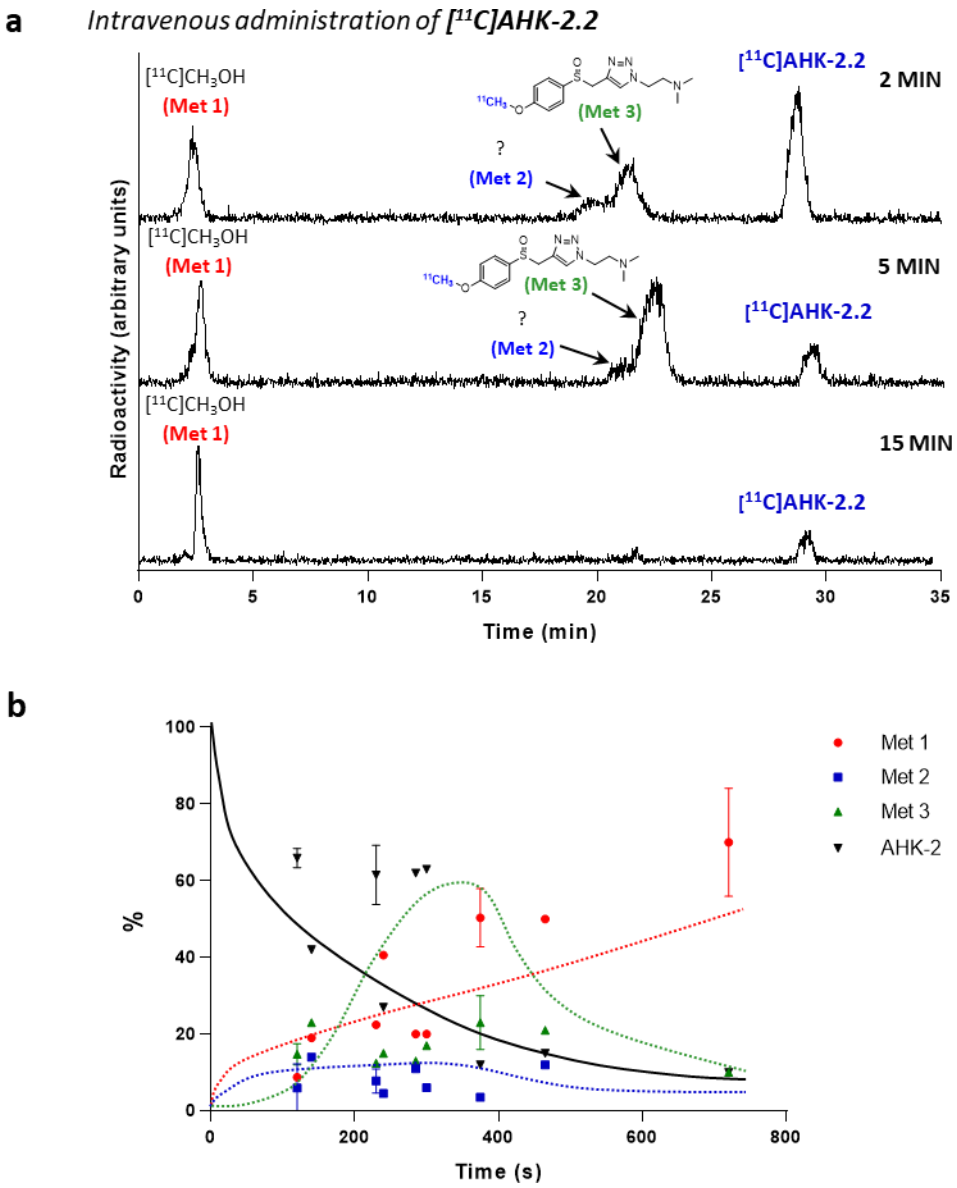

Fig. 5.12: a) Representative chromatograms corresponding to the *in vivo* (radioactivity detector) after intravenous administration of [^{11}C]AHK-2.2 (1 µg/Kg). The position of the peaks corresponding to the identified metabolites are shown. b) Metabolite kinetics profile after intravenous administration of [^{11}C]AHK-2.2 (1 µg/Kg). Data are expressed as percentage obtained from HPLC chromatograms.

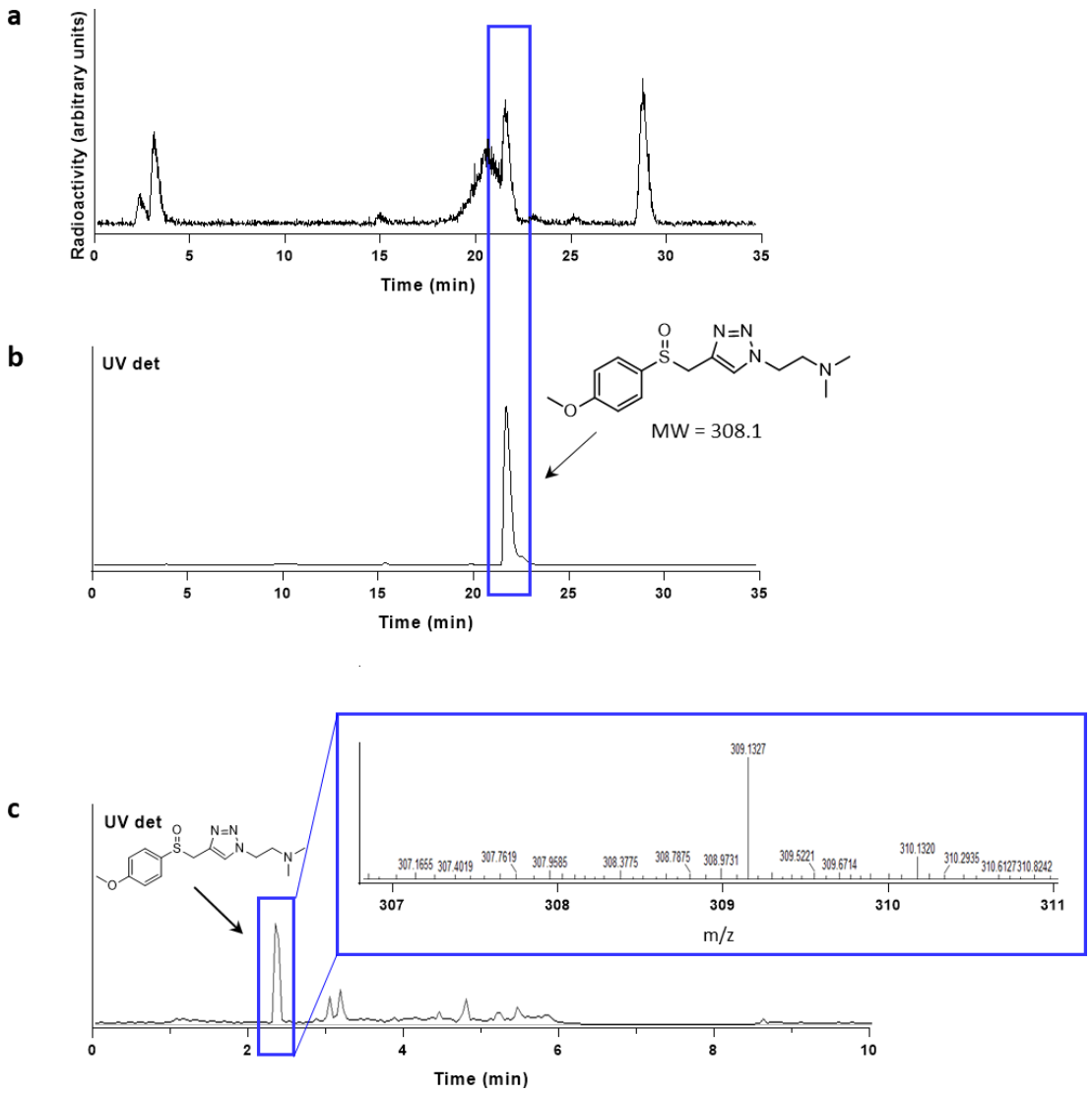

Fig. 5.13: a) Representative chromatogram corresponding to the *in vivo* metabolism (radioactivity detector) after intravenous administration of [^{11}C]AHK-2.2 (1 µg/Kg). The position of the peak with the same retention time of the sulfoxide derivative (H_3COAr-S=O-R) is shown. b) Chromatogram (UV detector) corresponding to the reference of the sulfoxide derivative. The retention time coincides with the chromatogram in a. c) Chromatogram (UV detector) corresponding to the analysis of the plasmatic fraction after intravenous administration of AHK-2 (5 mg/Kg). The mass spectrum corresponding to the sulfoxide derivative (highlighted in blue in the chromatogram) confirmed its formation *in vivo*.

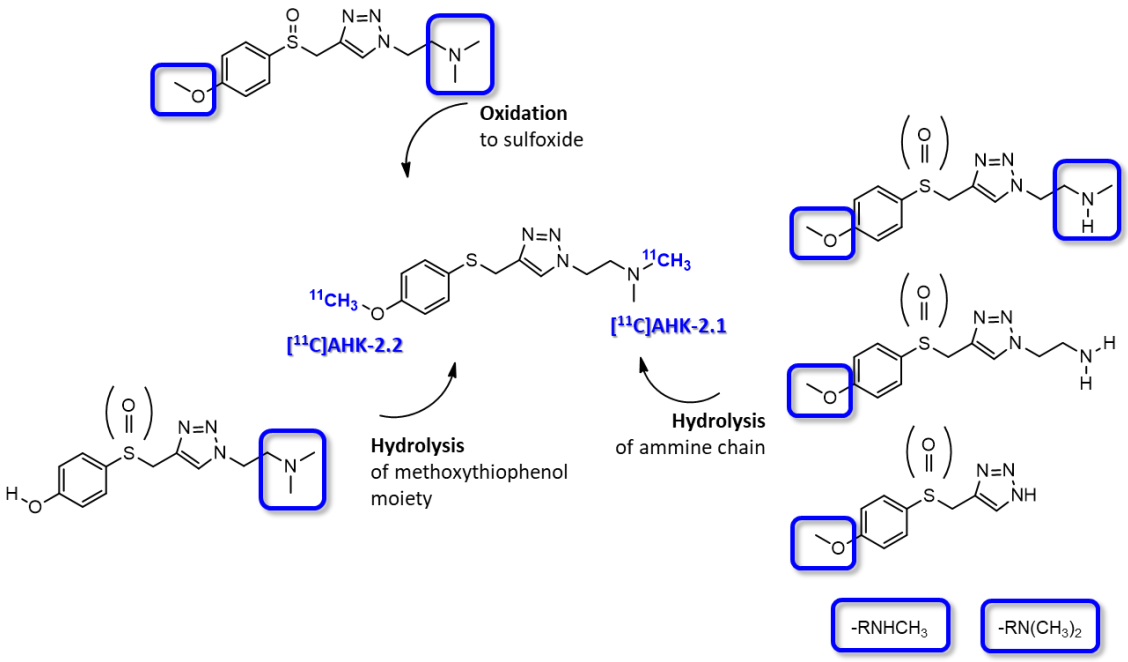

Fig. 5.14: Metabolic route hypothesized to try to identify the radioactive metabolites observed after the intravenous administration of [^{11}C]AHK-2.1 and [^{11}C]AHK-2.2.

Also for the compound AHK-2 data of plasma concentration of radioactivity corresponding to the parent compound versus time obtained from the HPLC analysis were fitted to Hill-type function to obtain a continuous time course of plasma parent concentration. The resulting Hill functions (for dose= 1 µg/Kg and 5 mg/Kg, respectively; Fig. 5.15b) were used to transform the arterial plasma TACs (Fig. 5.15a) into metabolite-corrected arterial plasma TACs (Fig. 5.15c). Optimal fit was obtained when *d*=1, indicating a slower metabolism compared to AHK-1. Values for *a* were 0.075 and 0.29 (dose = 1 µg/Kg and 5 mg/Kg, respectively) again suggesting a dose-dependent (non-linear) pharmacokinetics.

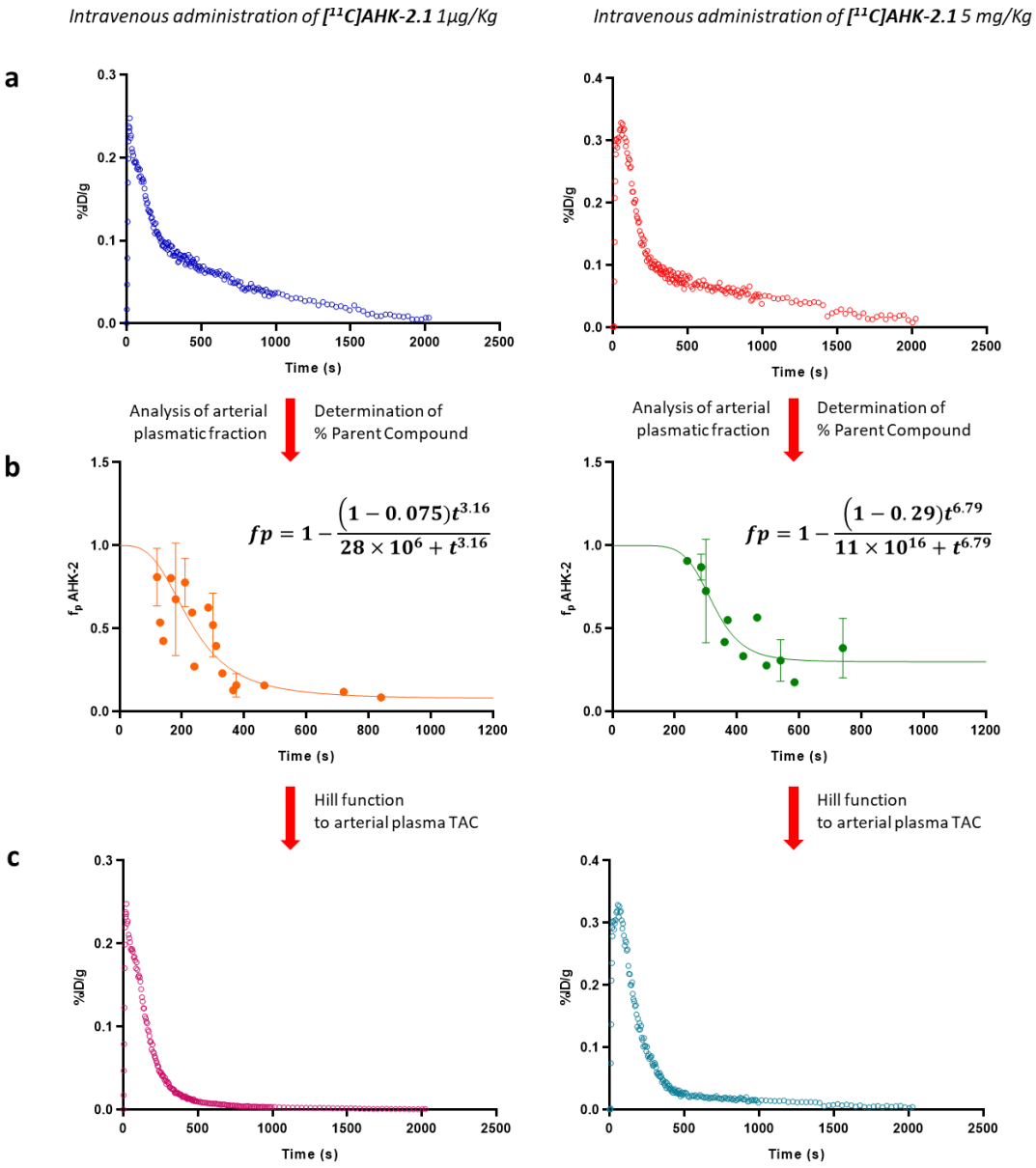

Fig. 5.15: a) Representative arterial plasma Time Activity Curves (TACs) after intravenous administration of [^{11}C]AHK-2.1 at [1 µg/Kg] (left) and [5 mg/Kg] (right). b) Graphic representation of plasma concentration over time of AHK-2 after intravenous administration of [^{11}C]AHK-2.1 and [^{11}C]AHK-2.2 at [1 µg/Kg] (left) and [5 mg/Kg] (right). The experimental values of unmetabolized parent compound (dots in the figure) were interpolated using Hill type function (line) to obtain a continuous time course of plasma parent concentration. c) Metabolite-corrected arterial plasma Time Activity Curves (TACs) after intravenous administration of [^{11}C]AHK-2.1 at [1 µg/Kg] (left) and [5 mg/Kg] (right). The curves were obtained by applying the Hill type function in b to the curve in a.

5.3.2 DETERMINATION OF METABOLITE-CORRECTED ARTERIAL PLASMA TIME ACTIVITY CURVES (TACS) AFTER ORAL ADMINISTRATION

Oral administration of drugs is the most common administration route since it is both convenient and economical. However, the choice of the administration route depends not only on the convenience and patient compliance but also on the drug's pharmacokinetics and pharmacodynamic profile. After oral administration, drugs need to be absorbed in a process that involves several steps such as the passage through the intestinal walls and liver before reaching the systemic circulation. During this process the drug can be partially absorbed and/or undergo biotransformation, in a process called first passage. Because the amount of drug that will be finally bioavailable depends on these steps, the pharmacokinetics could be different compared to when the same dose is administrated intravenously (Fig. 5.16).

Because the bioavailability and, consequently the biodistribution, of the drug strongly depends on the administration route and dosage, the second objective of this part of the PhD thesis was the determination of the metabolite-corrected arterial plasma TAC for compounds AHK-1 and AHK-2 after oral administration. This was achieved following the experimental approach previously described for the intravenous administration, using extracorporeal catheterization and online blood sampling.

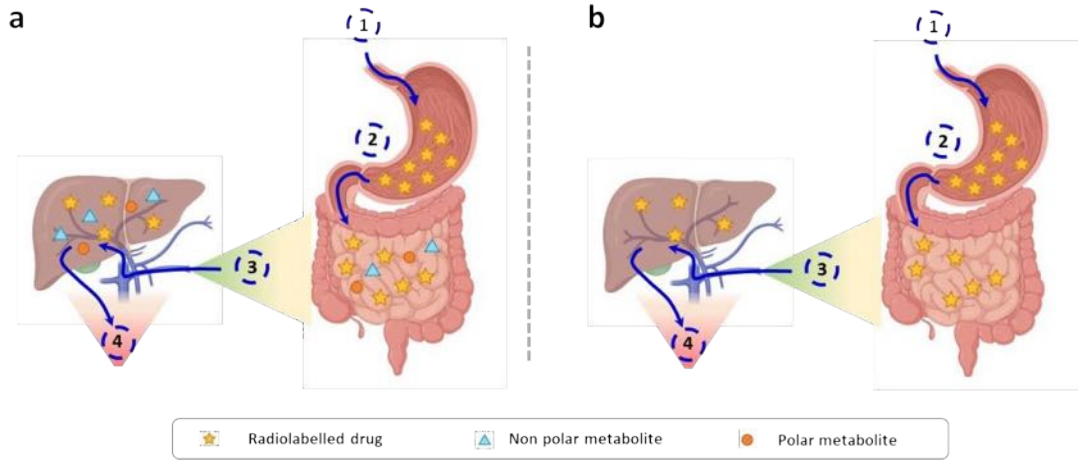

Fig. 5.16: Schematic representation of the absorption steps after the oral administration of a drug. Part of the (radiolabeled) drug is metabolized in the stomach and in the liver before reaching the bloodstream (a). The unmetabolized drug is partially absorbed to the gastrointestinal tract and reach the bloodstream, where it can successively undergo to biotransformation (b).

Distribution between plasma and red blood cells

As described in the previous sections for intravenous administration, the HCT was calculated by centrifuging a small amount of blood in a hematocrit capillary while C_B and C_P values were calculated by measuring in an automatic gamma counter the amount of radioactivity of arterial blood and plasma samples. The blood-to-plasma ratio was then calculated as well the C_{RBC} by using Eq. 6.

The HCT, C_{RBC} , plasma-to-blood ration (C_P/C_B) and the percentage of compound present in plasma or bound to the red blood cells are summarized in the **table 5.2**.

Compound	HCT[1]	C_{RBC}[2]	$C_p/C_{b\ experimental}$[3]	% Plasma	% RBC
AHK-1*	0.44±0.01	6.18±3.44 KBq/ml	1.44±0.20	81.15	18.84
AHK-2*	0.44±0.04	6.29±4.72 KBq/ml	1.44±0.18	81.24	18.75

[1]Hematocrit, [2]red blood cells concentration, [3]plasma-to-blood ratio, [4]percentage of compound in plasma, [5]percentage of compound penetrate or bound the surface of red blood cells.
* Considering results obtained after the administration of [^{11}C]AHK-1.2.
** Considering results obtained after the administration of [^{11}C]AHK-2.1 and [^{11}C]AHK-2.2.

The results summarized in the table 5.2 show that, similarly to intravenous administration, after oral administration of the radiolabelled compounds all the species that reach the systemic circulation persist in the plasma and are not sequestered by red blood cells.

In vivo metabolism of [^{11}C]AHK-1.2 after oral administration

As results obtained in section 5.3.1 showed that compound [^{11}C]AHK-1.1 was immediately hydrolysed to the free acid form, this compound was not investigated for oral route. Hence, only the results obtained after oral administration of compound [^{11}C]AHK-1.2 at two different doses (1 µg/Kg and 5 mg/Kg) will be discussed in this section.

Radio-HPLC analysis of arterial blood samples withdrawn at different time points after oral administration of [^{11}C]AHK-1.2 showed a similar metabolism pathway to that obtained after intravenous administration. Differences in the metabolism kinetics were observed suggesting that the absorption and/or the first passage effect are playing a role. The radioactive metabolites observed in arterial plasma, in this case, could in fact be the result of first passage metabolism and subsequent absorption of metabolites, and/or metabolism of the parent compound after its

partial absorption (Fig. 5.16). No trace of the unmetabolized compound was found, due to the fast hydrolysis of the ester to the carboxylic acid form. Overall, four radioactive peaks with retention times = 2, 4.7, 18 and 20 min were observed (Figure 5.17a). The one with retention time = 2 min probably corresponds to the formation of [^{11}C]CH_3OH. The peaks with retention time = 5 and 18 min could not be identified, while the peak with retention time = 20 min probably corresponds to the carboxylic acid (([^{11}C]H_3CO-Ar-COOH), as previously discussed (Fig. 5.17).

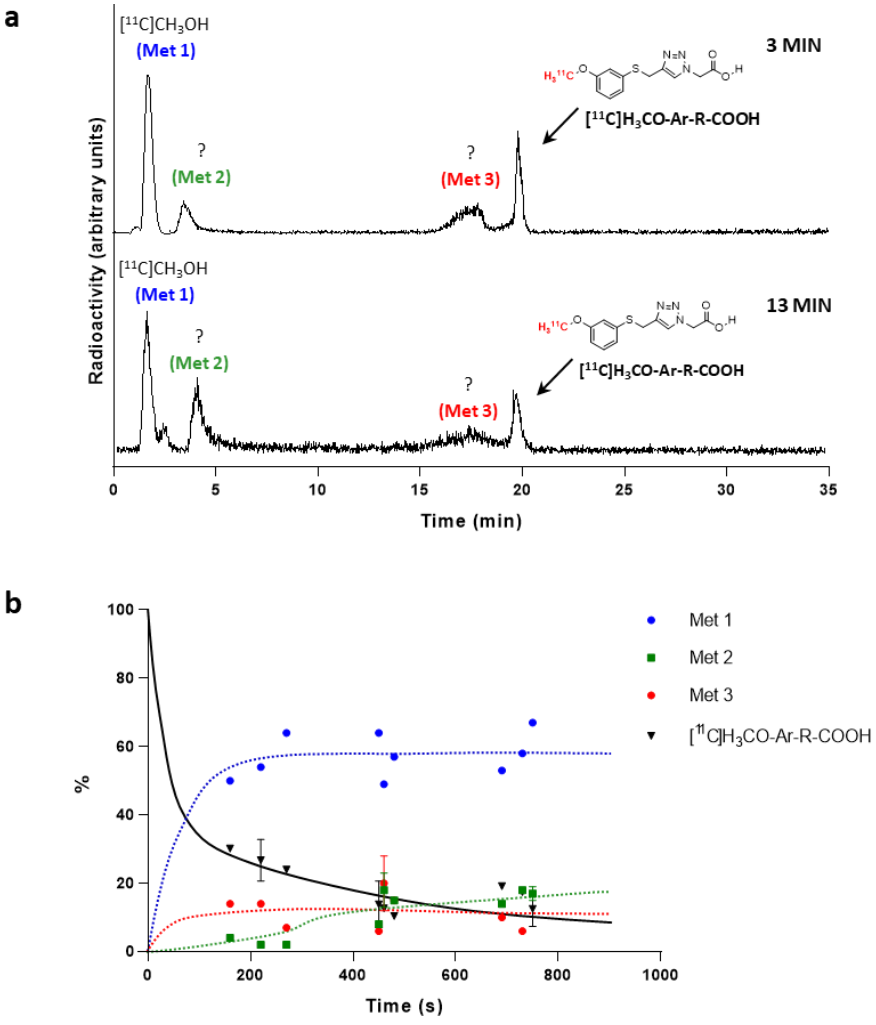

Fig. 5.17: a) Chromatograms corresponding to the *in vivo* metabolism (radioactivity detector) after oral administration of [^{11}C]AHK-1.2. The position of the peaks corresponding to the identified metabolites is shown. b) Metabolite kinetics profile after oral administration of [^{11}C]AHK-1.2. Data are expressed as percentage of total radioactivity, obtained from HPLC chromatograms.

The data obtained from radio-HPLC analysis of the arterial plasma fraction were fitted to the Hill function and a continuous function of the concentration of parent compound over time was calculated. The arterial plasma TACs obtained from extracorporeal circulation were thus finally corrected to obtain the metabolite-corrected arterial plasma TACs (Fig. 5.18).

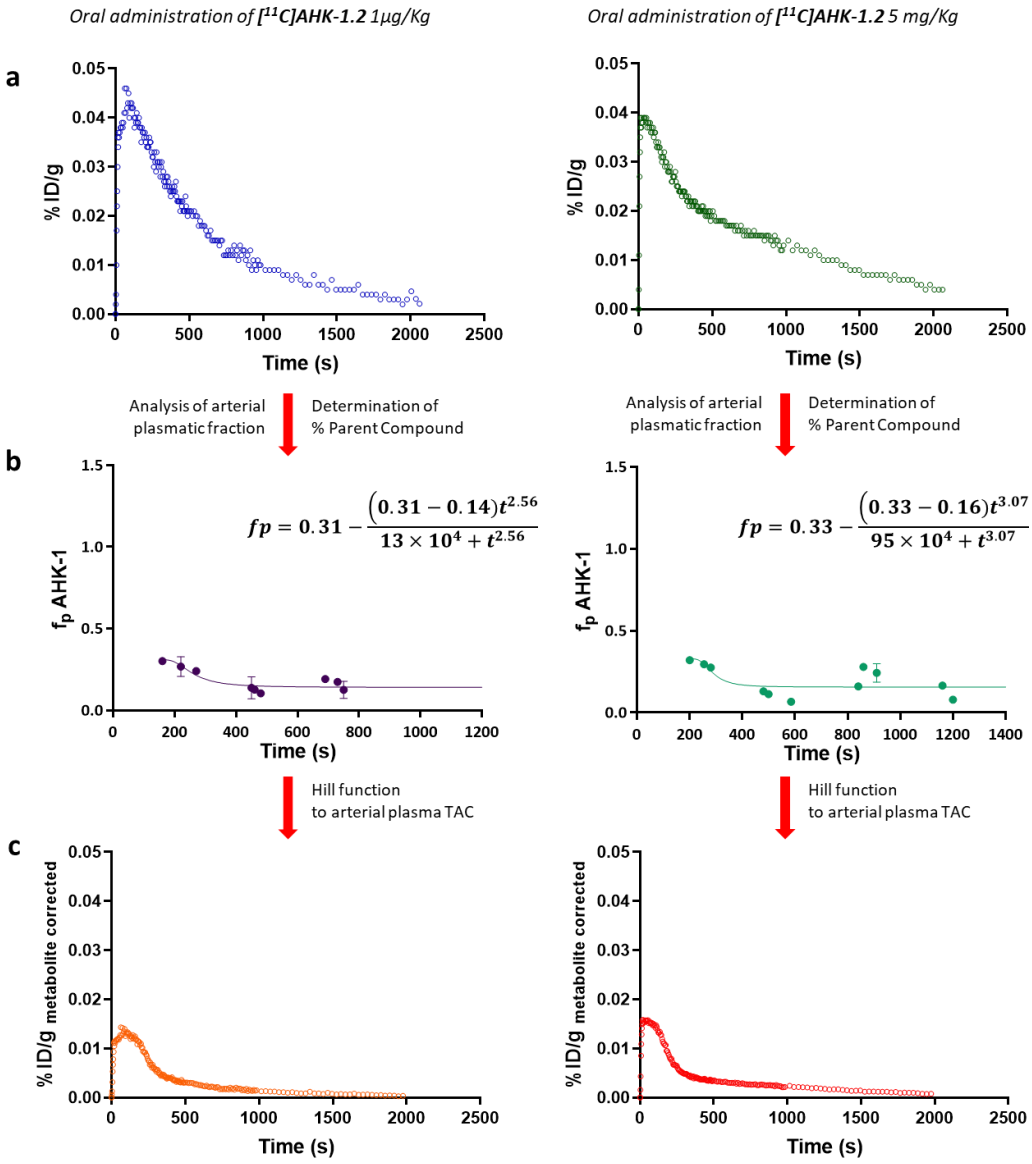

Fig. 5.18: a) Representative arterial plasma Time Activity Curves (TACs) after oral administration of [^{11}C]AHK-1.2 at doses of 1 µg/Kg (left) and 5 mg/Kg (right). b) Graphic representation of plasma concentration over time for carboxylic acid of AHK-1 ([^{11}C]H_3CO-Ar-COOH) after intravenous administration of [^{11}C]AHK-1.2 at doses of 1 µg/Kg (left) and 5 mg/Kg (right). The experimental values of unmetabolized parent compound (dots in the figure) were interpolated using Hill type function (line) to obtain a continuous time course of plasma parent concentration. c) Metabolite-corrected arterial plasma Time Activity Curves (TACs) after intravenous administration of [^{11}C]AHK-1.2 at doses of 1 µg/Kg (left) and 5 mg/Kg (right). The curves were obtained by applying the Hill type function in (b) to the curve in (a).

Comparison of the results with those obtained after intravenous administration suggests that oral administration results in lower initial plasma concentration of the drug and slightly higher at longer times, indicating the progressive absorption of the compound over time. In fact, the best-fit value for the parameter *d,* corresponding to the initial level of compound, was *ca.* 0.30 and *ca.*0.40 after oral and intravenous administration respectively, while the best-fit value for the parameter *a,* corresponding to the plateau, was *ca.* 0.15 after oral administration and, 0.013 and 0.064 after 1 µg/Kg or 5 mg/Kg intravenous administration, respectively.

Regarding metabolism kinetics, [^{11}C]CH_3OH (Met 1, blue dots in Fig. 5.17) is the major metabolite present in the arterial plasmatic fraction. This metabolite is rapidly formed and remains constant over time afterwards. The fraction of radioactivity present as metabolite with retention time = 5 min (Met 2, green squares in Fig. 5.17) was similar to that obtained for intravenous administration (green squares in Fig. 5.6), whereas for the metabolite with retention time = 18 min (Met 3, red dots in Fig. 5.17 and Fig. 5.6) the kinetics differed depending on the administration route. While after oral administration its concentration does not exceed 20% and remains almost constant over the duration of the study (Fig 5.17), after intravenous administration it is the major metabolite at early time points and its concentration decreases over time (Fig. 5.6). From these results, it is clear that the compound is partially metabolized by enzymes in the intestinal walls and/or liver before reaching the systemic circulation. This result is expected, as enzymes responsible for drug metabolism are mainly localized in the liver.

In vivo metabolism of [^{11}C]AHK-2.1 and [^{11}C]AHK-2.2 after oral administration

The *in vivo* metabolism of compound AHK-2 after oral administration was also investigated at two different doses: 1 µg/Kg and 5 mg/Kg. In this case, both labelled compounds ([^{11}C]AHK2.1 and [^{11}C]AHK2.2) were investigated (see Fig. 5.10). Radio-HPLC analysis of arterial blood samples showed the same metabolic pathway already observed after the intravenous administration. When [^{11}C]AHK-2.1 was administrated, the analysis of the plasmatic fraction showed the presence of four radioactive metabolites with retention times = 2, 3, 21 and 22 min, respectively (Fig. 5.19). When compound [^{11}C]AHK-2.2 was administrated, the formation of three radioactive metabolites with retention times = 2, 21 and 22 min, respectively, could be detected (Fig. 5.20).

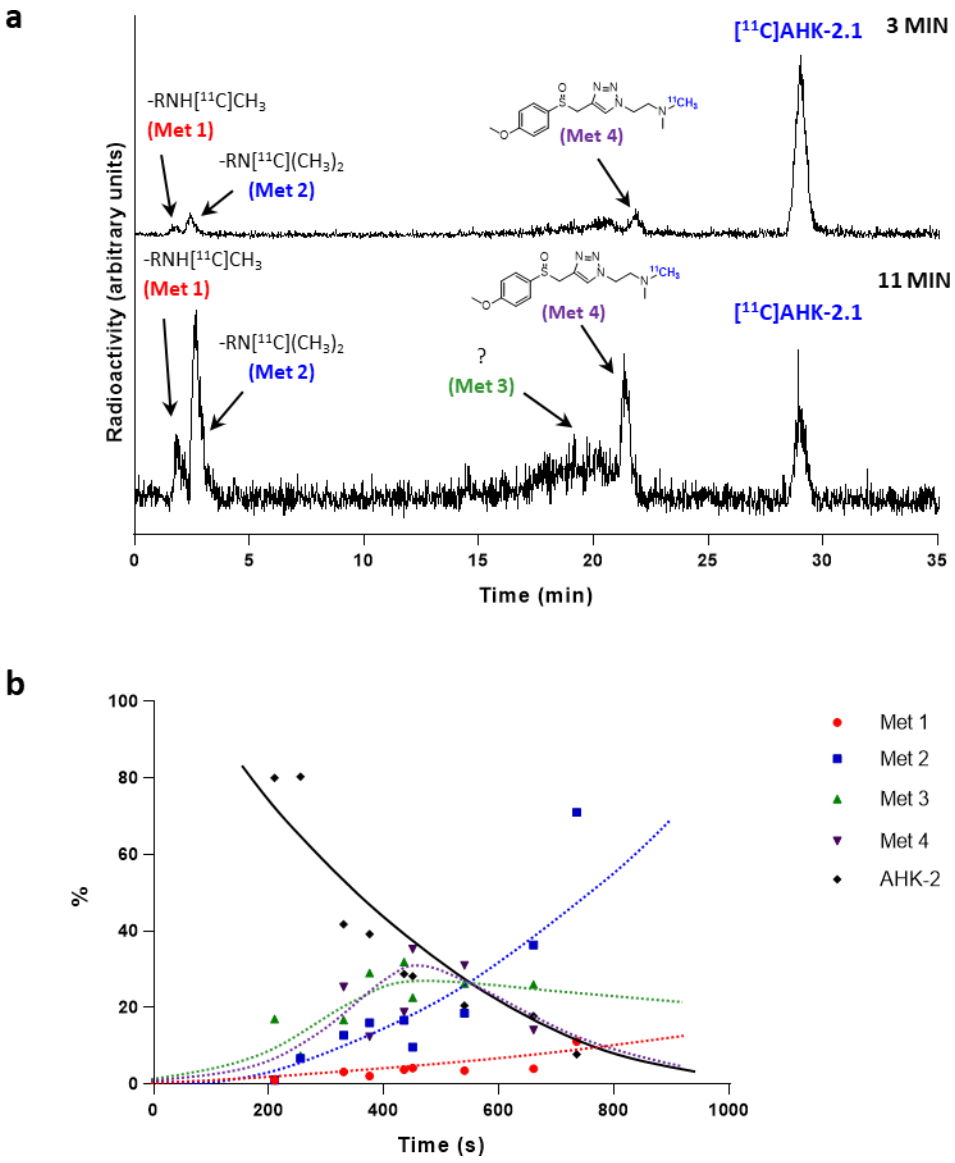

Fig. 5.19: a) Representative chromatograms corresponding to the *in vivo* HPLC analysis (radioactivity detector) of plasma samples after oral administration of [^{11}C]AHK-2.1 (1 µg/Kg). The position of the peaks corresponding to the identified metabolites are shown. b) Metabolite kinetics profile after intravenous administration of [^{11}C]AHK-2.1 (1 µg/Kg). Data are expressed as percentage of total radioactivity, obtained from HPLC chromatograms.

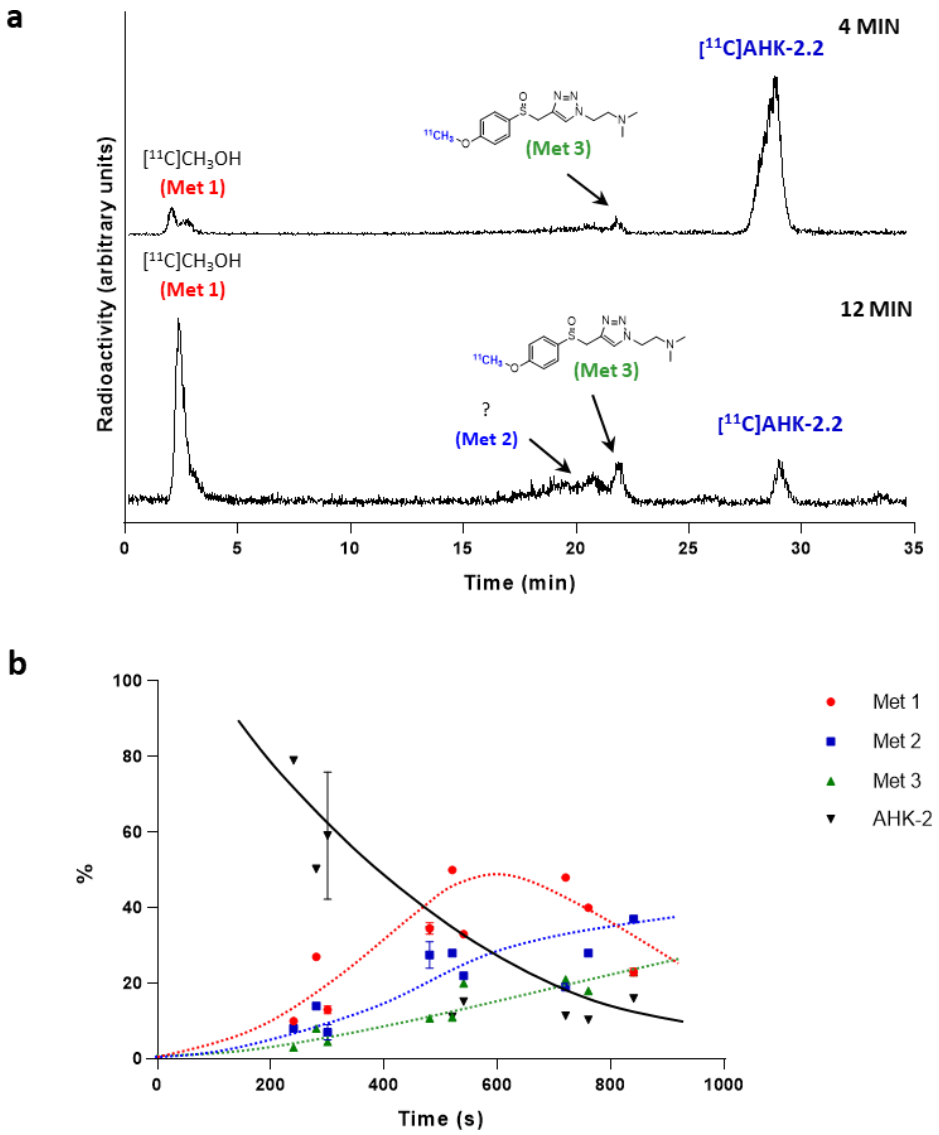

Fig. 5.20: a) Representative chromatograms corresponding to the *in vivo* HPLC analysis (radioactivity detector) of plasma samples after oral administration of [^{11}C]AHK-2.2 (1 µg/Kg). The position of the peaks corresponding to the identified metabolites are shown. b) Metabolite kinetics profile after intravenous administration of [^{11}C]AHK-2.2 (1 µg/Kg). Data are expressed as percentage of total radioactivity, obtained from HPLC chromatograms .

As previously described, data obtained from radio-HPLC analysis of the arterial plasma fraction after oral administration were fitted to the Hill function and continuous functions of the concentration of parent compound over time were calculated. The arterial plasma TACs were thus finally corrected to obtain the metabolite-corrected arterial plasma curves (Fig. 5.21).

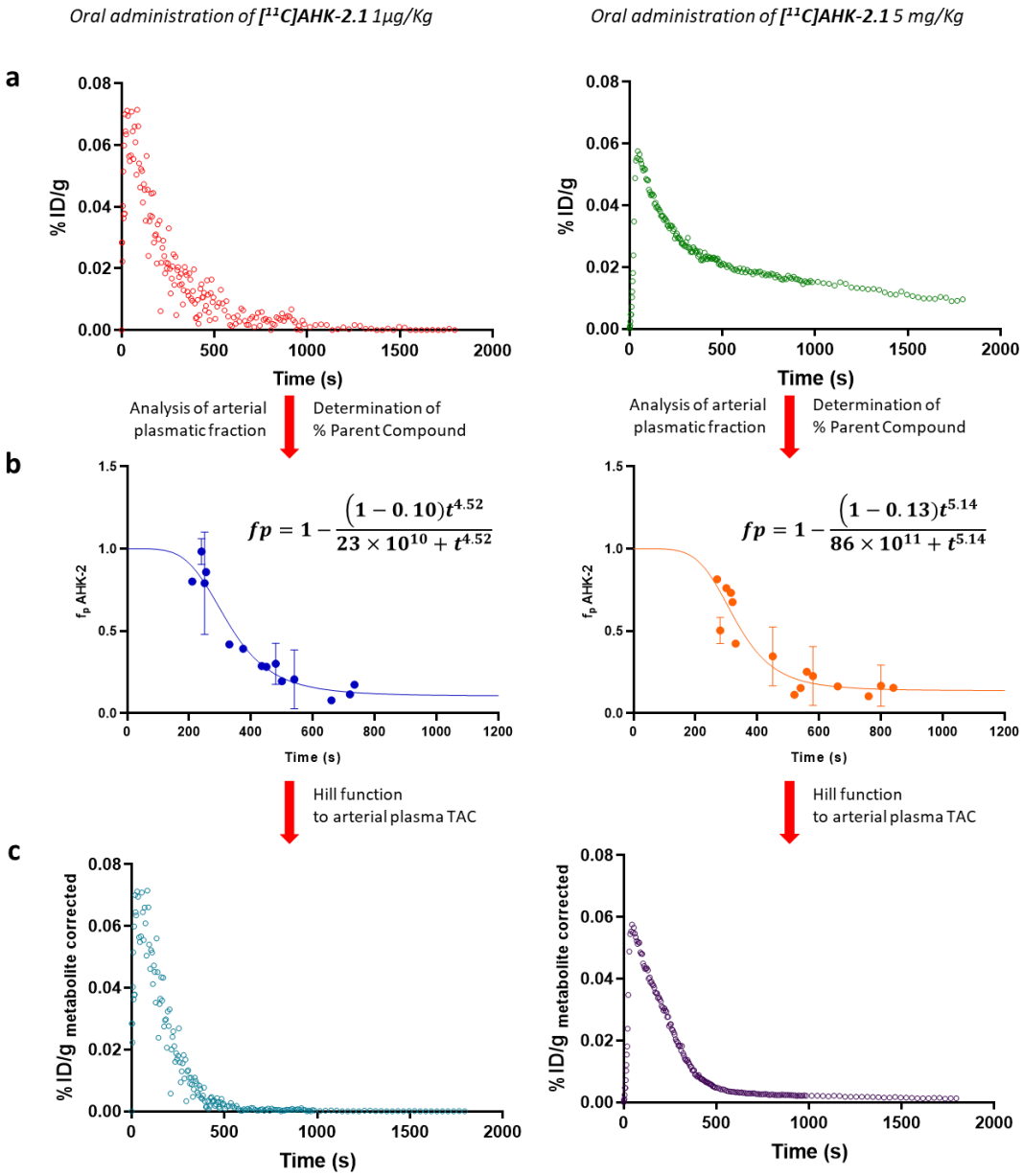

Fig. 5.21: a) Representative arterial plasma Time Activity Curves (TACs) after oral administration of [^{11}C]AHK-2.1 at doses of 1 µg/Kg (left) and 5 mg/Kg (right). b) Graphic representation of plasma concentration over time for [^{11}C]AHK2 after oral administration of [^{11}C]AHK-2.1 and [^{11}C]AHK-2.2 at doses of 1 µg/Kg (left) and 5 mg/Kg (right). The experimental values of unmetabolized parent compound (dots in the figure) were interpolated using Hill type function (line) to obtain a continuous time course of plasma parent concentration. c) Metabolite-corrected arterial plasma Time Activity Curves (TACs) after oral administration of [^{11}C]AHK-2.1 at doses of 1 µg/Kg (left) and 5 mg/Kg (right). The curves were obtained by applying the Hill type function in b to the curve in a.

As for intravenous administration, the best-fit value for parameter *d* was 1. However, after oral administration, no significant differences were found for the parameter *a* when 1 µg/Kg or 5 mg/Kg were administered, with values of 0.10 and 0.13, respectively. Focusing on metabolism kinetics, the metabolite with retention time = 2 min (Met 1, red dots in Fig. 5.19) reaches higher plasmatic concentration at longer time points compared with the intravenous administration of the same labelled compound (Fig. 5.11c). These results suggest that demethylation of the ammine group partially occurs before absorption. The trend of the other metabolites was quite similar to those obtained after intravenous administration. For compound [^{11}C]AHK-2.2, the metabolite [^{11}C]CH_3OH still remains as the main observed metabolite (Met 1, red dots in Fig. 5.20).

5.3.3 BIODISTRIBUTION AND PHARMACOKINETICS EVALUATION OF THE TRIAZOLE-BASED FKBP12-RYR STABILIZERS AHK-1 AND AHK-2 AFTER INTRAVENOUS ADMINISTRATION

Once the metabolite-corrected arterial plasma TACs had been determined for both compounds after intravenous bolus injection and oral administration at two different doses (1µg/kg and 5mg/kg), we tackled the evaluation of the biodistribution and the determination of the most important pharmacokinetics parameters. We will firstly discuss the results obtained after the intravenous administration of compound AHK-1 and AHK-2.

Biodistribution studies

Imaging studies performed in rats enabled the determination of the biodistribution pattern of the labelled compounds. Additionally, the inclusion of the label in the two different positions was used to gain information about the biodistribution of the major metabolites. With that aim, animals were injected with the labelled compounds and images were acquired immediately after administration (total acquisition time of 80 min).

Dynamic PET imaging, after intravenous administration (Fig. 5.22), showed elimination via urine when [^{11}C]AHK-1.2 and [^{11}C]AHK-2.2 were administered, probably reflecting the biodistribution of [^{11}C]methanol as the major metabolite. Contrarily, accumulation in the gastrointestinal track was observed after administration of [^{11}C]AHK-2.1, majorly reflecting the biodistibution of the sulfoxide derivative as one of the major metabolites. Delineation of volumes of interest (VOIs) in major organs (brain, heart, lungs, liver, kidneys, and bladder) and determination of the uptake

as % of injected dose per cm^3 (%ID/cm^3, see Fig. 5.23) revealed similar profiles, irrespective of the compound and the position of the label. Major accumulation at short times after IV administration was observed in the kidneys. For this organ, values at the first time point were 6.5±1.2 %ID/cm^3 for compound AHK-1 and 5.2±1.4 %ID/cm^3 for compound AHK-2. These values progressively decreased with time to reach values close to 2 %ID/cm^3 at t = 80 min for both compounds. The presence of radioactivity in the bladder at long times after administration confirms elimination via urine in all cases. The different biodistribution pattern observed when [^{11}C]AHK-2.1 or [^{11}C]AHK-2.2 is administered suggest that metabolism studies are paramount to interpret PET images.

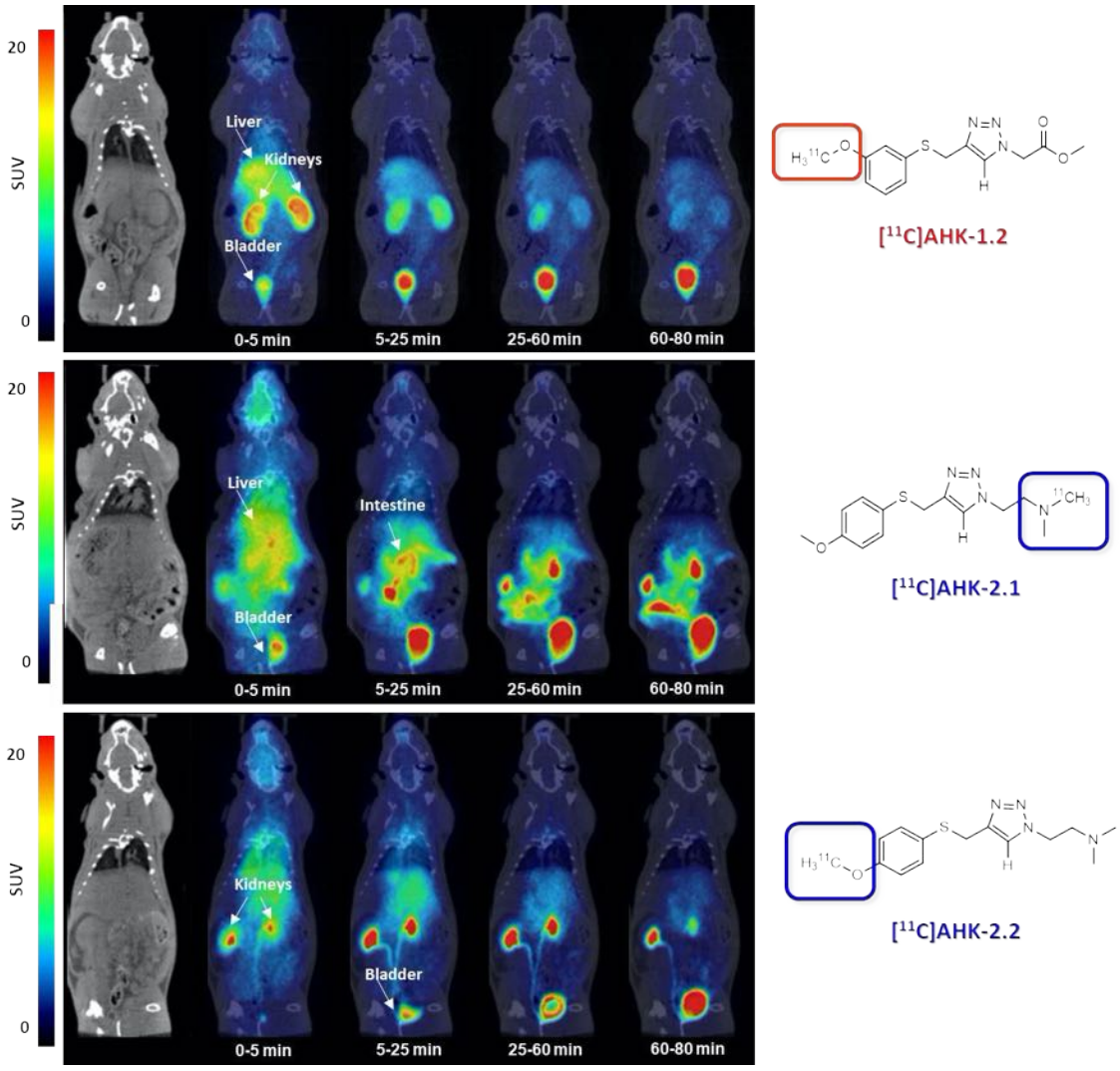

Fig. 5.22: Biodistribution of [^{11}C]AHK-1.1, [^{11}C]AHK-2.1 and [^{11}C]AHK-2.2 (from top to bottom) after intravenous administration (dose = 1 µg/Kg). Representative whole body coronal PET images (projections) obtained at different time points after administration. PET images have been co-registered with a representative CT slide for the localization of the radioactive signal. Positions of the major organs are indicated. The chemical structure of the corresponding radiolabelled compound is also shown in the right part of the image.

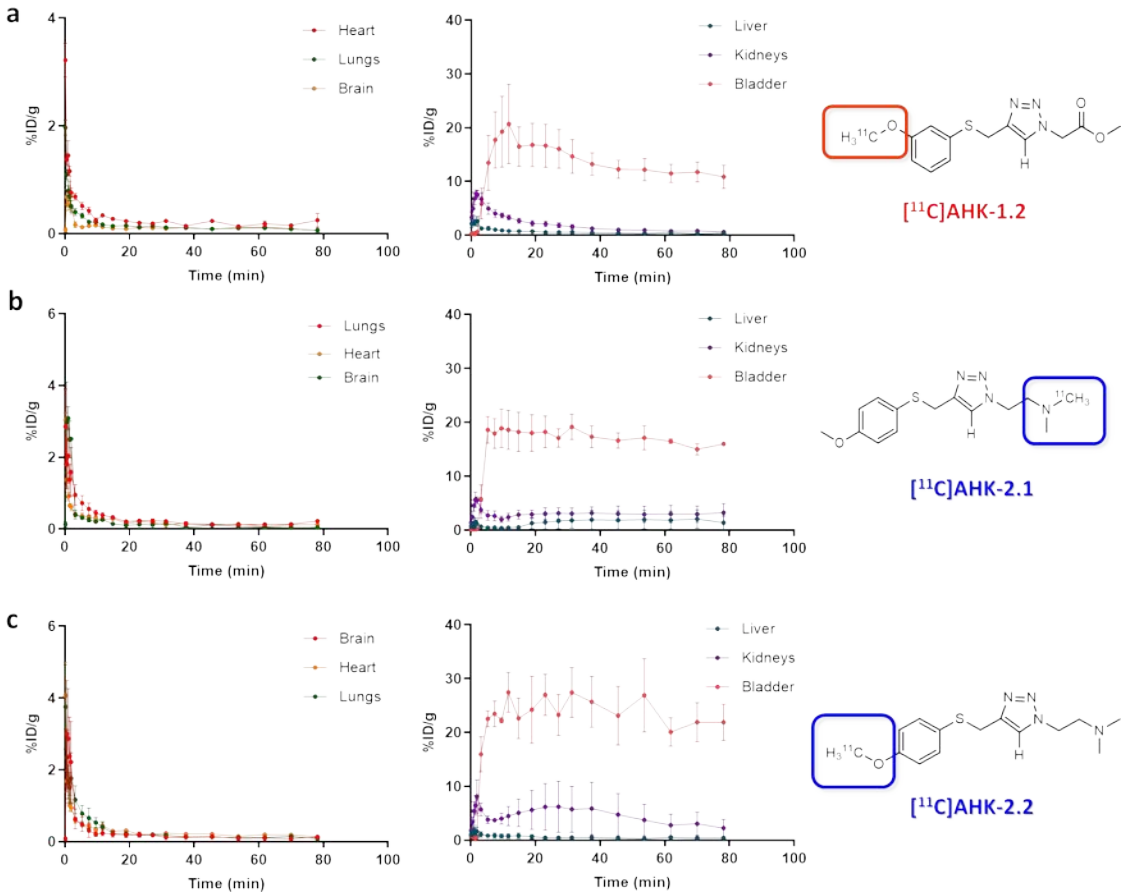

Fig. 5.23: Concentration of radioactivity in the different organs as determined from PET images after intravenous administration of [^{11}C]AHK-1.2, [^{11}C]AHK-2.1 and [^{11}C]AHK-2.2 (from top to bottom). Values are expressed as %ID/g. Values correspond to mean ± standard deviation, n=3 per radiolabelled compound.

Pharmacokinetics evaluation

In order to obtain reliable pharmacokinetics data, the selection of the appropriate software, model, and method to evaluate the reliability of the fitting is paramount. Nowadays, several software tools are available in the market. Among them, we selected PKSolver, a freely available add-in program for Microsoft Excel which, compared with professional software, provides satisfactory results, and simplifies the analysis [10] . Hence the initial estimates of the pharmacokinetic parameters were computed using the curve stripping technique by the add-in

[10] Zhang, Y., Huo, M., Zhou, J., Xie, S. PKSolver: An add-in program for pharmacokinetic and pharmacodynamic data analysis in Microsoft Excel. *Computer Methods and Programs in Biomedicine* (2010) doi:10.1016/j.cmpb.2010.01.007.

program PKSolver. The metabolite-corrected arterial plasma concentration versus time data from each animal were fit to one-, two-, three- and non-compartmental models, and the best fit was chosen based on the Akaike Information Criterion (AIC)[11]. Area under the curve (AUC) was calculated using the log-linear trapezoidal method. This method is a combination of the linear trapezoidal method used when concentration is increasing, as in the absorption phase, and the logarithmic trapezoidal method used when the concentration is decreasing, as occurs during the elimination process. An unpaired t test was run to compare the non-carried added (NCA; administered dose = 1µg/kg) and the carrier added (CA; administered dose = 5mg/kg) groups. The confidence level was set to 95% and a two-tail test was selected for the output P values. The pharmacokinetics parameters (Tables 5.3 and 5.4, entries 1-6) were: elimination half-life ($t_{1/2}$), plasma clearance (Cl), volume of distribution at final state (Vz), volume of distribution at the steady state (Vss), area under the curve (AUC) and mean residence time (MRT).

Table 5.3: AHK-1 main pharmacokinetic parameters obtained from metabolite-corrected arterial plasma time activity curves.

Entry	Parameter	Value*	Value**	P_{value}	Value***
1	$t_{1/2}$	7.36±0.65	6.14±1.06	0.27	6.99±1.38
2	Cl	1.24±0.09	1.67±0.97	0.46	1.41±0.54
3	V_z	838.59±124.42	780.78±340.95	0.69	822.5±196.2
4	V_{ss}	523.91±65.76	504.88±201.79	0.78	516.3±111.6
5	AUC	80.80±6.23	71.77±41.65	0.71	77.19±21.85
6	MRT	7.01±0.38	5.40±1.09	0.28	6.34±1.10

$t_{1/2}$: elimination half-life, expressed in minutes; **Cl**: plasma clearance, expressed in ml/s; **V_z**: volume of distribution at final state, expressed in ml; **Vss**: volume of distribution at the steady state, expressed in ml; **AUC**: area under the curve, expressed as %IDxs/ml; **MRT**: mean residence time, expressed in minutes.

* NCA group. Mean and standard deviation values, n=3

** CA group. Mean and standard deviation values, n=3

*** Considering both NCA and CA groups. Mean and standard deviation values, n=6

[11] Akaike, H. A new look at the statistical model identification. *IEEE Transactions on Automatic Control* (1074) doi:10.1109/tac.1974.1100705.

Table 5.4: AHK-2 main pharmacokinetic parameters obtained from metabolite-corrected arterial plasma time activity curves.

Entry	Parameter	Value*	Value**	P_{value}	Value***
1	$t_{1/2}$	11.67± 3.22	13.60± 3.42	0.38	12.63±3.29
2	Cl	1.91±0.41	1.87±0.73	0.71	1.89±0.55
3	V_z	1996.50±429.72	2335.03±608.77	0.66	2165.76±1125.06
4	V_{ss}	1026.88±695.33	1126.13±443.15	0.75	1076.50±808.72
5	AUC	53.99±11.04	59.39±19.76	0.60	56.69±15.36
6	MRT	8.48±3.76	8.59±5.23	0.67	8.53±4.30

$t_{1/2}$: elimination half-life, expressed in minutes; **Cl**: plasma clearance, expressed in ml/s; **V_z**: volume of distribution at final state, expressed in ml; **Vss**: volume of distribution at the steady state, expressed in ml; **AUC**: area under the curve, expressed as %IDxs/ml; **MRT**: mean residence time, expressed in minutes.
* NCA group. Mean and standard deviation values, n=5
** CA group. Mean and standard deviation values, n=5
*** Considering both NCA and CA groups. Mean and standard deviation values, n=10

According to AIC criterion, in which the smaller the AIC the better is the fitting, the pharmacokinetics parameters for both compounds were best described by a non-compartmental analysis of metabolite-corrected arterial plasma TACs with intravenous constant fast infusion input. No significant differences on pharmacokinetics were found when doses of 1 µg/Kg and 5 mg/Kg were used for each compound, indicating that the pharmacokinetics is linear in this dose range. The P value in all cases is > 0.05 confirming that there are no statistical differences between the two groups (NCA, 1 µg/kg administered dose; and CA, 5 mg/Kg administered dose). Because of that, all data for each compound (irrespective of the administered dose) were pooled to calculate the parameters included in Tables 5.3 and 5.4.

Comparison of the pharmacokinetics parameters obtained for AHK-1 and AHK-2 showed significant differences. Compound AHK-2 has higher $t_{1/2}$ values than compound AHK-1. Usually, this can be associated either with a large V_d or/and a slow clearance. In fact, the larger the V_d, the lower the fraction of the drug that can be eliminated over time and the longer the half-life. However, in this particular case the difference in $t_{1/2}$ seems to be associated with the V_d, since no substantial differences were observed for clearance values. The higher value found for V_d, and consequently for $t_{1/2}$, in the case of AHK-2, could be expected considering the different metabolism of the two drugs. As a matter of fact, drugs which are more polar or highly ionized,

as in the case of AHK-1 which is instantaneously hydrolysed to the corresponding carboxylic acid, have lower volumes of distribution.

5.3.4 BIODISTRIBUTION AND PHARMACOKINETICS EVALUATION OF THE TRIAZOLE-BASED FKBP12-RYR STABILIZERS AHK-1 AND AHK-2 AFTER ORAL ADMINISTRATION

The biodistribution and the most important pharmacokinetics parameters were also determined for oral administration.

Biodistribution studies

In this case, animals were kept in a fasting condition for 5 hours before the imaging session to prevent the presence of food in the stomach, and the labelled compounds were administrated using a flexible plastic gavage needle. Static PET acquisitions were recorded at 0, 30, 60, 90, 120, 160 min.

Visual inspection of PET images (Fig. 5.24) showed no translocation to remote organs for both compounds indicating that the absorption was too low to be measured by PET imaging. This could be a result of the low bioavailability of the compound, together with the short half-life of the radionuclide, which dramatically decreases the sensibility of the technique at long times after administration.

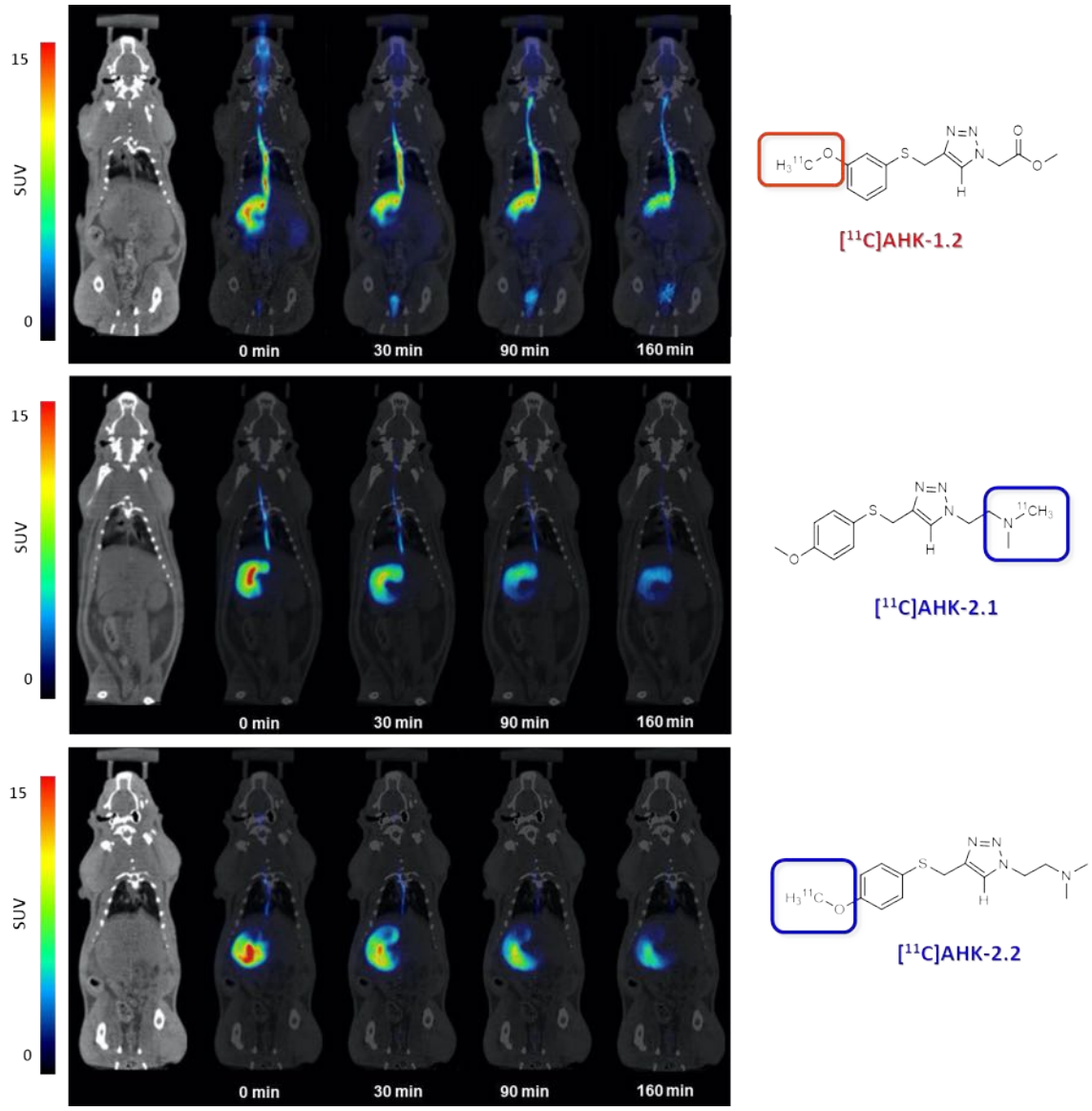

Fig. 5.24: Biodistribution of [^{11}C]AHK-1.1, [^{11}C]AHK-2.1 and [^{11}C]AHK-2.2 (from top to bottom) after oral administration (1 µg/Kg). Representative whole body coronal PET images (projections) obtained at different time points after administration. PET images have been co-registered with a representative CT slide for the localization of the radioactive signal. Positions of the principal organs are indicated. The chemical structure of the correspondent radiolabelled compound is also shown in the right part of the image.

Pharmacokinetics evaluation

The evaluation of the most important pharmacokinetics parameters was carried out as previously described for intravenous administration, with the difference that among the parameters calculated the bioavailability (F) was included. Experimentally, the metabolite-corrected arterial plasma concentration versus time data for each animal were fit to one-, two-, three- and non-compartmental models, and the best fit was chosen based on the AIC criterion. AUC was calculated using log-linear trapezoidal method. An unpaired t test was run to compare the NCA (administrated dose 1µg/kg) and the CA (administrated dose 5mg/kg) group. The confidence level was set to 95% and a two-tail test was selected for the output P value. The pharmacokinetics parameters (Tables 5.5 and 5.6, entries 1-6) were: elimination half-life ($t_{1/2}$), plasma clearance (Cl), volume of distribution at final state (Vz), area under the curve (AUC), mean residence time (MRT) and bioavailability (F).

Table 5.5: AHK-1 main pharmacokinetic parameters obtained from metabolite-corrected arterial plasma time activity curves.

Entry	Parameter	Value*	Value**	P_{value}	Value***
1	$t_{1/2}$	9.96±2.66	9.41±4.26	0.78	9.64±3.31
2	Cl	1.97±1.26	1.66±0.54	0.75	1.79±0.77
3	V_z	1378.11±453.25	1345.77±657.56	0.38	1360±575.1
4	AUC	6.86±0.26	12.69±11.50	0.54	10.36±8.74
5	MRT	12.50±3.66	11.46±4.66	0.71	11.88±3.82
6	F				0.134

$t_{1/2}$: elimination half-life, expressed in minutes; **Cl**: plasma clearance, expressed in ml/s; **V_z**: volume of distribution at final state, expressed in ml; **Vss**: volume of distribution at the steady state, expressed in ml; **AUC**: area under the curve, expressed as %IDxs/ml; **MRT**: mean residence time, expressed in minutes; **F**: bioavailability.

* NCA group. Mean and standard deviation values, n=3

** CA group. Mean and standard deviation values, n=3

*** Considering both NCA and CA groups. Mean and standard deviation values, n=6

Table 5.6: AHK-2 main pharmacokinetic parameters obtained from metabolite-corrected arterial plasma time activity curves.

Entry	Parameter	Value*	Value**	P_{value}	Value***
1	$t_{1/2}$	9.16±3.78	12.97±11.06	0.60	11.34±8.44
2	Cl	4.23±3.58	1.57±0.69	0.29	2.71±2.55
3	V_z	2728.14±1252.35	1624.28±1299.35	0.31	2097.36±1309.61
4	AUC	6.68±4.35	13.35±5.08	0.32	10.49±5.65
5	MRT	8.51±2.69	9.36±8.51	0.88	9.00±6.93
6	F				0.185

$t_{1/2}$: elimination half-life, expressed in minutes; **Cl**: plasma clearance, expressed in ml/s; **V_z**: volume of distribution at final state, expressed in ml; **AUC**: area under the curve, expressed as %IDxs/ml; **MRT**: mean residence time, expressed in minutes; **F**: bioavailability

* NCA group. Mean and standard deviation values, n=3

** CA group. Mean and standard deviation values, n=4

*** Considering both NCA and CA groups. Mean and standard deviation values, n=7

According to AIC criterion, for both compounds, the pharmacokinetics parameters were best described by a non-compartmental analysis of metabolite-corrected arterial plasma TACs with extravascular input. No significant differences on pharmacokinetics were found when doses of 1 µg/Kg and 5 mg/Kg were used, indicating that the pharmacokinetics is linear in this dose range. The P value in all cases was > 0.05 confirming that the differences observed for the two groups (NCA, 1 µg/kg administered dose and CA, 5 mg/Kg administered dose) were non-significant.

Pharmacokinetic parameters obtained after oral administration are quite similar to those obtained after intravenous administration for both compounds. This is expected considering that once absorbed, the unaltered compound undergoes the same processes as when administered intravenously. The only differences are observed for AUC values. The AUC, which describes the variation of a drug concentration in blood plasma as a function of time, reflects the bioavailability of the drug. The bioavailability is practically 100% (F=1) following an intravenous administration and lower (F≤1) for other routes of administration as in the case of oral administration. The bioavailability after oral administration was 0.134 for compound AHK-1 and 0.185 for compound AHK-2.

5.3.5 PLASMA PROTEIN BINDING (PPB)

The binding of administered drugs to plasma proteins has long been of interest since protein-bound drug is practically non-diffusible, or at least less diffusible across capillary membranes into tissue. Only the free fraction of the drug can pass across biological membranes and reach the target, therefore only the free fraction is pharmacologically active[12]. This could affect the efficacy of a drug but also the clearance and toxicity since all these processes include passage through a membrane. However, it is worth mentioning that a high plasma protein binding (PPB) does not necessarily means unavailability for distribution and that different examples in the literature can be found explaining that paradoxically some drugs are successful despite the high percentage of PPB[13,14]. Plasma protein binding in fact can be considered a sort of storage deposit. Because a chemical in any tissue compartment is in equilibrium with its free concentration in blood, storage is dynamic. Removal of free chemical from the body by metabolism or excretion shifts the equilibrium in such a way that the stored chemical is released. Hence, at longer times, also the protein-bound fraction could become available. Overall, the plasma protein binding, although does not necessary determine if a drug will be successful or not, is a paramount parameter to consider in the drug development process since it could influence important pharmacokinetic and thus pharmacodynamics processes[15].

Protein binding studies are typically carried out either with plasma o serum. Equilibrium dialysis (ED) and ultrafiltration (UF) are commonly used experimental techniques for protein-binding measurements. Among them, we selected the ultrafiltration technique, which offers significant advantages in terms of analysis time, simplicity, and lack of dilution effects since the separation of free and protein-bound drug can be carried out directly using plasma without addition of buffer. However, beside its advantages, the results obtained using this method can be questionable if the nonspecific binding on membrane filters and plastic devices are not

[12] Smith, D. A.; Di, L., & Kerns, E. H. The effect of plasma protein binding on in vivo efficacy: misconceptions in drug discovery. *Nature Reviews Drug Discovery,* (2010) doi:10.1038/nrd3287.

[13] https://www.cambridgemedchemconsulting.com/resources/ADME/distribution.html

[14] Gallo, M., Matteucci, S., Alaimo, N., Pitti, E., Orsale, M. V., Summa, V., Cicero, D. O., Monteagudo, E. A Novel Method using Nuclear Magnetic Resonance for Plasma Protein Binding Assessment in Drug Discovery Programs. *Journal of Pharmaceutical and Biomedical Analysis,* (2019). doi:10.1016/j.jpba.2019.01.049.

[15] Mehvar, R. Role of Protein Binding in Pharmacokinetics. *American Journal of Pharmaceutical Education,* (2005). doi:10.5688/aj69051526.

considered and corrected for[16]. For that reason, we verified the presence of nonspecific binding by absorption of the drug to the membrane and corrected the results with a positive control, which consisted of filtrating a volume of only radiolabelled compound. Noteworthy, since this is an *ex vivo* experiment and therefore no metabolism is expected, these studies were only carried out on one of the labelled analogues per each compound ([^{11}C]AHK-1.2 for AHK1; [^{11}C]AHK-2.2 for AHK2). Experimentally, rat plasma was incubated with [^{11}C]AHK-1.2 or [^{11}C]AHK-2.2 for 15 minutes. 300 µl of the incubated solution were transferred to an Amicon® Ultra Centrifugal filter and centrifugated for 20 minutes at 2000 rpm. Filters with molecular weight cut-off values of 10 and 30 KDa were used, to ensure that all the major protein present in the plasma such as albumin (67 KDa), alpha-1 acid glycoprotein (38-48 KDa) and lipoprotein (>200 KDa) were retained in the filter, irrespectively of the pore size. After centrifugation, the filtrate and the filter were separated, and the amount of radioactivity was measured in a gamma counter. We finally corrected the results considering the unspecific binding. The percentage of unbound drug resulted to be about 60% classifying both compounds as medium/weak binding.

In **table 5.7** the percentage of nonspecific binding, plasma protein binding and free drug for each compound are summarized.

Compound	% NCB[1*] (n=3)	% PPB[2*] (n=3)	% Unbound drug[3*] (n=3)	% NCB[1**] (n=3)	% PPB[2**] (n=3)	% Unbound drug[3**] (n=3)
[^{11}C]AHK-1	24.3±0.8	41.7±3.5	58.3±3.5	17.6±0.9	36.6±4.7	63.4±4.7
[^{11}C]AHK-2	27.8±2.0	42.0±1.6	58.0±1.6	16.4±0.5	44.2±2.3	55.8±2.3

[1] percentage of nospecific binding, [2] percentage of plasma protein binding, [3] percentage of unbound drug
* 10 KDa Amicon® Ultra Centrifugal filters
** 30 KDa Amicon® Ultra Centrifugal filters

[16] Lee, K. ; Mower, R.; Hollenbeck, T.; Castelo, J.; Johnson, N.; Gordon P.; Sinko, P. J.; Holme, K.; Lee, Y. Modulation of nonspecific binding in ultrafiltration protein binding studies, *Pharm. Res*. (2003) doi:10.1023/a:1024406221962.

5.4 CONCLUSION

The evaluation of pharmacokinetics is paramount during the drug development process of new drugs. In the work presented in this chapter, the pharmacokinetics evaluation of the triazole-based compounds was tackled using Positron Emission Tomography (PET) after intravenous and oral administration of two different concentrations, 1 µg/Kg and 5 mg/Kg. For the determination of the metabolite-corrected arterial plasma TAC, which represents the concentration of the non-metabolized compound in arterial plasma, the catheterization and online blood sampling, by using an in-house developed monitoring system which enable the extracorporeal circulation blood, resulted to be appropriate. The multi-position labelling approach was used to gain information about the *in vivo* metabolism of AHK-1 and AHK-2. In the case of AHK-1, the *in vivo*

metabolism results show instantaneous hydrolysis of the ester moiety to form the corresponding carboxylic acid, suggesting that the AHK-1 could be a pro-drug. In the case of AHK-2, the main metabolic pathway was the demethylation of the CH_3O-Ar residue followed by oxidation of the thioether group into sulfoxide and demethylation of $–N(CH_3)_2$. For the determination of the most important pharmacokinetics parameters such as elimination half-life ($t_{1/2}$), plasma clearance (Cl), volume of distribution at final state (Vz), volume of distribution at the steady state (Vss), area under the curve (AUC), mean residence time (MRT) and bioavailability (F), the metabolite-corrected arterial plasma TACs were fit to different kinetic models by using the add-in program PKSolver. For both compounds and both administration routes, the pharmacokinetics were best described by a non-compartmental model. The results indicate high plasma clearance, linear pharmacokinetics in the dose-range investigated, and low bioavailability when the drug was administrated orally. Investigation of the biodistribution pattern after intravenous administration of the radiolabelled compounds in experimental rats using PET show accumulation in kidneys and liver at early time points and elimination via urine for the compound [^{11}C]AHK-1.2. In the case of the compound AHK-2, when [^{11}C]AHK-2.1 was intravenously administrated PET images show accumulation in the gastrointestinal tract at early time points and accumulation in kidneys at the same time points when [^{11}C]AHK-2.2 was administrated, probably reflecting the biodistribution of [^{11}C]methanol as major metabolite, suggesting that knowledge about metabolic pathways is paramount to interpret images. In both cases, elimination via urine was observed at late time points. Investigation of the biodistribution pattern after oral administration of the same radiolabelled compounds, show no translocation to remote organs. *Ex vivo* evaluation of the plasma protein binding showed that the percentage of unbound drug resulted to be about 60%, classifying AHK-1 and AHK-2, as medium/weak binding.

5.5 EXPERIMENTAL PART

5.5.1 GENERAL CONSIDERATIONS

Female Sprague-Dawley rats (8-9 weeks old, Janvier Labs) were used to investigate pharmacokinetics (biodistribution, metabolism and excretion) of the triazole-based FKBP12-RyR stabilizers AHK-1 and AHK-2. The animals were maintained and handled in accordance with the Guidelines for Accommodation and Care of Animals (European Convention for the Protection of Vertebrate Animals Used for Experimental and Other Scientific Purposes) and internal guidelines. All experimental procedures were approved by ethical committee of CIC biomaGUNE and local authorities before conducting experimental work. All animals were housed in ventilate cages and fed on standard diet *ad libitum*.

5.5.2 METABOLITE-CORRECTED ARTERIAL PLASMA TIME ACTIVITY CURVES (TACS)

Animal surgery

During experiment, rats were kept normothermic using a heating blanket (Homeothermic Blanket Control Unit; Bruker). Anaesthesia was induced with 5% isoflurane (IsoFlo®, Abbott Laboratories) and maintained by 2% of isoflurane in 100% O_2. The rat was positioned in supine position on an operating table and the two distal hind limbs were fixed forming an approximately 30° angle with the horizontal plane. The surgical region was scrubbed using Betadine, starting in the centre, and making a circular sweep outward. A skin incision was made in the femoral region. Soft tissue was dissected to expose the femoral neurovascular bundle, consisting of femoral vein, artery, and nerve. Fine tip forceps were placed between the artery, vein and nerve and were slowly opened to separate the vessels, exposing an approximately 1 cm length section of artery/vein. The vena profunda femoris was sutured to avoid retrograde bleeding via this vessel, and the sapheno-femoral junction was cauterized. A few millimetres from venatomy, a vascular clip was inserted in the direction of the catheter (to control the flow) and a suture was applied in the opposite direction (to avoid retrograde bleeding). The same operation was carried out both on the femoral vein and femoral artery. An appropriate syringe filled with 50 U/ml Heparin/physiologic saline solution was fixed at the terminus of the catheters and these were filled with heparinized saline solution. On the upper half of the vessel circumference, at a 45° angle, an incision was done and the catheter (fine bore polythene tubing: ID 0.58 mm, OD 0.98

mm) was inserted through the venotomy and advanced to the vascular clip. The vascular clip was then removed, and the catheter advanced distally towards the level of the inguinal ligament. The catheter was finally secured to the femoral vein/artery proximally and distally with 2 single knots using 4-0 braided silk suture. The catheters were connected to an in-house developed system composed by a peristaltic pump and gamma-radiation coincidence detector (Bioascan, B-FC-4100). The femoral artery catheter, the gamma detector, the peristaltic pump and the femoral vein catheter were thus connected in series, to enable the extracorporeal circulation of blood (flow 150 µl/s from femoral artery to femoral vein) and continuous measurement of radioactivity in the blood.

The labelled compounds were administrated through two different ways:

1. Intravenous constant infusion. *Ca.* 37 MBq in 300 µL of saline solution was injected concomitantly with the start of the acquisition through the femoral vein catheter.
2. Oral bolus administration. Animals were kept in a fasting condition for 5 hours. The radioactive dose (*ca.* 74 MBq in 300 µL of saline solution) was administered using a flexible a 20-gauge disposable flexible PTFE feeding needles (Fine Science Tools, F.S.T.) and a small animal Laryngoscope (Penn-Century, Model LS-2) for the correct visualization of the oesophagus. The time gap between oral administration and start of acquisition was *ca.* 30 seconds.

For each compound, the study was conducted under no carrier added (NCA, 1 µg/Kg) and carrier added (CA) condition. In this case, all experiments were performed by adding non-radioactive compound to a final dose of 5 mg/Kg. In all cases, data were imported in real time to an excel sheet using PLX-DAX add-on for Microsoft Excel (measured in volts per second).

Distribution between plasma and blood to obtain arterial plasma TACs

In order to determine the haematocrit, hence the relationship between plasma and blood, arterial blood samples were withdrawn from the femoral artery catheter and introduced into a capillary (Microhaematocrit capillaries 75x1.55, Nahita). Samples were centrifuged at 11000 rpm for 10 minutes and the haematocrit was determined.

To determine arterial plasma TACs another blood sample was withdrawn and the amount of activity, of a fixed volume (10 µL), was measured in an automatic gamma counter (2470 Wizard, PerkinElmer) to convert data imported with PLX-DAX (Volts per seconds) into Bq/s using a

calibration curve obtained from previous measurement of a known amount of radioactivity in the automatic gamma counter. Values were than expressed as percentage of injected dose per gram of blood (% ID/g). The blood sample was then centrifuged at 14800 rpm for 10 minutes to separate the plasma and the amount of radioactivity of a fixed volume (10 µL), was measured in an automatic gamma counter (2470 Wizard, PerkinElmer) to calculate the real plasma-to-blood ratio. Finally, the TACs were corrected to be expressed as percentage of injected dose per gram of plasma (% ID/g_{plasma}).

In vivo metabolism studies. Metabolite-corrected arterial plasma TACs

At different time points, arterial blood samples (150 µL) were withdrawn. Blood samples were processed to separate the plasma, which was further processed to determine the presence of radioactive metabolites. With that aim, plasma fractions were diluted with the same volume of acetonitrile. After mixing vigorously for 20 s, samples were centrifuged at 14800 rpm for 4 minutes. The liquid phase was separated from the precipitate by decantation and was injected into the HPLC system, using an Agilent 1200 Series HPLC system with a multiple wavelength UV detector (λ = 254 nm) and a radiometric detector (Raytest). A RP-C18 column (Mediterranean Sea18, 4.6x150 mm, 5 µm particle size) was used as stationary phase, with an Eclipse XDB-C18 (4.6×12.5 mm, 5 µm particle size) guard column. For compound AHK-1.2, the mobile phase was 10 mM ammonium formate solution (pH = 3.9)/Acetonitrile. For compounds AHK-2.1 and AHK-2.2, the mobile phase was 10 mM ammonium formate solution (pH = 8.3)/Acetonitrile. In all cases, chromatographic runs were performed under gradient conditions, at a flow rate of 1 mL/min, with a total chromatographic time of 35 min (0-5 minutes 5% ACN; 5-25 minutes 60% ACN for compound AHK-1 / 50% ACN for compound AHK-2; 25-30 minutes 60% ACN for compound AHK-1 / 50% ACN for compound AHK-2; 30-35 minutes 5% ACN).

The arterial plasma TACs were corrected by metabolism to represent the plasma concentration of radioactivity corresponding to the parent compound. The corresponding metabolite-corrected arterial plasma TACs were further used for the determination of the most important pharmacokinetics parameters.

5.5.3 PHARMACOKINETICS ANALYSIS

The pharmacokinetics parameters of compounds AHK-1 and AHK-2 after intravenous and oral administration at two different doses were calculated by using the add-in program PKSolver. The

area under the curve (AUC) was calculated using log-linear trapezoidal method. The maximum concentration in plasma (C_{max}) and the time taken to reach the maximum plasma concentration (T_{max}) were obtained from arterial plasma data. The pharmacokinetic parameters were fitted into different compartment models and the best fit model was based on Akaike Information Criterion (AIC). The unpaired *t*-test was run to compare the data obtained under no carrier (NCA, administered dose 1µg/Kg) and under carrier added (CA, administered dose 5mg/Kg) conditions.

5.5.4 BIODISTRIBUTION STUDIES

Intravenously administered triazole-based FKBP12-RyR stabilizers

Rats were anesthetized by inhalation of 5% isoflurane (IsoFlo®, Abbott Laboratories) in pure O_2 and maintained by 1.5-2% isoflurane in 100% O_2. During imaging, rats were kept normothermic using a heating blanket (Homeothermic Blanket Control Unit; Bruker). Once the animal was under anesthesia, one of the lateral tail veins was catheterized with a 24-gauge catheter (Introcan Certo®, Bbraun) and [^{11}C]AHK-1.2, [^{11}C]AHK-2.1 or [^{11}C]AHK-2.2 was injected using saline solution as the vehicle (n=3 for each radiolabelled compound, *ca.* 26 MBq) concomitantly with the start of a PET dynamic acquisition. Whole body dynamic images were acquired in 4 bed positions (21 frames: 5x5s, 5x30s, 5x60s, 6x120s; total acquisition time = 79.6 min) in the 400-700 keV energetic window using an eXploreVista-CT small animal PET-CT system (GE Healthcare). After each PET scan, CT acquisitions were also performed (140µA intensity, 40kV voltage) to provide anatomical information of each animal as well as the attenuation map for the later reconstruction of the PET images. PET images were reconstructed using 2D OSEM reconstruction algorithm and applying random, scatter and attenuation corrections. After reconstruction, PET-CT images of the same animal were co-registered and analysed using PMOD image processing tool (PMOD Technologies Ltd, Zürich, Switzerland). Volumes of interest (VOIs) were manually placed on different organs of rat body (brain, lungs, heart, liver, stomach, kidneys and bladder). Time–activity curves (decay corrected) were obtained as cps/cm^3 in each organ. Curves were transformed into real activity (Bq/cm^3) curves by using a calibration factor, obtained from previous scans performed on a phantom (micro-deluxe, Data spectrum Corp.) under the same experimental conditions (isotope, reconstruction algorithm and energetic window) and finally into %ID/ cm^3.

Orally administered triazole-based FKBP12-RyR stabilizers

Animals were kept in a fasting condition for 5 hours before the imaging session. Deep sedation was induced to the animals by inhalation of 5% isoflurane in pure O_2. As soon as anaesthesia was accomplished, the animals were placed on an angled board at 90° (vertical head up) by hanging the upper incisor teeth on the incisor loop of the board. The radioactive dose (*ca.* 74 MBq in 300 µL of saline solution) was administered using a flexible a 20-gauge disposable flexible PTFE feeding needles (Fine Science Tools, F.S.T.) and a small animal Laryngoscope (Penn-Century, Model LS-2) for the correct visualization of the oesophagus. Administration was followed by whole body static images in 4 bed positions at different time points (0, 30, 60, 90, 120, 160 min) and high-resolution CT acquisitions as above. After image reconstruction, PET-CT images were analysed using PMOD image processing tool as above.

5.5.5 Plasma Protein Binding (PPB)

Test compounds were incubated for 15 minutes in fresh blood. Samples were centrifuged at 14800 rpm for 10 min to pellet the red blood cells and 300 µl of the supernatant plasma was transferred to a cellulose centrifugal filter (Amicon® Ultra-0.5) with molecular cut-off of 10 and 30 KDa. Samples were centrifuged for 20 minutes at 2000 rpm. The filter and the filtrate were analysed using MUCHA detector (Raytest). The unspecific binding was calculated incubating test compounds with saline solution (pH 7.4). The samples were treated as above.

CHAPTER 6: GENERAL CONCLUSION

1. The triazole-based FKBP12-RyR stabilizers, AHK-1 and AHK-2, can be efficiently radiolabelled by the incorporation of either positron or beta emitters. The labelling with the positron emitters was achieved by C-11 methylation using $[_{11}C]CH_3I$ as labelling agent.

2. The multi-radionuclide/multi-position labelling approach resulted to be useful to get a good overview of metabolism and the identification of some of the metabolites. Preliminary *in vitro* metabolism studies, by using rat liver microsomes, suggested that the main metabolic pathway for the compound AHK-1 is the hydrolysis of the ester to form the corresponding carboxylic acid (–COOH) and $[^{11}C]CH_3OH$. For the compound AHK-2 the main metabolic pathway was the demethylation of the CH_3O-Ar residue followed by oxidation of the thioether group into sulfoxide and demethylation of $–N(CH_3)_2$.
3. The online measurement of the AIF by creating an extracorporeal circulation of the arterial blood, resulted to be the most appropriate method for our subsequent pharmacokinetics studies. It allows the determination of a real arterial input function and, enables arterial blood sample collection and processing (eventually enabling metabolite analysis) and subsequent correction.
4. Positron Emission Tomography is perfectly suited to investigate the pharmacokinetics properties of drugs AHK-1 and AHK-2.
5. For both compounds and both administration routes (IV and OR), the pharmacokinetics were best described by a non-compartmental model. The results indicate high plasma clearance, linear pharmacokinetics in the dose-range investigated (1µg/Kg and 5mg/Kg), and low bioavailability when the drug was administrated orally.
6. Investigation of the biodistribution pattern after intravenous administration of the radiolabelled compounds show different pattern depending on the labelling position, suggesting that knowledge about metabolic pathways is paramount to interpret images.
7. *Ex vivo* evaluation of the plasma protein binding showed that the percentage of unbound drug resulted to be about 60%, classifying, AHK-1 and AHK-2, as medium/weak binding.

ACKNOWLWDGMENTS

First, I would like to express my sincere appreciation to my research supervisor **Dr. Jordi Llop**. Thank you for giving me the opportunity to carry out this doctoral thesis in your group, but above all for your guidance and direction throughout these years. Thanks to you and your attitude, I have been able to discover new qualities as a researcher through a wonderful learning process.

Many thanks also to **Dr. Jesús Maria Aizpurua** for making me part of this project.

Also a big thank you to the **PET3D** project that has made this PhD thesis possible by giving me the opportunity to participate in many invaluable activities. All this, thanks to the fantastic people which has welcomed me, our project manager Dr. Debbie McLaggan and the project coordinator Prof. Matteo Zanda. Furthermore, for the opportunity of secondments at the AstraZeneca many thanks to **Dr. Charles Elmore** and all his team, especially to Jonas, Lee, Malvika and Marcus for your help and contribution to my research, and for the "fika" and the very early lunches (☺).

Special thanks also to **Dr. Vanessa Gómez-Vallejo** for your invaluable personal and professional support, and to all my former and current colleges in the **Radiochemistry and Nuclear Imaging Group**: Ana B., Ane, Ángel, Irene, Kepa B., Kepa Z., Krishna, Luka, Marcos, Oscar, Riccardo and Zuriñe.

Gracias a la **muchitanga de radioquímica**, Víctor, Aitor, Xabi, Unai, pero sobre todo a mis neskak, Pilar, Ana y Cristina. Podría escribir otra tesis para contar todos los momentos inolvidables que he vivido con vosotras en estos años. Hemos compartido, aprendido, llorado, pero sobre todo hemos rellenado de recuerdos maravillosos todos los sitios por donde hemos pasado.

A **César**. El comienzo de esta tesis ha sido también el comienzo de nuestra vida juntos, nunca podré olvidar aquel momento. Gracias por estar a mi lado y por haberme enseñado que la vida es algo maravilloso y que cada instante es bueno para pasárselo bien.

Alla mia **famiglia**, ai grandi e ai piccoli membri. Senza il vostro appoggio niente di tutto ció sarebbe stato possibile. Tra di noi non sono mai state necessarie tante parole per esprimere l'amore che proviamo l'uno verso l'altro. Ció che ci unisce e ci supporta é un sentimento che racchiudiamo dentro ognuno di noi. GRAZIE DI TUTTO.

ACKNOWLEDGMENTS

A **Chiara**. Da quel “Ciao” timido tra i banchi de La Sapienza, l’affetto che ci unisce non ha mai smesso di crescere. Sei una costante della mia vita. Grazie.

A **Chiara M., Mavi y Anais**. Con vosotras tuve la suerte de empezar mi vida en España. Gracias por enseñarme que no hay distancia que nos pueda separar. Siempre estáis a mi lado.

Y por último a todas las personas que me han acogido en esta maravillosa ciudad haciéndome sentir una más. A mis **númer@s danzarin@s**, mi **best english team** y **Maite**. ESKERRIK ASKO.